PWHT-Free Cast Stainless Steels

PWHT-Free Cast Stainless Steels

by

Michael O. Annor

A Dissertation

Presented to the Graduate and Research Committee

of Lehigh University

in Candidacy for the Degree of

Doctor of Philosophy

in

Materials Science and Engineering

Lehigh University

May 2024

Approved and recommended for acceptance as a dissertation in partial fulfillment of the requirements for the degree of Doctor of Philosophy

Michael O. Annor

PWHT-Free Cast Stainless Steels

_____

Defense Date

_____

Dissertation Director

_____

Approved Date

Committee Members:

_____

John N. DuPont

_____

Wojciech Z. Misiolek

_____

Masashi Watanabe

_____

Herman F. Nied

Acknowledgements

I would like to thank Dr. John DuPont for giving me the opportunity to undertake graduate studies under his tutelage. I am grateful his support and patience throughout this time, and for the wealth of knowledge that he has generously passed down to me.

I am grateful to the Steel Founders' Society of America (SFSA) and the Defense Logistics Agency (DLA) for the funding that made this project possible. To the staff at SFSA, Dave Poweleit, Ryan Moore and Diana David, I say thank you for the logistical support and technical discussions.

I would also like to thank the graduate students of my research group – Chris Farnin, Jonah Duch, Thomas Siggillino, Nick Yang, Jason Langevin, and Campbell Zantop-Zimlinghaus - for their invaluable support, helping me out with various equipment and making all those useful suggestions whenever I was stuck. My heartfelt appreciation goes to the staff of the Department of Materials Science and Engineering – Lisa Arechiga, Carly Campbell, Mike Rex, Laura Moyer, Bill Mushock, Rob Keyes, Leslie O'brien, and Sz Chian Liou – all your help is very much appreciated.

Finally, I would like to thank my wife, Theodora, and daughter, Afriyie. They have been very patient with me and supported me in any way they could. I am eternally grateful to you guys.

Table of Contents

List of Tables

List of Figures

Abstract

Standard specifications set forth by the American Society for Testing and Materials (ASTM) for the production of stainless steel castings require the castings to be heat treated after welding. The post weld heat treatment (PWHT) is designed to dissolve chromium-rich carbides that may form during welding. Chromium-rich carbides can precipitate on grain boundaries in the heat affected zone (HAZ), depleting their immediate surroundings of chromium, which is an essential element for corrosion resistance. This phenomenon is known as sensitization. Even though sensitization-resistant grades have been developed that mitigate this problem, the PWHT requirements in the ASTM standards do not distinguish between improved and susceptible compositions, leading to potentially redundant heat treatments. It has become necessary to investigate the possibility of waiving the PWHT requirement for grades that may not need it. Two groups of cast stainless steel (CF and CN grades) and their associated weld metals were investigated under different welding conditions to determine their sensitization resistance using thermodynamic simulation, HAZ simulation, electrochemical corrosion tests, and energy dispersive spectroscopy (EDS) in the scanning electron microscope (SEM) and transmission electron microscope (TEM). The alloys, which comprised CF3, CF8C, CF3MN, CF8, CN3MCu and CN7M, were selected to include sensitization-resistant grades. The results showed that the high carbon grades CN7M and CF8 together with their weld metals were strongly sensitized as expected and therefore need the post-weld solution anneal. The low carbon grades (CF3 and CN3MCu) and the niobium-stabilized grade (CF8C) were only mildly sensitized. Their degree of sensitization (DOS) values were low enough to potentially permit use in the as-welded state for applications where corrosive attack is not severe. It

was however recommended that the PWHT requirement be maintained for them to pre-empt serious attack in more corrosive environments. Although not sensitized, the as-deposited welds for CF3 and CF8C (made with E308L and E347 filler metals respectively) experienced boundary dissolution, which was eliminated after the PWHT. It was concluded that the change in ferrite morphology and amount caused by the post-weld solution anneal contributed to mitigating the corrosion earlier observed. The CN3MCu welds (made with E320LR) had excellent resistance to sensitization. Results from thermodynamic and kinetic modelling suggest that adding nitrogen to CN3MCu can potentially improve its sensitization resistance to levels that would permit the CN3MCu/E320LR base metal/weld pair to be used without PWHT. The nitrogen-bearing CF3MN and its weld metal E316L showed the best resistance to intergranular corrosion without PWHT. None of their samples reactivated in the corrosion tests nor showed any boundary dissolution. Further tests are recommended for this base metal/weld metal pair to generate more comprehensive data on sensitization resistance before the PWHT requirement is completely removed.

Chapter 1: Literature Review

Stainless Steels

Stainless steels are ferrous alloys that contain the minimum chromium content required to form a protective passive layer in a particular environment. Eleven (11) wt% is the minimum amount of chromium required for corrosion resistance in an unpolluted atmosphere.[1–3] Stainless steels are very popular for the corrosion resistance they offer in various services. The chromium oxide layer which is very stable and self-healing in a lot of atmospheres, acts as an effective barrier between the metal substrate and the environment to prevent corrosion of the metal.[4–6] Stainless steels are also known for their good mechanical properties, which allow them to be used in structural applications.[7,8]

Stainless steels are classified according to their microstructure at room temperature. The major classes are austenitic, ferritic, martensitic, duplex and precipitation hardened stainless steels. Austenitic and ferritic grades are mostly austenitic and ferritic at room temperature respectively. The major alloying element in ferritic grades is chromium, with type 430 (17 wt% Cr) being the most basic.[1] Ferritic stainless steels are known to possess good resistance to chloride stress corrosion cracking, pitting corrosion, and crevice corrosion but do not have impressive mechanical properties.[9,10] Some of problems with using ferritic grades are high ductile-to-brittle-transition temperatures, high temperature embrittlement, formation of sigma, chi and laves phases at elevated temperatures and low impact strength.[11–14] They are often used in applications where corrosion resistance is more critical than mechanical strength. Austenitic stainless steels on the other hand are known to have good mechanical properties, they are popular in cryogenic applications

because they have good low temperature toughness.[15,16] They also do well in applications requiring good atmospheric or elevated temperature corrosion resistance. The primary alloying elements here are Cr and Ni, with type 304 (18 wt% Cr, 8 wt% Ni) as the most basic grade.[7] The martensitic grades are designed to have a fully austenitic structure at elevated temperatures that transforms to martensite under a wide range of cooling rates, even by air cooling. The requirement to stabilize austenite at high temperatures means these steels cannot contain a lot chromium.[17] Type 410, which is the most traditional martensitic stainless steel, has 12 wt% chromium. The main alloying elements here are carbon and chromium. The low chromium level means corrosion is not stellar in this grade, but they do have high hardness values because of their relatively high carbon content. Type 410 has 0.15 wt% carbon. The martensitic grades are used in applications that require high hardness and corrosion resistance in ambient atmospheric conditions. The duplex grades are designed to contain about 50% austenite and 50% ferrite. They combine the strength and toughness of the austenite phase and the superior corrosion resistance of the ferrite phase. They offer good strength to weight ratios.[18,19] This combination of desirable properties makes them popular in industries where structural components are exposed to aggressive service fluids like in the oil and gas industry. Type 2205 is a popular duplex stainless steel, which has a nominal composition of 22wt% chromium, 5-6wt% nickel, 3wt% molybdenum and 0.2wt% nitrogen. Nitrogen is an important austenite-stabilizing addition to these steels that helps achieve the required phase balance. Precipitation-hardened stainless steels are able to deliver exceptional tensile strength and toughness values, with corrosion resistance comparable to some austenitic grades. Most of their strength is from precipitates that form upon heat treatment.[20,21] They can be further subclassified as

martensitic, austenitic or semiaustenitic according to their predominant microstructures at room temperature. A popular member of this family of stainless steels is 17-4PH. They are used in select applications, like nuclear submarine launch tubes or space shuttle engines, where high strength steels do not provide enough corrosion resistance.

The most commonly used stainless steel naming system was designed by the American Iron and Steel Institute (AISI). It has 3-digit designations for wrought stainless steel grades that are very popular with industry. Under this naming system, austenitic stainless steels are assigned to the 200 and 300 series, while ferritic and martensitic are assigned to the 400 series. Some of the commonly used austenitic grades are 201, 304 and 316. Type 304 is the most basic of the 300 series with a nominal 18-8 composition (18wt% Cr and 8wt% Ni). Adding 2-3 wt% of molybdenum to 304 gives type 316, which has a higher resistance to corrosion in harsh chemical environments. The low carbon version of these grades, 304L and 316L, are popular for welded applications because they minimize the precipitation of chromium carbides in the heat affected zone (HAZ) and reduce the risk of intergranular corrosion. The most popular AISI designated ferritic and martensitic grades are 430 and 410 respectively. Duplex and precipitation-hardened stainless steels are known by trade names or their Unified Numbering System (UNS) designation except AISI type 329. An example of this is the precipitation-hardened stainless steel type 630 which is very commonly referred to by its tradename 17-4 PH. It is worth mentioning here that there seems to some ambiguity about the proper use of the term “duplex” when referring to stainless steel grades. There are texts that refer to some austenitic grades as duplex because they have some ferrite (about 10-20 vol %) in their austenitic structure at room temperature. While this is technically correct, it should be noted that the duplex grades mentioned in

standards refer to stainless steel grades that have been designed to have approximately 50% austenite and 50% ferrite at room temperature. Austenitic grades are not designed this way, but they are processed to retain a little ferrite to improve weldability. Figure 1-1 shows the various grades of stainless steels with their major alloying elements and properties.

The American Society for Testing and Materials (ASTM) adopts designations originated by the Alloy Casting Institute (ACI) for cast stainless steels in some of its specifications like ASTM A743, A744 and A351. Table 1 shows the ACI designations and composition ranges for heat-resistant and corrosion-resistant cast stainless steels. The names of corrosion-resistant alloys begin with "C" in the table. The third column in the table shows wrought equivalents of the cast alloys but it should be noted that the chemical compositions of the wrought and cast equivalents are not necessarily the same. Some alloying elements can have significant influence on workability or castability, and so different amounts of such elements may be specified to enhance mill processes.[22] Among the different cast stainless steel families, the CF grades are some of the most commonly used. They have a nominal composition of 19-9 (19wt% Cr and 9wt% Ni) and are austenitic, with about 10-20 vol% ferrite.[23] The CF8 and CF8M grades are the cast equivalents of 304 and 316 respectively. Their low carbon versions, CF3 and CF3M, are also equivalent to 304L and 316L respectively. Examples of other cast stainless steels are CN7M (20Cr, 29Ni) from the fully austenitic CN series, CA-6NM (13Cr, 4Ni) from the martensitic CA series and CD-4MCu (26Cr, 5Ni) from the duplex CD series.[23]

Cast stainless steels are used for complex-shaped parts that need to be corrosion resistant, like valve and pump casings, flanges, pipe fittings and other pressure containing parts.

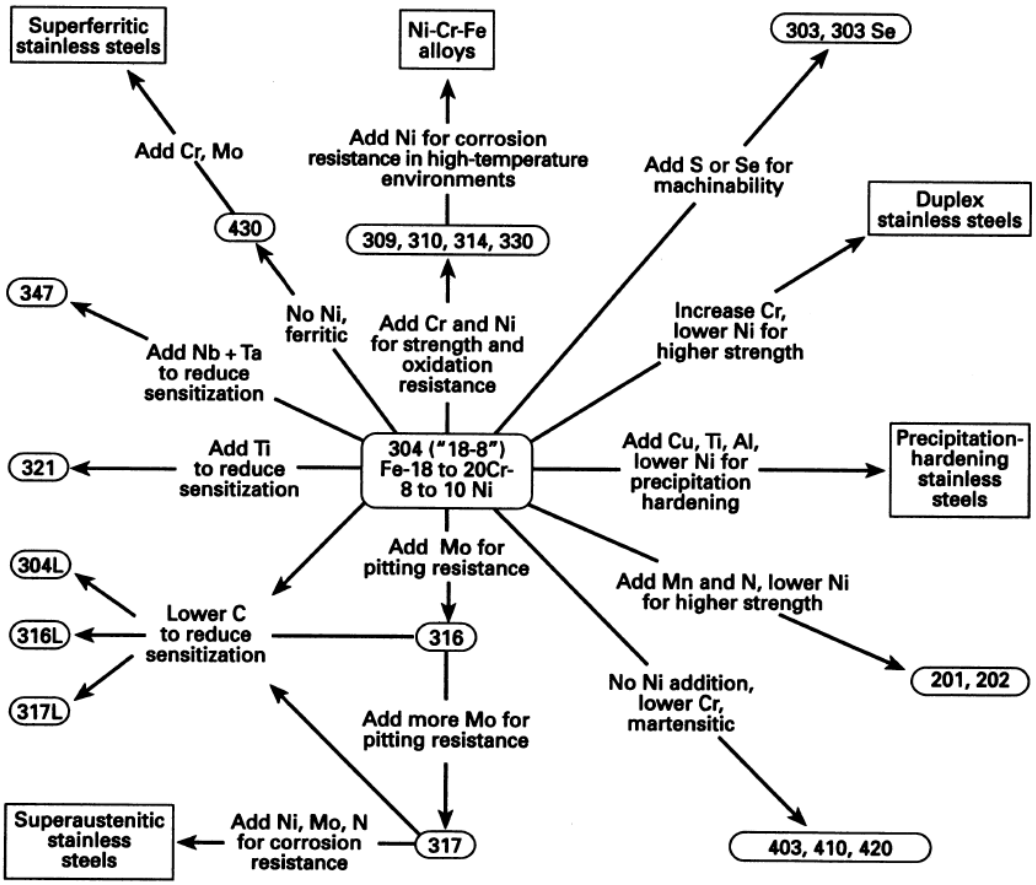

Figure 1- 1:Various grades of stainless steels showing alloying additions and properties. [1]

Table 1- 1: ASTM alloy designations and chemical composition ranges for heat-resistant and corrosion-resistant castings. [22]

Table C-1 ACI Alloy Designations and Chemical Composition Ranges for Heat- and Corrosion-Resistant Castings

Cast alloy designation	UNS No.	Wrought alloy type (see Note A)	Composition(a)—percent (balance Fe) C	Mn	Si	P	S	Cr	Ni	Other elements
CA-15	J91150	410[W]	0.15	1.00	1.50	0.04	0.04	11.5-14	1	Mo 0.5(b)
CA-15M	J91151	...	0.15	1.00	0.65	0.04	0.04	11.50-14.0	1.00	Mo 0.15-1.00
CA-40	J91153	420[W]	0.20-0.40	1.00	1.50	0.04	0.04	11.5-14	1	Mo 0.5(b)
CA-6NM	J91540	F6NM[Z]	0.06	1.00	1.00	0.04	0.03	11.5-14.0	3.5-4.5	Mo 0.4-1.0
CA-6N	J91650	...	0.06	0.50	1.00	0.02	0.02	10.5-12.0	6.0-8.0	
CB-30	J91803	431[W]	0.30	1.00	1.50	0.04	0.04	18-21	2	...
CB-7Cu-1	J92180	17-4[Y]	0.07	0.70	1.00	0.035	0.03	14.0-15.5	4.5-5.5	Cb 0.15-0.35, N 0.05, Cu 2.5-3.2
CB-7Cu-2	J92110	15-5[Y]	0.07	0.70	1.00	0.035	0.03	14.0-15.5	4.5-5.5	Cb 0.15-0.35, N 0.05, Cu 2.5-3.2
CC-50	J92615	446[W]	0.50	1.00	1.50	0.04	0.04	26-30	4 max	...
CE-30	J93423	...	0.30	1.50	2.00	0.04	0.04	26-30	8-11	...
CF-3	J92500	304L[W]	0.03	1.50	2.00	0.04	0.04	17-21	8-21	...
CF-8	J92600	304[W]	0.08	1.50	2.00	0.04	0.04	18-21	8-11	...
CF-20	J92602	302[W]	0.20	1.50	2.00	0.04	0.04	18-21	8-11	...
CF-3M	J92800	316L[W]	0.03	1.50	1.50	0.04	0.04	17-21	9-13	Mo 2.0-3.0
CF-8M	J92900	D319(316)[W]	0.08	1.50	2.00	0.04	0.04	18-21	9-12	Mo 2.0-3.0
CF-8C	J92710	347[W]	0.08	1.50	2.00	0.04	0.04	18-21	9-12	Cb 8 × C min, 1.0 max
CF-16F	J92701	303[W]	0.16	1.50	2.00	0.17	0.04	18-21	9-12	Mo 1.5, Se 0.20-0.35
CG-12	J93001	...	0.12	1.50	2.00	0.04	0.04	20-23	10-13	...
CG-8M	J93000	317[W]	0.08	1.50	1.50	0.04	0.04	18-21	9-13	Mo 3.0-4.0
CH-20	J93402	309[W]	0.20	1.50	2.00	0.04	0.04	22-26	12-15	...
CK-20	J94202	310[W]	0.20	2.00	2.00	0.04	0.04	23-27	19-22	...
CN-7M	N08007	...	0.07	1.50	1.50	0.04	0.04	19-22	27.5-30.5	Mo 2.0-3.0, Cu 3.0-4.0
CN-7MS	J94650	...	0.07	1.00	2.50-3.50	0.04	0.03	18-20	22-25	Mo 2.0-3.0, Cu 1.5-2.0
CY-40	N06040	...	0.40	1.50	3.00	0.03	0.03	14-17	Bal	Fe 11.0
CZ-100	N02100	...	1.00	1.50	2.00	0.03	0.03	...	Bal	Fe 3.0, Cu 1.25
HA		...	0.20	0.35-0.65	1.00	0.04	0.04	8-10	...	Mo 0.90-1.20
HC		446[W]	0.50	1.00	2.00	0.04	0.04	26-30	4 max	Mo 0.5(b)
HD		327[W]	0.50	1.50	2.00	0.04	0.04	26-30	4-7	Mo 0.5(b)
HE		...	0.20-0.50	2.00	2.00	0.04	0.04	26-30	8-11	Mo 0.5(b)
HF		302B[W]	0.20-0.40	2.00	2.00	0.04	0.04	18-23	8-12	Mo 0.5(b)
HH		309[W]	0.20-0.50	2.00	2.00	0.04	0.04	24-28	11-14	Mo 0.5(b) N 0.2
HI		...	0.20-0.50	2.00	2.00	0.04	0.04	26-30	14-18	Mo 0.5(b)
HK		310[W]	0.20-0.60	2.00	2.00	0.04	0.04	24-28	18-22	Mo 0.5(b)
HL		...	0.20-0.60	2.00	2.00	0.04	0.04	28-32	18-22	Mo 0.5(b)
HN		...	0.20-0.50	2.00	2.00	0.04	0.04	19-23	23-27	Mo 0.5(b)
HP		...	0.35-0.75	2.00	2.50	0.04	0.04	24-28	33-37	Mo 0.5(b)
HP-50WZ		...	0.45-0.55	2.00	2.00	0.04	0.04	24-28	33-37	W 4.0-6.0, Zr 0.2-1.0
HT		330[W]	0.35-0.75	2.00	2.50	0.04	0.04	15-19	33-37	Mo 0.5(b)
HU		...	0.35-0.75	2.00	2.50	0.04	0.04	17-21	37-41	Mo 0.5(b)
HW		...	0.35-0.75	2.00	2.50	0.04	0.04	10-14	58-62	Mo 0.5(b)
HX		...	0.35-0.75	2.00	2.50	0.04	0.04	15-19	64-68	Mo 0.5(b)
CA28MWV	J91422	422[W]	0.20-0.28	0.50-1.00	1.00	0.030	0.030	11.0-12.5	0.50-1.00	Mo 0.90-1.25, W 0.90-1.25, V 0.20-0.30
CD4MCU & 1A	J93370	255[Y]	0.04	1.00	1.00	0.040	0.040	24.5-26.5	4.75-6.00	Mo 1.75-2.25, Cu 2.75-3.25
CE8MN & 2A	J93345	...	0.08	1.00	1.50	0.040	0.040	22.5-25.5	8.00-11.00	Mo 3.00-4.50, N 0.10-0.30
CD6MN 3A	J93371	...	0.06	1.00	1.00	0.040	0.040	24.0-27.0	4.00-6.00	Mo 1.75-2.50, N 0.15-0.25
CD3MN 4A	J92205	2205[Y]	0.03	1.50	1.00	0.04	0.020	21.0-23.5	4.5-6.5	Mo 2.5-3.5, Cu 1.00 max, N 0.10-0.30
CE3MN 5A	J93404	...	0.03	1.50	1.00	0.04	0.04	24.0-26.0	6.0-8.0	Mo 4.0-5.0, N 0.10-0.30
CF10SMnN	J92972	Nitronic 60[X1]	0.10	7.00-9.00	3.50-4.50	0.060	0.030	16.0-18.0	8.0-9.0	N 0.08-0.18
CQ6MMN	J93790	Nitronic 50[X1]	0.06	4.00-6.00	1.00	0.04	0.03	20.5-23.5	11.5-13.5	Mo 1.50-3.00, Cb 0.10-0.30, V 0.10-0.30, N 0.20-0.40
CK3MCuN	J93254	254SMO[XZ]	0.025	1.20	1.00	0.045	0.010	19.5-20.5	17.5-19.5	Mo 6.0-7.0, Cu 0.5-1.00, N 0.180-0.24
CN3MN	...	AL6XN[X3]	0.03	2.00	1.00	0.040	0.010	20.0-22.0	23.5-25.5	Mo 6.0-7.0, Cu 0.75 max, N 0.18-0.26
CWZM	N26455	CA[Y]	0.02	1.00	0.80	0.03	0.03	15.0-17.5	Bal	Mo 15.0-17.5, Fe 2.0 max, Cb 1.0 max
CW6M	N30107	...	0.07	1.00	1.00	0.040	0.030	17.0-20.0	Bal	Mo 17.0-20.0, Fe 3.0 max
CW6MC	N26625	625[Y]	0.06	1.00	1.00	0.015	0.015	20.0-23.0	Bal	Mo 8.0-10.0, Fe 5.0 max, Cb 3.15-4.50
CW12MW	N30002	C[Y]	0.12	1.00	1.00	0.040	0.030	15.5-17.5	Bal	Mo 16.0-18.0, Fe 4.5-7.5, W 3.75-5.25, V 0.20-0.40
CX2MW	N26022	C22[Y]	0.02	1.00	0.80	0.025	0.025	20.0-22.5	Bal	Mo 12.5-14.5, Fe 2.0-6.0, W 2.5-3.5, V 0.35 max
CY5SnBiM	N26055	...	0.05	1.50	0.5	0.03	0.03	11.0-14.0	Bal	Mo 2.0-3.5, Fe 2.0 max, Bi 3.0-5.0, Sn 3.0-5.0
M255	N24025	...	0.25	1.50	3.5-4.5	0.03	0.03	...	Bal	Cu 27.0-33.0, Fe 3.50 max

(continued)

Table 1-1 (contd): ASTM alloy designations and chemical composition ranges for heat-resistant and corrosion-resistant castings[22]

Table C-1 ACI Alloy Designations and Chemical Composition Ranges for Heat- and Corrosion-Resistant Castings (continued)

Cast alloy designation	UNS No.	Wrought alloy type (see Note A)	Composition(a)—percent (balance Fe)							
			C	Mn	Si	P	S	Cr	Ni	Other elements
M30C	N24130	...	0.30	1.50	1.0-2.0	0.03	0.03	...	Bal	Cu 26.0-33.0, Fe 3.50 max, Cb 1.0-3.0
M30H	N24030	...	0.30	1.50	2.7-3.7	0.03	0.03	...	Bal	Cu 27.0-33.0, Fe 3.50 max
M35-1	N24135	400[Y]	0.35	1.50	1.25	0.03	0.03	...	Bal	Cu 26.0-33.0, Fe 3.50 max, Cb 0.5 max
M35-2	N04020	400[Y]	0.35	1.50	2.00	0.03	0.03	...	Bal	Cu 26.0-33.0, Fe 3.50 max, Cb 0.5 max
N-7M	N30007	B2[Y]	0.07	1.00	1.00	0.040	0.030	1.0	Bal	Mo 30.0-33.0, Fe 3.00 max
N-12MV	N30012	B[Y]	0.12	1.00	1.00	0.040	0.030	1.0	Bal	Mo 26.0-30.0, Fe 4.0-6.0, V 0.20-0.60
D3MWCuN & 6A	J93380		0.03	1.00	1.00	0.030	0.025	24.0-26.0	6.5-8.5	Mo 3.0-4.0, Cu 0.5-1.0, W 0.5-1.0, N 0.20-0.30
CU5MCuC	...	825[Y]	0.05	1.00	1.00	0.030	0.030	19.5-23.5	38.0-44.0	Mo 2.5-3.5, Cu 1.50-3.50, Cb 0.60-1.20
CF3MN	J92804	316LN	0.03	1.50	1.50	0.040	0.040	17.0-22.0	9.0-13.0	Mo 2.0-3.0, N 0.10-0.20

(a) Maximum, unless Range is given. (b) Molybdenum not intentionally added. Designations with the initial letter "C" indicate alloys generally used to resist corrosive attack at temperatures less than 1200 °F. Designations with the initial letter "H" indicate alloys generally used under conditions where the metal temperature is in excess of 1200 °F. The second letter represents the nominal chromium-nickel type; the nickel content increasing in amount from "A" to "Z." For example, "F" stands for the 19% Cr-9% Ni, "K" for the 25% Cr-20% Ni, and "W" for the 12% Cr-60% Ni alloy types. Numerals following the letters indicate the *maximum* carbon content of the corrosion-resistant alloys; carbon content may also be designated in the heat-resistant grades by following the letters with a numeral to indicate the *midpoint* of a ±0.05% carbon range. If special elements are included in the composition they are indicated by the addition of a letter to the symbol. Thus, "CF-8M" is an alloy for corrosion-resistant service, of the molybdenum-containing 19% Cr-9% Ni type with a maximum carbon content of 0.08%. Note A: Wrought alloy type numbers are listed only for the convenience of those who want to determine corresponding wrought and cast grades. Because the cast alloy chemical composition ranges *are not the same* as the wrought composition ranges, buyers should use cast alloy designations for proper identification of castings. Note B: Most of the standard grades listed are covered for general applications by American Society for Testing and Materials specifications A 743, A 890, and A 297. ASTM specifications A 217, A 351, A 447, A 451, A 452, A 744, and A 757 also apply to some of the grades. Note C: For additional alloy designations consult the current SFSA Handbook Supplement on specifications. W: Common description, formerly used by AISI. X: Proprietary trademark, (1) Armco Inc. (2) Avesta Sheffield AB. (3) Allegheny Ludlum Corp. Y: Common name used by two or more producers; not a trademark. Z: ASTM designation

Sensitization

Sensitization is a condition in welded stainless steels or stainless steels subjected to elevated temperatures where chromium carbides precipitate along grain boundaries and cause the regions next to the carbides/grain boundaries to be depleted in chromium.[24–26] If the chromium in the depleted zone falls below the minimum required to form a stable protective passive layer, that region becomes susceptible to corrosive attack. The sensitized material then suffers intergranular corrosion (IGC) when exposed to corrosive media. For intergranular corrosion to occur, there must be some interaction between a corrosive medium and the chromium-depleted area that leads to degradation. For example, in the heating and cooling of a very thick steel plate section, sensitization could happen at the

center of the plate where cooling is very slow, but apart from exposed plate edges, intergranular corrosion may not be observed in such a part since the sensitized area at the center of the plate is shielded from the environment.[27] Another possible phenomenon is that, precipitation of chromium carbides may not result in detrimental chromium depletion. The decreased chromium content may not always fall below the minimum required for passivation. There would be no risk of intergranular corrosion in such a situation.[27] This is why identification of chromium carbide through metallographic examination alone may not be enough to conclude that sensitization has occurred.

In austenitic stainless steels, chromium carbides are known to precipitate in the 500ºC-900ºC temperature range.[28–30] Sensitization happens when there is the right combination of composition and thermal cycle to promote chromium carbide precipitation. This can happen in the part of a weld heat affected zone where the peak temperature falls within the chromium carbide precipitation temperature range. It can also happen in stainless steels that have been exposed to temperatures within the precipitation temperature range either in service or through a heat treatment.

The amount of carbon in solution has significant influence on the kinetics of the carbide formation. Therefore, one of the ways to prevent sensitization is to reduce the amount of carbon in solution. Low carbon stainless steel grades like 304L, 316L, CF3 and CF3M contain a maximum carbon concentration of 0.03 wt%, which has been proven to slow down the precipitation kinetics enough to prevent chromium-rich carbides from forming within the timescales seen in welding.[31,32] Another way to prevent sensitization is to tie the carbon up with niobium or titanium before it can be precipitated as chromium carbide. Titanium and niobium carbides form in the temperature range 870ºC-1150ºC while

chromium carbide forms in the 500ºC-900ºC temperature range. Thus given a high enough temperature, titanium and niobium carbides will form preferentially to chromium carbides, preventing the problem of chromium been drawn out of the matrix.[1,28–30] Stainless steels designed to avoided sensitization by precipitating titanium or niobium carbides are called stabilized grades. Examples of such grades are AISI 321, which is alloyed with titanium, and AISI 347, which is alloyed with niobium and tantalum. Stabilized grades are known to be susceptible to another form of intergranular corrosion known as Knife-line attack.[33,34] This happens in the part of the HAZ closest to the fusion line where peak temperature is high enough to dissolve the niobium or titanium carbides and prevent their re-precipitation due to the rapid cooling conditions.

If the steel has already been sensitized, a solution treatment at temperatures high enough to dissolve the carbides and eliminate the chromium depletion, followed by quenching or rapid cooling, is usually enough to restore the corrosion resistance of the steel. The solution anneal temperature recommended for most grades in ASTM A744 is 1040ºC.

In most texts, sensitization is defined in relation to the formation of chromium carbides. However, the phenomenon of chromium depletion that results in the destabilization of the protective layer, is not exclusive to chromium carbide formation.[35] It is possible that the formation of chromium-rich intermetallic phases, like sigma phase, could pull enough chromium out of solution to make a material vulnerable to intergranular attack.[35,36] Sedriks et al.[27] found that intergranular attack did not happen in 316L exposed to seawater except when it was heat treated within the sigma phase formation temperature range. Part of the results from this work is shown in Table 2 below. The results show which heat treatment produced intergranular attack in 316, 316L and 317 after exposure to seawater.

This suggests that sigma phase can lead to chromium depletion in the surrounding matrix. Tests that characterize susceptibility to intergranular corrosion in stainless steels based on the instability of the oxide layer in chromium-depleted areas may not be able to show the cause of chromium depletion. Further metallographic examination would be required in such a situation to identify the cause of the chromium depletion. Therefore, if the several chromium-rich phases are present in a sample, the researcher should consider that any of them could contribute ton sensitization and intergranular corrosion.

Table 1- 2: Shows the effect of thermal history on occurrence of intergranular attack in 316, 316L and 317 in seawater. [27]

Type	Condition*	Intergranular attack†
316L	Annealed	No
	1 h, 675°C, AC	No
	4 h, 870°C, AC + 1 h, 675°C, AC	Yes‡
	As welded, matching filler	No
	Welded + 1 h, 705°C, AC	No
	Welded + 1 h, 870°C, AC	Yes‡
316	Annealed	No
	2 h, 620°C, AC	No
	1 h, 675°C, AC	No
	As welded, matching filler	No
	Welded + 1 h, 870°C, AC	Yes
317	Annealed	No
	4 h, 595°C, AC	No
	1 h, 675°C, AC	Yes
	As welded, matching filler	No
	Welded, 1 h, 705°C, AC	Yes

*AC Air cooled following indicated heat treatment.
†Attack often initiated in the creviced area of the mounting hole before spreading along grain boundaries.
‡σ may form at 870°C in Type 316L.

Factors that affect sensitization in cast stainless steels

Following the classical definition given above, most researchers focus on chromium carbide precipitation when investigating sensitization. Stansbury et al.[26] looked at the

effects of carbon content, molybdenum content and ferrite content on sensitization in cast stainless steels subject to weld repair. Their work investigated welding-induced sensitization in CF3, CF3M, CF8 and CF8M using ASTM A262 practice A, ASTM A262 practice B, Single Loop Electrochemical Potentiokinetic Reactivation (SL-EPR) test and Double Loop Electrochemical Potentiokinetic Reactivation (DL-EPR) test. The ASTM Practice A is the oxalic acid etch test, and Practice B is the ferric sulfate-sulfuric acid test. The SL-EPR test results showed that the Mo-bearing (CFM) grades containing up to 0.08wt% carbon were immune to sensitization. For Mo-free (CF) grades, only samples containing up to 0.03 wt% carbon were immune to sensitization. This showed that molybdenum helped sensitization resistance. They concluded that the presence of Mo has two different effects on sensitization; in the beginning of sensitization, Mo delays the onset of chromium carbide precipitation, but at longer sensitization times or for more severe sensitization conditions, the effect of Mo is related to its contribution to the formation of a more stable passive layer. The second effect is corroborated by the work of other researchers who found that Mo is present in the passive layer of Mo-bearing stainless steels.[37] Aside from this positive influence of Mo in reducing sensitization, they noticed that in the CF8M, the molybdenum encouraged the formation of what could be sigma phase within the ferrite pools, which then became sites for corrosive attack. In general, the Mo-bearing samples seemed to provide better protection against sensitization. Another observation they made was that, increasing ferrite content reduced susceptibility to sensitization. The researchers made samples with three different ferrite numbers; 5, 12 and 18 to represent low, intermediate, and high ferrite content respectively. The different ferrite numbers were achieved by changing the Cr/Ni ratio. They found that for CF grades with

carbon above 0.06 wt%, only the samples with high ferrite numbers resisted sensitization, while the intermediate and low ferrite CF samples were sensitized. This observation was explained as follows: in stainless steels like the CF/CFM grades that have both austenite and ferrite phases, the austenite-ferrite boundaries are the most preferred for chromium carbide precipitation, followed by austenite-austenite boundaries and then twin boundaries. Since in an austenitic stainless steel, the austenite-austenite boundary network is the most pervasive, precipitation of chromium carbides at this boundary can easily lead to a continuous network of chromium-depleted areas. If there are enough austenite-ferrite boundaries, they could serve as preferred precipitation sites instead of the austenite-austenite boundaries. Care must be taken however to avoid a continuous ferrite network. The right amount of ferrite will form just enough discontinuous austenite-ferrite boundaries to prevent a chromium carbide network. This is why they observed better sensitization resistance at high ferrite numbers. They however did not establish an upper limit for ferrite content beyond which sensitization resistance would be reduced. The practical application of this effect of ferrite is that, designers can find the critical ferrite content that creates enough ferrite-austenite boundaries but avoids a continuous ferrite network. The ferrite-austenite boundaries will attract all or most of the carbides, but since the ferrite is only in discrete pools, there would be no continuous path of chromium depletion around grains to cause grain dropping. Lastly, this study further confirmed that lower carbon content provides better resistance to sensitization. Lower carbon is known to slow the kinetics of chromium carbide formation and prevent its formation in most welding operations.[38]

McCaul et al.[39] investigated the sensitization susceptibility of CN7MS, which is a fully austenitic cast stainless steel. The CN7MS and CN7M alloys, unlike the CF grades, are

fully austenitic and contain very little to no ferrite. The ASTM A744, which is the standard for Fe-Cr-Ni stainless steels used in severe corrosive applications, requires heat treatment after weld repair without considering whether a particular grade's composition makes it resistant to sensitization or not. The requirement for heat treatment after welding only considers the extent of repair and the nature of the surface on which the repair was done. It has been argued that the call for heat treatment after welding may be overreaching and redundant especially for grades that are not susceptible to sensitization. Manufacturers may be spending money on unnecessary heat treatments with its attendant high scrapping rate due to dimensional distortion. All this could be avoided if the heat treatment requirement in ASTM A744 can be properly streamlined. Producers of fully austenitic stainless steels like CN7M and CN7MS stand to benefit a great deal, especially if it is proven that any of the fully austenitic grades does not require heat treatment after welding. This would not only benefit foundries but field construction activities too if field welding can be performed on these cast stainless steel products without the need to heat treat afterwards. This was the motivation for McCaul's[39] work on the sensitization susceptibility of CN7MS. The study used four CN7MS plates, all with maximum carbon and sulfur content at 0.03 wt% and 0.015 wt% respectively. He tested for corrosion susceptibility using ASTM A262 Practices A and B and used acceptance criteria of 1.22mm/year for the Practice B test results. ASTM A262 does not set acceptance criteria for any of its weight loss tests, however, Brown[40] conducted an extensive evaluation of Practices A, B and C and concluded that a maximum corrosion rate of 1.22mm/year in Practice B corresponded to absence of sensitization. McCaul[39] used this acceptance criteria and found that, none of the samples was sensitized after welding. It was then concluded that CN7MS could be used in the as-welded state

without any loss in corrosion resistance in the weld or heat affected zone under the following conditions: that the carbon content of the parent material should be below 0.03 wt% and that low carbon filler metal should be used and the interpass temperature must be strictly monitored. Interpass temperature and heat input were limited to 93^{o}C and 1180 Jmm^{-1} in this study.

In another study, Beck et al.[23] studied the effects of ferrite and sensitization on the intergranular corrosion behavior of cast stainless steels. They studied intergranular corrosion in solution annealed and sensitized versions of CF3, CF3M, CF8, CF8M, CF20, CF8C using ASTM A262 Practice C, which is the nitric acid test. For each alloy, ferrite number was varied between 0 and 40. Ferrite number in this study loosely translated to volume percent of ferrite phase. A fundamental finding of this study was that, lowering carbon levels in the Mo-free (CF) grades helped curb corrosion rates in the sensitized samples. This agrees well with the effects of carbon found by other researchers.[26,38,39] For the Mo-bearing (CFM) grades however, carbon seemed to have the opposite effect. Lower carbon samples rather saw bigger jumps in the corrosion rates comparing the solutionized and sensitized states. This is an unusual observation as lower carbon is traditionally known to produce lower levels of sensitization and hence lower intergranular corrosion rates. It is also contrary to the outcome of other works described above. It is worth noting that all the works reviewed so far used ASTM A262 Practices A and B while Beck used practice C. Nitric acid (used in practice C) is known to be among the most oxidizing corrodents. There are corrosive attacks on stainless steels that are unique to nitric acid service. An example is that nitric acid in known to attack sigma phase in Mo-bearing stainless steels.[41] This could be linked to the unusual effect of carbon in the cast Mo-bearing samples. Beck's[23]

study also covered wrought grades 316 and 316L in the solutionized and sensitized states. The observation in the wrought grades was as expected, where the lower carbon samples exhibited smaller jumps in corrosion rate between the solutionized and sensitized samples. The other outcome of Beck's work[23] was that increasing ferrite content helped reduce susceptibility to intergranular corrosion in all solution annealed alloys. Again, this is in good agreement with Stansbury's[26] work. However, in the sensitized alloys, increasing ferrite content only reduced sensitization in the Mo-free (CF) samples. The sensitized Mo-bearing (CFM) alloys showed increased susceptibility to intergranular corrosion with increasing ferrite content. Molybdenum is a ferrite former, and also encourages the formation of sigma phase in sensitized stainless steel.[38] Increasing ferrite content in the presence of molybdenum, and exposing such a material to a sensitization treatment will lead to profuse sigma phase formation which will then be attacked by the nitric acid used in this study. This is could explain why increased ferrite content in the sensitized Mo-bearing stainless steels did not reduce intergranular corrosion.

So far, the major factors that have been seen to influence sensitization and intergranular corrosion in cast stainless steels are carbon content, molybdenum content, ferrite content, history of thermal cycle and the environment (or more specifically, the corrodent).

Tests to Detect Susceptibility to Intergranular Corrosion in Cast Stainless Steels

Weight Loss Tests

Hot Acid/ boiling acid/ weight loss tests are very popular ways to test susceptibility to intergranular corrosion caused by sensitization. The first boiling acid tests were developed as simulated service tests, to help predict a material's response to a particular corrosive service fluid.[42] Over time, their use has changed from directly predicting service life to detecting the presence and severity of factors that cause intergranular corrosion, but they can still be designed to directly predict service life. This is one of the reasons the acid immersion tests are popular. They usually require measuring weight loss after a period of immersion in boiling acid. The weight loss is then converted to corrosion rate. The relatively simple interpretation of the test results is another reason hot acid tests are popular. To get appreciable levels of intergranular corrosion, ASTM A262 requires that hot acid tests are conducted on sensitized steel. ASTM A262 is the ASTM standard for detecting susceptibility to intergranular attack in austenitic stainless steels. All but one of the corrodents in ASTM A262 attack areas with reduced chromium levels associated with chromium carbide precipitation. The exception here is oxalic acid in practice A, which attacks the chromium carbides directly.[26] Nitric acid in practice C additionally attacks sigma phase, submicroscopic sigma phase precursors, other carbides, and sigma phase constituents.[26,38,41,43] As expected, materials may exhibit different corrosion behaviors in different corrodents, therefore, results of a hot acid test may not be directly applicable in predicting corrosion response a certain service fluid. For example, a nitric acid test may

not be suitable to predict service life in hydrochloric acid. A thorough understanding of the material's interaction with the acid is very essential in designing an effective test.

The American Society for Testing and Materials (ASTM) has a number of specifications that standardize tests to detect susceptibility to intergranular corrosion. Two of them that are discussed in this review are ASTM A262 and ASTM G108. The ASTM A262 standard was designed for austenitic stainless steels, it has five tests that help detect susceptibility to intergranular corrosion in different corrodents, which are known as practices A, B, C, E and F.[44] Practice A is an oxalic acid etch test. This test is not a standalone test, rather it is intended as a screening test for the other more lengthy tests in this specification. It can be used to accept a sample but not reject one. Its purpose is to identify samples that will pass the other longer and more expensive tests, and so save the researcher time and resources. The test is done at room temperature and involves electrolytically etching a sample in 10% oxalic acid for 1.5 minutes at $1A/cm^2$. The severe etching conditions over-etch the surface so that interpreting the etch structure is simple enough even for non-technical people. This gives qualitative results that are solely based on the appearance of the etch structure. The etch structure is classified as "step" for non-susceptible alloys, "ditch" for susceptible alloys and "dual" for alloys that lie in between. The oxalic acid dissolves material at grain boundaries with profuse chromium carbide precipitation. This creates "ditches" or "grooves" around grains in sensitized materials. If one or more grains are completed surrounded by ditches, the structure is classified as ditch structure. In materials that have not been sensitized, the oxalic acid wears down adjacent phases and grains at different rates and creates the "step" structure. The "dual" structure is assigned to materials that show a mix of step and ditch structures, but there is no one grain is completely surrounded by a

ditch. Figures 1-2, 1-3 and 1-4 show examples of the step, ditch, and dual structures respectively. Samples that show ditch and dual structures need to be examined with the other more comprehensive tests to establish the severity of the sensitization. The other tests; practices B, C, E and F are the more comprehensive tests. With the exception of method E, they all measure weight loss as a measure of susceptibility to intergranular corrosion. Method E, which gives qualitative results, uses a bend test at the end of the immersion period to evaluate susceptibility to intergranular corrosion. The sample is embedded in copper shots or grindings in a boiling solution of copper sulfate and 16% sulfuric acid for 15 hours. Acceptance or rejection is based on the appearance of fissures that traverse the corroded grain boundaries after the bend test. The tests in ASTM A262 detect susceptibility caused by one or more of the following: chromium carbide precipitation, sigma phase formation and end grain exposure.[41,42] Since end grain corrosion is not a major concern in cast products, the tests for this study need not have the ability to detect that. The alloys being investigated require that the tests be able to detect intergranular corrosion from chromium carbide and sigma phase. Practices B, C, E, F are all able to detect corrosion from chromium carbide but only Practices B and C can additionally detect corrosion related to sigma phase formation.[44] ASTM A262 also states that Practices B and C are able to detect intergranular corrosion due to the formation of sigma phase constituents in stabilized wrought grades 321 and 347.[44] Even though CF8C, which is the cast equivalent of 347, is not explicitly mentioned in ASTM A262, it appears that it can also be investigated with Practices B and C. Practice B basically involves 120-hour exposure of the sample in a boiling ferric sulfate – 50% sulfuric acid solution, followed by weight loss determination. The ferric sulfate is a specific additive that

establishes and controls the corrosion potential. It is a corrosion inhibitor that causes passivation in stainless steels in the presence of sulfuric acid.[42] It was first derived during a study of the acid corrosion of stainless steels and its inhibition by ferric sulfate.[41] It was found that even though ferric salts effectively inhibited corrosion of stainless steels, they could not prevent intergranular attack in sensitized material. This makes it excellent for studying intergranular corrosion in stainless steels since this form of attack stands out in this corrodent. Research has shown that the intergranular corrosion happens even though the grain faces and grain boundaries of stainless steels in a ferric sulfate- sulfuric acid solution are actually at the same potential, i.e the grain boundaries are not active relative to the grains.[42] Robert Baboian[42] explains that in the passive state, the protective film is in a dynamic process of dissolution and repair to maintain the film. The protective film dissolves in the acid and is repaired by dissolving metal. In sensitized steel, the corrosion current or dissolution of the chromium-depleted area surrounding chromium carbides on grain boundaries is much more aggressive. A lot of the chromium-depleted material needs to dissolve to keep up with the repair of the passive film. This is what causes the grain boundary attack of sensitized stainless steels in the ferric sulfate-sulfuric acid solution.[42] The corrosion rate in practice B is controlled by the reduction of the ferric ions to ferrous ions. The copper sulfate in the sulfuric acid solution in practices E and F play the same role as the ferric sulfate in practice B. Practice C is a 240-hour exposure in 65% nitric acid, followed by weight loss determination. In this corrodent also, Baboian[42] asserts the grain faces and grain boundaries of stainless steels in nitric acid are at the same potential. Nitric acid is known to be very oxidizing and attacks stainless steels in ways not seen in other acidic corrodents. Nitric acid is known to attack directly sigma phase and precursors of

sigma phase in stainless steels, even in the absence of chromium carbides.[41] It also dissolves other carbides like titanium carbides in stabilized grades, creating pits that exacerbate corrosion rates. Hexavalent chromium, which is a corrosion product in nitric acid, is known to increase corrosion rate.[41] This is why ASTM A262 recommends that the nitric acid solution be changed every 48 hours when doing the nitric acid test (practice C). The dissolution of titanium carbides and other inclusions, and subsequent rise in the concentration of hexavalent chromium in the resultant pits, makes materials prone to end grain attack in nitric acid.[41,43] Cross sections of these elongated inclusions and carbides are exposed to the nitric acid at cross sections of hot worked products. Due to the severely oxidizing nature of practice C, the nitric acid test, ASTM A262 advises that it be used when the material being tested is intended for a nitric acid service. Table 3 shows a summary of all the tests in ASTM A262, Practice D has been withdrawn.

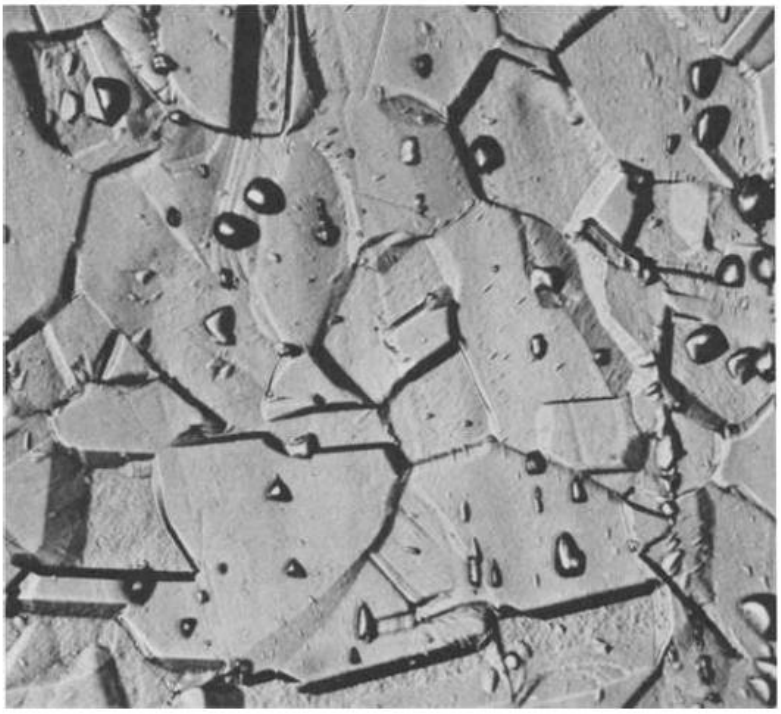

Figure 1- 2: Step structure in ASTM A262 Practice A, oxalic acid etch test. 500x [41]

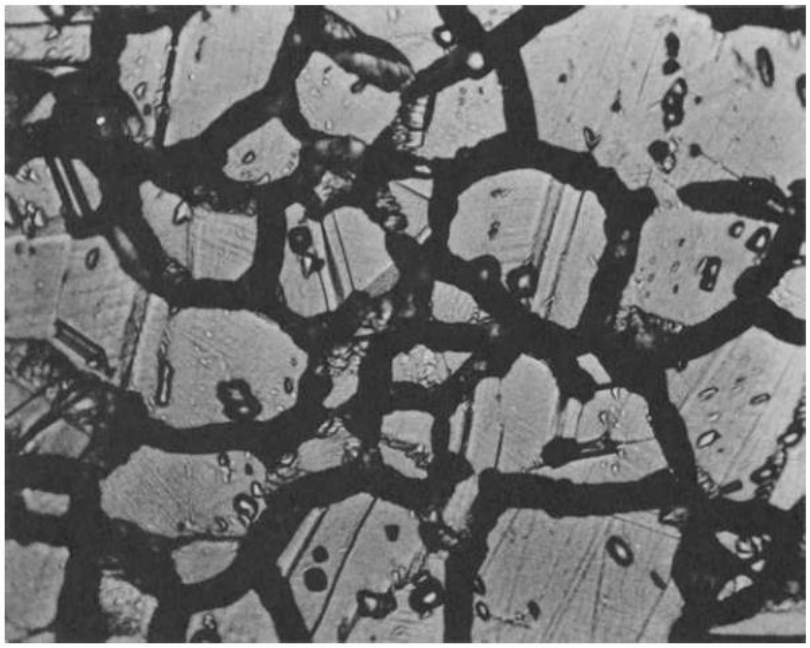

Figure 1- 3: Ditch structure in ASTM A262 Practice A, oxalic etch test. 500x [41]

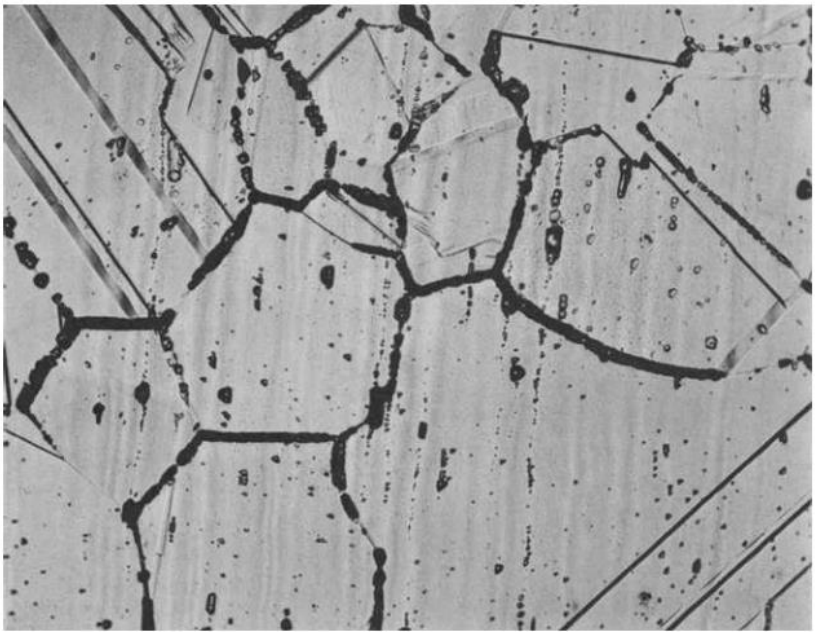

Figure 1- 4: Dual structure in ASTM A262 Practice A, oxalic etch test. 250x [41]

Table 1- 3: Summary of tests methods in ASTM A262. Practice D has been withdrawn. [42]

Designation	Test	Temperature	Testing Time	Applicability	Evaluation Method
Practice A	Oxalic Acid Etch Screening Test	ambient	1.5 min	Chromium carbide sensitization only	Microscopic Examination; Classification of etch structure
B	Ferric Sulfate-50% Sulfuric Acid	boiling	120 h	Chromium carbide	Weight-loss/corrosion rate
C	65% Nitric Acid	boiling	240 h	Chromium carbide and sigma phase	Weight-loss/corrosion rate
D	10% Nitric-3% Hydrofluoric Acids (This test is being removed from A 262)	70°C	4 h	Chromium carbide in 316, 316L, 317, 317L	Ratio of corrosion; Rates of "unknown" over that of a solution annealed specimen
E	6% Copper Sulfate 16% Sulfuric Acid with metallic copper	boiling	24 h	Chromium carbide	Examination for fissures after bending
F	Copper Sulfate 50% Sulfuric Acid with metallic copper	boiling	120 h	Chromium carbide in cast 316 and 316L	Weight-loss/corrosion rate

Electrochemical Potentiokinetic Reactivation (EPR) Tests

The EPR test was designed as a fast, quantitative, and non-destructive method for detecting the presence and /or extent of sensitization.[42] It produces results in about 15 minutes compared to the 15 hours – 240 hours required for the immersion tests. It uses an electrochemical cell to polarize the sample through the active region and record the highest corrosion current as a measure of sensitization.[45] There are two versions of this test currently in use; the single loop EPR (SL-EPR) and the double loop EPR (DL-EPR). The single loop test has been standardized in ASTM G108 for 304 and 304L alloys. For the single loop test, the sample must be prepared to a 1μm diamond polish, and tested in a solution of 0.5M sulfuric acid and 0.01M potassium thiocyanide at 30°C +/-1°C.[46] The potassium thiocyanide is added as an activator to increase the corrosion currents. The test involves first identifying the corrosion potential, E_{corr} of the sample in the prescribed solution, which has been found to be approximately -400mV vs saturated calomel electrode (SCE) for type 304 stainless steel. Then the sample is held at a potential of +200mV vs

SCE (in the passive region) for about two minutes to form the passive layer. After this, the potential is reduced back to the corrosion potential at a scan rate of 6V/hour. The reduction reactivates the sample, causes a preferential break down of the protective film at grain boundaries that have chromium carbides and produces a big jump in the corrosion current. The single loop test involves only one scan from the passive region towards the corrosion potential as shown in Figure 1-5 below. Figure 1-5 is a plot of potential at the anode vs log of the corrosion current at the anode. The area under the loop generated is proportional to the total charge, Q passed in coulombs. A sensitized sample will produce a bigger loop and Q value because it will record a higher corrosion current. The bigger the area under the loop, the more sensitized the material is. The total charge, Q is then normalized with the area from which the charge originated, which is assumed to be the grain boundaries. The formula to normalize the charge is shown below[46]

$P_a = Q/X$, where;
P_a = normalized charge
Q = total charge which is equal to area under the loop
X = total grain boundary area = $A_s [5.1 \times 10^{-3} e^{0.35G}]$
A_s = specimen area (cm2)
G = grain size at 100x (in accordance with Test Methods ASTM E112)

The assumptions made in this test and calculation are as follows:[46]

a) The corrosive attack is restricted to only grain boundaries
b) The attack is distributed uniformly over the grain boundaries
c) The width of each attacked grain boundary is $2 \times (5 \times 10^{-5})$ cm

Since the charge is assumed to be coming from only the grain boundaries, the normalization is done with only the grain boundary area. This may not actually be the case in a sample that has a lot of pitting or inclusions on the surface. Nonmetallic inclusions, pits and even uniform corrosion can contribute to the corrosion current, so it might be necessary to examine the sample under a microscope to confirm the type of corrosion that was responsible for the measured charge. The single loop test is known to be sensitive to sample surface finish[45], which is why a 1μm diamond polish finish is required, but this requirement makes it difficult to apply this procedure as a field test.

The double loop test was developed to work with a less stringent surface finish. It has been asserted that the double loop test can work with a 100 grit SiC paper finish.[45] It uses the same set up and test solution as the single loop test with slight modifications to the process. The double loop test involves two scans; the first scan starts at the corrosion potential (-400mV vs SCE for type 304 stainless steel) and proceeds in the anodic direction into the passive region (+200mV vs SCE). As soon as the potential in the passive region is reached, the scan direction is reversed and the potential reduced back to the corrosion potential.[45,47] Both scans are done at a rate of 6V/hour. Figure 1-6 below is a plot of the potential at the anode vs log of the corrosion current at the anode, it shows a schematic diagram of the double loop forward and reverse scans. Because the first scan begins in the active region without the passive layer and proceeds in the anodic direction, it generates a big loop due to the high corrosion current. The maximum current for this scan direction is denoted I_a. The reverse (reactivation) scan generally produces a lower current and loop because of the passive layer that formed when the sample reached the passivation potential. The size of the second loop depends on the presence and severity of sensitization. Severely sensitized

steel will generate a large loop while a non-sensitized steel will generate a smaller loop, with a maximum current I_r. The degree of sensitization is evaluated with the ratio I_r/I_a. A bigger ratio signifies more sensitization. Normalization by the total grain boundary area is not required for this test. The advantages of the double loop over the single loop method are that, it is independent of surface finish, results are not affected by pits, it is more reproducible than the single loop and it is less sensitive to changes in scan rate and solution composition.[42]

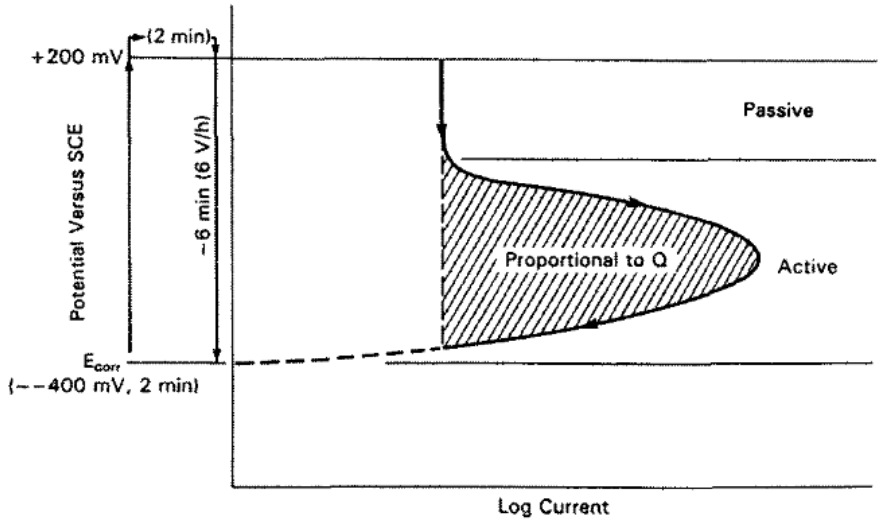

Figure 1- 5: Schematic diagram of single loop EPR reactivation scan.

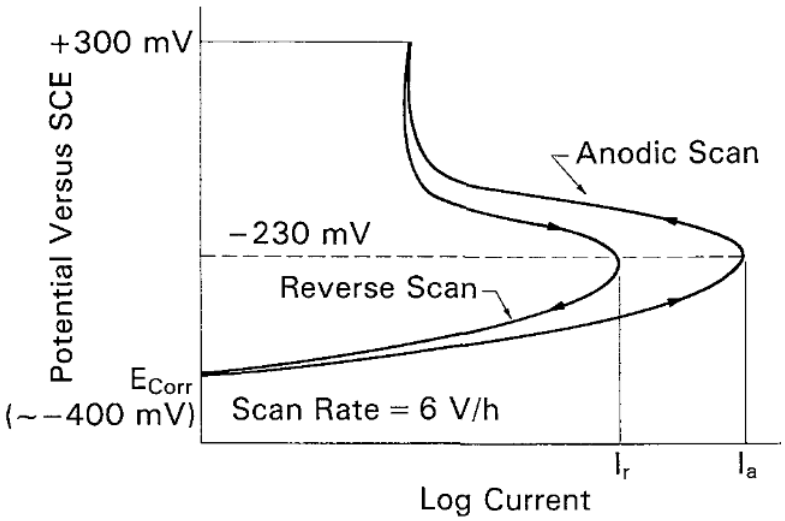

Figure 1- 6: Schematic diagram of doble loop EPR forward and reverse scans.

Comparing results from EPR tests and immersion tests

In deciding which test to use in sensitization studies, it is important to know how results from the different tests compare with each other, especially for the material being tested and the test conditions to be used. This helps to ensure consistency and reproducibility of results. Studies by Lackner et al.[48] and Majidi et al.[45] comparing the ferric sulfate-sulfuric acid test, oxalic etch test and the EPR test show good agreements among the results produced by these tests as seen in Figure1- 7. Both investigations concluded that the boiling acid tests and the EPR tests produce identical results when there is enough corrosion in the acid test to cause grain dropping. The boiling acid tests detect susceptibility to intergranular corrosion by weight loss caused by grain dropping. Even though intergranular attack is the more dominant form of corrosion in sensitized steel, dissolution of the grain boundaries alone does not lead to discernible weight loss. Material dissolved at the grain boundaries is so little that it does not result in appreciable weight loss. Grains need to fall out for the

test to produce quality data in terms of weight reduction. For the grains to fall out, there needs to be enough corrosion of the grain face in addition to the intergranular corrosion.[42] This could be a source of discrepancy when comparing results for the same sample from the weight loss test and EPR test conducted on cast products. Due to the large grain sizes of cast products, it may take considerably more wear and time for grains to be completely surrounded and for them to drop. So even though a cast stainless steel may be severely sensitized, it may not drop as many grains as a wrought product.

Majidi et al.[45] and Stansbury et al.[26] found that both the single loop and double loop were very sensitive in detecting little or mild levels of sensitization but the boiling acid test does not show much sensitivity in that range because grain dropping is not profound under such conditions. However, at medium and severe levels of sensitization, the boiling acid test shows more sensitivity than the EPR test, which levels off at high sensitization levels. Figure 1-8 from Majidi's[45] work shows results from the oxalic acid etch test, the ferric sulfate – sulfuric acid test and the double loop EPR test conducted on the same sample. It is observed that there is good agreement among the results of all three tests. The ditch structure in the oxalic acid test, which signifies severe sensitization, corresponds to the highest corrosion rates from the other tests. The samples that showed step and dual structures in the oxalic acid test were only mildly sensitized, and they rightly corresponded to low corrosion rates in the other tests. But it is noticed that the double loop EPR test does a better job distinguishing these samples than the boiling acid test, hence the conclusion that the double loop EPR test is very sensitive to low and mild levels of sensitization. As corrosion rates increase into the regime of ditch structure samples, the double loop test measurements of corrosion rate level off and does not distinguish very well among samples

in this band. The ferric sulfate – sulfuric acid test rather does a better job in this range. The oxalic acid test is seen here to be a good indicator of the sensitization state of a sample, but since it is qualitative, the other tests are needed to predict the corrosion rate. Figure 1-9, also from Majidi's[45] work, shows results from the oxalic acid test and the ferric sulfate – sulfuric acid test compared with the single loop EPR test. The major difference between the results in Figure 1-8 and 1-9 is that, there is an overlap between the step and dual structure samples. Another overlap is seen between the dual and ditch structure samples. The researchers concluded that the overlaps were due to currents contributed by pits on the surfaces of the sample. Pitting is known to affect the results of single loop EPR tests.[26] Clarke et al.[49] selected 2.0 coulomb/cm^2 as the upper acceptance limit for incoming stainless steel. The limit ensured "a lack of discernible intergranular carbide precipitation". Majidi et al.[45] found that this limit agreed well with the findings of their work.

The other boiling acid tests work much the same way as the ferric sulfate-sulfuric acid test, so the comparisons discussed above may be extended to those as well.

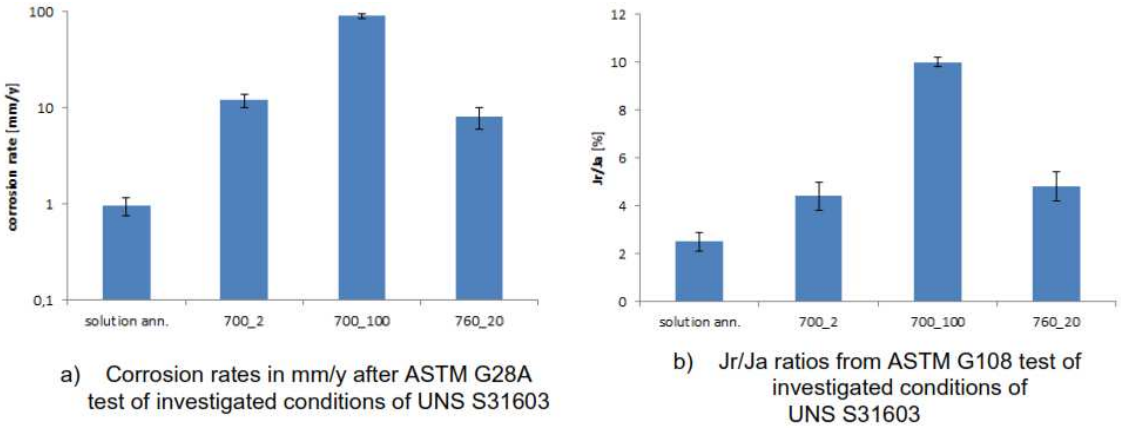

a) Corrosion rates in mm/y after ASTM G28A test of investigated conditions of UNS S31603

b) Jr/Ja ratios from ASTM G108 test of investigated conditions of UNS S31603

Figure 1- 7: Comparison of corrosion tests conducted on AISI 316 stainless steel samples with the same thermal histories. (a) ferric sulfate-sulfuric acid test in ASTM G28 and (b) single loop EPR test from ASTM G108. [48]

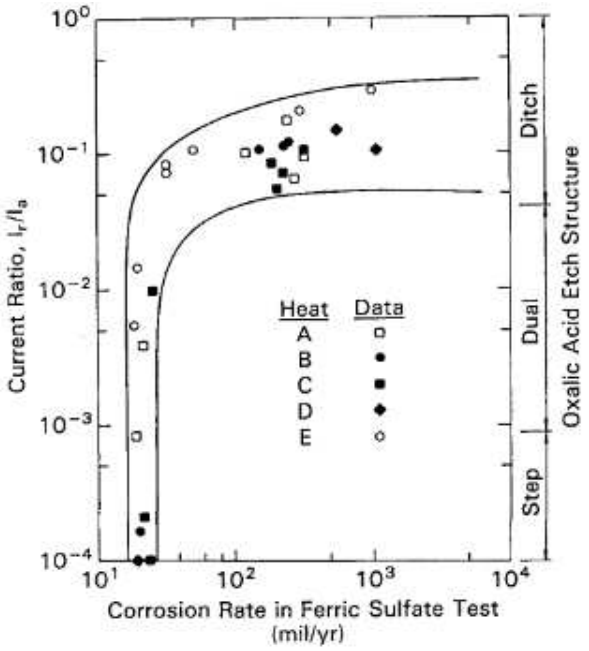

Figure 1- 8: Plot comparing results from the double loop EPR test, oxalic acid test and ferric sulfate-sulfuric acid test conducted on AISI 304 stainless steel samples with identical thermal histories. [45]

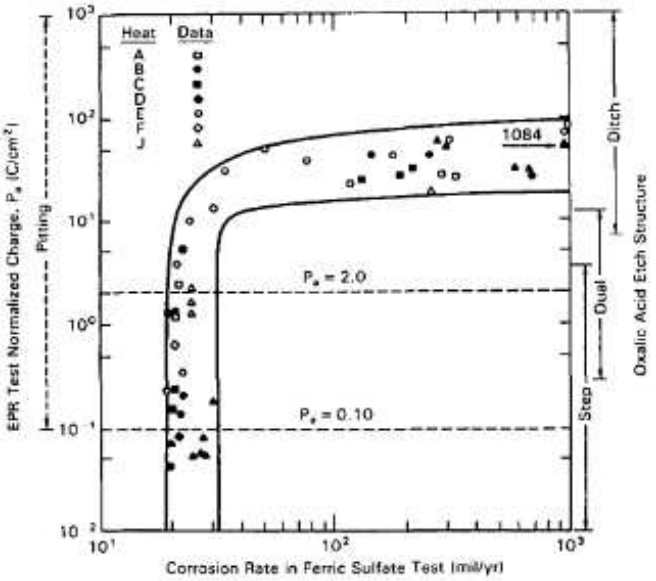

Figure 1- 9: Plot comparing results from the single loop EPR test, oxalic acid test and ferric sulfate-sulfuric acid test conducted on AISI 304 and AISI 304L stainless steel samples with identical thermal histories. [45]

References

1. A.J. Sedriks: Corrosion of Stainless Steels , 2nd ed., John Wiley & Sons, Inc, 1996.
2. D.A. Jones: Principles and Prevention of Corrosion, 2nd edition., Prentice Hall, Upper Saddle River NJ, 1996.
3. R.J. Schmitt and C.X. Mullen: in Stainless Steel for Architectural Use, ASTM International, 1969.
4. Z. Wang, E.-M. Paschalidou, A. Seyeux, S. Zanna, V. Maurice, and P. Marcus: Front Mater, 2019, vol. 6, pp. 1–12.
5. T. Ohmi, Y. Nakagawa, M. Nakamura, A. Ohki, and T. Koyama: Journal of Vacuum Science & Technology A: Vacuum, Surfaces, and Films, 1996, vol. 14, pp. 2505–10.

6. I. Olefjord: Materials Science and Engineering, 1980, vol. 42, pp. 161–71.
7. J. Lippold and D. Kotecki: Welding Metallurgy and Weldability of Stainless Steels, 1st edition., John Wiley & Sons, Inc, Hoboken, New Jersey, 2005.
8. R.K. Desu, H. Nitin Krishnamurthy, A. Balu, A.K. Gupta, and S.K. Singh: Journal of Materials Research and Technology, 2016, vol. 5, pp. 13–20.
9. W.R. Cieslak and D.J. Duquette: J Electrochem Soc, 1985, vol. 132, pp. 533–7.
10. G. Hultquist and C. Leygraf: Corros Sci, 1981, vol. 21, pp. 401–8.
11. A.C.T.M. Van Zwieten and J.H. Bulloch: International Journal of Pressure Vessels and Piping, 1993, vol. 56, pp. 1–31.
12. M. Yoshino, T. Tagawa, H. Li, and N. Takata: ISIJ International, 2022, vol. 62, p. ISIJINT-2021-506.
13. M.P. Sello and W.E. Stumpf: Materials Science and Engineering: A, 2010, vol. 527, pp. 5194–202.
14. T.J. Nichol, A. Datta, and G. Aggen: Metallurgical Transactions A, 1980, vol. 11A, pp. 573–85.
15. H. Ding, Y. Wu, Q. Lu, P. Xu, J. Zheng, and L. Wei: Cryogenics (Guildf), 2018, vol. 92, pp. 50–9.
16. C. Zheng and W. Yu: Materials Science and Engineering: A, 2018, vol. 710, pp. 359–65.
17. I. Calliari, M. Zanesco, M. Dabalà, K. Brunelli, and E. Ramous: Mater Des, 2008, vol. 29, pp. 246–50.
18. R. Francis and G. Byrne: Metals (Basel), 2021, vol. 11, p. 836.
19. S.D. Kahar: Int J Eng Res Appl, 2017, vol. 7, pp. 27–36.

20. M.F. McGuire: in Stainless Steels for Design Engineers, 1st edition., ASM International, 2008, pp. 137–46.
21. H. Nakagawa and T. Miyazaki: J Mater Sci, 1999, vol. 34, pp. 3901–8.
22. M. Blair, T.L. Stevens, and B. Linskey: Steel Castings Handbook - Chapter 20, 6th Edition., ASM International, Materials Park, Ohio.
23. F.H. Beck, J. Juppenlatz, and P.F. Wieser: Stress Corrosion - New Approaches, 1976, vol. ASTM STP 610, pp. 381–98.
24. C.L. Briant, R.A. Mulford, and E.L. Hall: Corrosion, 1982, vol. 38, pp. 468–77.
25. T.M. Devine: Corros Sci, 1990, vol. 30, pp. 135–51.
26. Steel Founders' Society of America: Sensitization Behavior of Cast Stainless Steels Subject to Weld Repair, Des Plaines IL, 1984.
27. A.J. Sedriks: International Metals Reviews, 1982, vol. 27, pp. 321–53.
28. H.D. Solomon: Corrosion, 1984, vol. 40, pp. 51–60.
29. E. Loria: J Test Eval, 1986, vol. 14, pp. 81–96.
30. G. Ma, W. Xian, H. Bi, and M. Li: Int J Electrochem Sci, 2022, vol. 17, p. 22097.
31. R. Pascali, A. Benvenuti, and D. Wenger: Corrosion, 1984, vol. 40, pp. 21–32.
32. E.A. Trillo, R. Beltran, J.G. Maldonado, R.J. Romero, L.E. Mun, W.W. Fisher, and A.H. Advani: Mater Charact, 1995, vol. 35, pp. 99–112.
33. M.G. Fontana: Ind Eng Chem, 1952, vol. 44, pp. 87A-90A.
34. M.L. Holzworth, F.H. Beck, and M.G. Fontana: Corrosion, 1951, vol. 7, pp. 441–9.
35. K.N. Adhe, V. Kain, K. Madangopal, and H.S. Gadiyar: J Mater Eng Perform, 1996, vol. 5, pp. 500–6.

36. S.K. Bonagani, K. Chandra, K. V. Ravikanth, H. Donthula, S. Roychowdhury, and V. Kain: Materials Science and Engineering: A, 2023, vol. 888, pp. 1–17.
37. M. Shirazi: The University of Saskatchewan, 1996.
38. K.E. Pinnow and A. Moskowitz: Weld J, 1970, vol. 49, pp. 278s–84s.
39. C. McCaul: British Corrosion Journal, 1991, vol. 26, pp. 239–43.
40. M.H. Brown: Corrosion, 1974, vol. 30, pp. 1–12.
41. M.A. Streicher: in Intergranular Corrosion of Stainless Steels, ASTM STP 656, R.F. Steigerwald, ed., ASTM International, 1978, pp. 3–84.
42. R. Baboian: Corrosion Tests and Standards: Application and Interpretation, 2nd edition., ASTM International, West Conshohocken, PA, 2005.
43. Oak Ridge National Laboratory: Sensitization, Intergranular Attack, Stress Corrosion Cracking, and Irradiation Effects on the Corrosion of Iron-Chromium-Nickel Alloys, Oak Ridge, TN, 1978.
44. ASTM International: ASTM A262 - 15, 2021, pp. 1–20.
45. A.P. Majidi and M.A. Streicher: Corrosion, 1984, vol. 40, pp. 584–93.
46. ASTM International: ASTM G108 - 94, 2015, pp. 1–9.
47. D.L. Reichert and G.E. Stoner: J Electrochem Soc, 1990, vol. 137, pp. 411–3.
48. R. Lackner, G. Mori, R. Egger, and F. Winter: Corrosion 2014, 2014, vol. Paper No. 3946, pp. 1–15.
49. W.L. Clarke, R.L. Cowan, and W.L. Walker: in Intergranular Corrosion of Stainless Steels, ASTM STP 656, R.F. Steigerwald, ed., ASTM International, 1978, pp. 99–132.

Chapter 2: PWHT-Free Cast CF Stainless Steel Grades

Abstract

The sensitization susceptibility of four CF grades and their associated weld metals was evaluated using heat affect zone simulations, electrochemical corrosion testing, scanning electron microscopy and transmission electron microscopy. The goal of this investigation was to determine if the post weld heat treatment (PWHT) requirement in industry standards can be waived for three of the alloys which are known in industry as sensitization-resistant. The CF3 and CF8C base metals showed low levels of sensitization under the welding conditions tested, indicating potential acceptable performance in mild environments. Their weld metals, E308L and E347, exhibited higher degrees of sensitization due to preferential attack of the austenite phase. The PWHT was found to improve the corrosion resistance of the welds by changing their ferrite morphology and amount. It also served as a stabilization treatment for E347, which is often recommended for stabilized grades to avert knife-line attack. The CF3MN and E316L base metal/weld metal pair presented the best resistance to sensitization under the welding conditions tested. They did not reactivate in the corrosion test or show any evidence of intergranular attack. It was recommended that the PWHT requirement be maintained for CF3, CF8, CF8C and their weld metals. Wider corrosion testing is encouraged for CF3MN/E316L pair to generate more comprehensive data on its sensitization resistance.

Introduction

Stainless steels are ferrous alloys that contain a minimum of 11wt% chromium, the amount required to form a stable protective layer in unpolluted atmospheres.[1–3] Cast stainless steels are manufactured into components like pump casings and valve bodies for use in the chemical processing industry. Among cast stainless steels, CF grades are popular because they are relatively low-alloyed but perform well in many media.[4,5] Since stainless steels are usually specified for their corrosion resistance, it is desired that they achieve and maintain passivity during fabrication and service life. A condition under which these alloys lose their passivity is sensitization. Sensitization is a condition where chromium-rich phases (usually carbides) form along grain boundaries in a stainless steel, depleting the surrounding matrix of chromium.[6,7] The depleted area is unable to maintain a stable passive layer and becomes vulnerable to selective attack in corrosive media. Since the carbides form on grain boundaries, the dissolution is often along these areas and is known as intergranular attack (IGA). Sensitization can happen in austenitic stainless steels during fabrication or in service when they are heated between 500ºC and 900ºC where these carbides are stable.[6] Welding can therefore be problematic for austenitic stainless steels since the heat affected zone (HAZ) experiences temperatures from the liquidus to room temperature. Grades more amenable to welding have since been designed to avoid sensitization, and they include low-carbon, stabilized and nitrogen-bearing austenitic stainless steels. Limiting carbon concentration to 0.03wt% has been found to significantly retard carbide formation during welding.[8,9] Stabilized grades use potent carbide formers, usually titanium or niobium, to tie up the carbon before it has the chance to combine with chromium.[10,11] Adding up to 0.2wt% nitrogen also helps mitigate sensitization by

inhibiting chromium diffusion in austenite.[12,13] These types of alloys have become popular in industry because of the considerable success they have exhibited. However, the American Society for Testing and Materials (ASTM) standards, A743 and A744, that regulate the production of cast stainless steels require post weld solution annealing for all grades, including the alloys with improved compositions. The post weld heat treatment (PWHT) is designed to restore corrosion resistance by dissolving any carbides that may have formed during welding. Some consider this requirement overreaching because experience in industry has shown that PWHT may be redundant for some grades. Also, heat-treating large castings can cause dimensional distortion, resulting in high scrap rates. The complex equipment set up makes PWHT difficult to execute in the field, so removing this barrier will open new possibilities for field fabrication and installation of cast components. It has therefore become necessary to investigate the possibility of waiving PWHT for the applicable grades.

These alloys already have a well-established reputation of being resistant to welding-induced sensitization. Time-temperature-sensitization (TTS) diagrams are often developed for low carbon grades to demonstrate their efficiency in this area. The results used to construct TTS diagrams come from qualitative tests such as ASTM A262 method E where corrosion test samples are bent and inspected for fissures in an optical microscope at 5x to 20x magnification.[14] The absence of fissures is interpreted as sensitization resistance. While these diagrams are widely used in industry, it is important to acknowledge their limitation in conclusively ruling out intergranular attack. Other researchers also employ weight loss tests to investigate sensitization resistance and often conclude that corrosion rate below a certain threshold signifies sensitization resistance. Again, this may not be

sufficient to determine general PWHT requirements for several reasons. First, low corrosion rates observed in laboratory tests are not always guaranteed in operating plants because service fluids often have contaminants that accelerate corrosion beyond results obtained in laboratory tests. These contaminants could be metal cations, which Streicher found to increase corrosion if present in certain amounts.[15] Secondly, a mildly sensitized sample that has chromium carbides may exhibit low corrosion rates in a weight loss test if the depletion zone is not wide or deep enough to cause grain dropping, but such samples can still corrode aggressively in media like oxalic acid, which attack chromium-rich carbides instead of chromium depleted zones. Stansbury et al. found that similarly processed CF8M and CF8 were equally attacked in oxalic acid even though the CF8M had performed better in an electrochemical corrosion test.[16] Thirdly, components that have pre-existing chromium carbides have been shown to be susceptible to further sensitization even at temperatures below the classic sensitization range. This phenomenon is known as low temperature sensitization (LTS).[17,18] Low temperature sensitization makes a component progressively more prone to attack even though the component may have exhibited low rates at the time of installation. For these reasons, a more rigorous proof of "no sensitization" is needed to modify existing standards and make generic PWHT recommendations.

Sensitization testing should also include all the different regions of a welded assembly under different welding conditions. The regions that will be investigated in this project are unaffected (solution-annealed) base metal, base metal heat affected zone (BM-HAZ), as-deposited weld and weld metal heat affected zone (WM-HAZ). A weld fusion zone

typically has residual solidification-induced segregation, which is expected to make the fusion zone more susceptible to sensitization relative to the base metal.

Experimental Procedure

The alloys selected for this investigation are listed in Table I along with their chemical compositions determined by optical emission spectroscopy (OES) except for the nitrogen concentrations, which were determined by inert gas infusion – thermal conductivity method. The alloys include a low carbon grade (CF3), a niobium-stabilized grade (CF8C), a nitrogen-bearing grade (CF3MN) and a high carbon grade (CF8). These base metals are paired with their respective weld wires as determined from foundry polls. The pairings are CF3/E308L, CF8/E308L, CF8C/E347 and CF3MN/E316L. The cast plates were solution annealed in the foundries according to ASTM A743/A744. The CF3 and CF8 plates were heated at 1066ºC (1950ºF) for one hour, CF8C was held at 1093ºC (2000ºF) for two hours and CF3MN was held at 1107ºC (2025ºF) for 2 hours. All the plates were quenched in water at the end of the heat treatment. Sensitized samples were included in the corrosion tests as controls. The sensitization treatment was done at 675ºC for two and half hours and quenched in water.

Ten welding procedure specifications (WPS) designed for these base metal/weld metal combinations where sourced from foundries around the country. From each, the maximum heat input was calculated and used to generate HAZ thermal cycles with peak temperatures from 500ºC to 900ºC in the SmartWeld program[19]. For each cycle, the total time spent in the sensitization range was calculated and plotted against peak temperature as shown in

Figure 2-1. Thermal cycles with peak temperature of 900ºC were found to be the most deleterious (i.e., spent the most time in the sensitization range) and selected to be applied in the Gleeble 3500 thermomechanical simulator at three heat input levels of 0.81kJ/mm, 1.78kJ/mm and 3.75kJ/mm, representing low, intermediate, and high heat inputs as calculated from the WPS's. Gleeble samples were φ12mm x 110mm long with threaded ends. All the Gleeble work was done under zero force conditions to avoid plastic deformation. After the thermal cycling, samples were cut at the point of thermocouple wire attachment, mounted and metallographically prepared.

All-weld metal samples were made by overlaying gas metal arc welds (GMAW) on 304L base plates to a thickness of 32mm with samples extracted from the top 16mm. Samples were machined to φ12mm x 110mm long as stated above. The welds were made with a Miller Jetline automated GMAW welder using 1.0kJ/mm heat input, 177ºC(350ºF) maximum interpass temperature and 98% Ar + 2% O_2 shielding gas.

The Double Loop Electrochemical Potentiokinetic Reactivation (DL-EPR) test was used for corrosion testing. Samples from the Gleeble test were cut, mounted in conductive Bakelite powder and metallographically prepared with silicon carbide paper, and then polished with 0.05microm colloidal silica. They were then thoroughly rinsed with deionized water to remove any contaminants. The corrosion tests were done with a saturated calomel electrode (SCE), Gamry 1010E potentiostat and Gamry ParaCell kit for flat specimens. Sample masks were used to isolate 1cm^2 of the sample surface for testing. The scan speed was 1.67mV/s, and the potential was cycled from the open circuit potential (around -400mV) to 200mV and back in a 0.5M H_2SO_4 + 0.01M KSCN solution at ambient temperature (approximately 24ºC). The electrolyte was prepared with ASTM type I

deionized water. After the corrosion testing, the samples were rinsed with deionized water and ethanol, dried and examined in the scanning electron microscope (SEM).

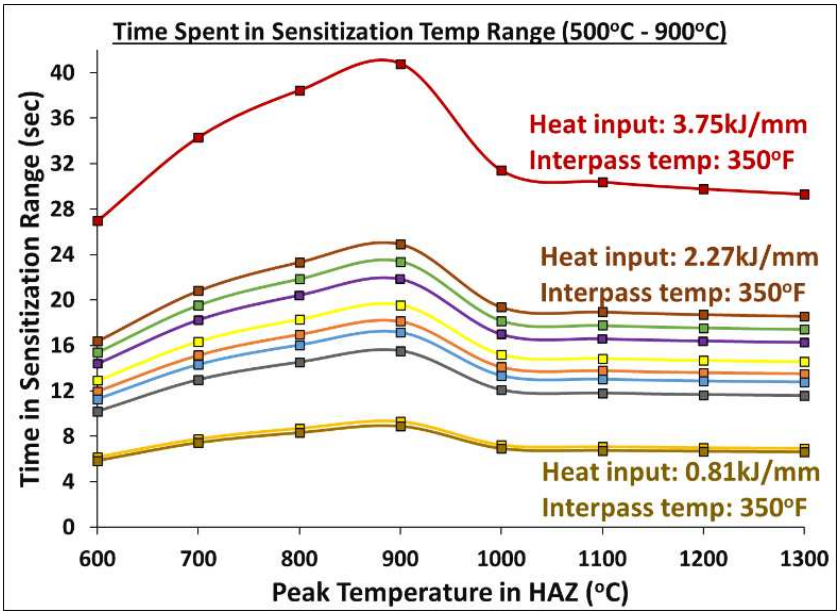

Figure 2- 1: Time spent in the sensitization time range vs peak temperature in HAZ. Time periods were calculated from thermal cycles generated with SmartWeld program.

Imaging was done in a Hitachi 4300 SEM with a backscattered electron detector and an Everhart Thornley secondary electron detector. All energy dispersive spectroscopy (EDS) line scans and maps were taken with the EDS detector in the same equipment using 15kV accelerating voltage and 7.68μs process time.

The transmission electron microscope (TEM) samples were prepared with a FEI Scios dual beam FIB using the standard lift-out procedure. A Jeol 2100 TEM operating at 200kV was used to take selected area diffraction (SAD) patterns. An aberration-corrected cold field

emission scanning transmission electron microscope Jeol ARM 200CF operating at 200kV was used to image ferrite pools in the welds and collect EDS line scans and maps.

Table 2- 1: Chemical composition of base metals and deposited weld metals. All values in weight percent.

CHEMICAL COMPOSITION OF BASE METALS.												
	C	**Mn**	**P**	**S**	**Si**	**Cr**	**Ni**	**Mo**	**Nb**	**Cu**	**N**	**Fe**
CF3	0.03	1.21	0.023	0.001	1.76	17.58	9.01	0.24	0.02	0.29	0.07	Bal
CF3MN	0.02	0.79	0.022	0.003	0.78	20.23	9.39	2.19	-	0.25	0.19	Bal
CF8C	0.03	0.92	0.030	0.002	1.28	18.44	9.70	0.29	0.43	0.32	0.11	Bal
CF8	0.05	1.19	0.023	0.001	1.74	17.83	9.04	0.24	0.02	0.29	0.07	Bal
CHEMICAL COMPOSITION OF DEPOSITED WELD METAL. All values in weight percent.												
E308L	0.04	1.49	0.023	<0.001	0.33	19.59	9.95	0.14	0.02	0.16	0.05	Bal
E316L	0.02	1.67	0.021	0.005	0.39	18.14	12.36	2.69	<0.01	0.19	0.03	Bal
E347	0.07	1.60	0.011	0.009	0.40	19.56	10.69	0.10	0.56	0.02	0.06	Bal

Results

Sensitization Mechanism

The chromium-rich carbides that cause sensitization mostly precipitate at grain boundaries or other interphase boundaries. Research has shown that the nature and shape of the interface affect carbide nucleation kinetics, with the austenite-ferrite boundary reported as the most preferred site for precipitation.[20–22] The sensitized CF8C samples were examined in the SEM to determine if the NbC boundaries in CF8C make any difference in this hierarchy. Figure 2-2 shows images of various boundaries in sensitized CF8C and EDS line scans taken across them. Figures 2-2A and 2-2B are for an austenite-NbC boundary,

Figures 2-2C and 2-2D are for an austenite-austenite boundary, and Figures 2-2E and 2-2F are for an austenite-ferrite boundary in a sensitized CF8C sample. Only niobium enrichment is seen at the austenite-NbC boundary while no enrichment exists at the austenite-austenite boundary. The austenite-ferrite boundary however shows chromium enrichment higher than was measured in the ferrite phase with the same EDS set up. This signifies the presence of chromium-rich carbides at that interface. A similar level of chromium is seen at an identical boundary in sensitized CF8C when the electron probe hits the $M_{23}C_6$ as clearly seen in Figure 2-3. The WinX-Ray version 1.4.2.1 program was used run Monte Carlo simulations for CF8C using 15kV accelerating voltage and 10nA beam current. It predicted an interaction volume width of approximately 1μm, which is larger than the niobium carbide in Figure 2-2 and chromium carbides in Figure 2-3. This means the electron and xray signals do not emanate exclusively from these particles when the electron probe hits them. This is why Figure 2-2B for example shows about 45wt% Nb in NbC instead of Nb greater than 80wt% as known for this phase. This notwithstanding, the set-up is still able to show relative element profiles across the region of interest. The concentrations shown on the y-axes in Figures 2-2B, 2-2D and 2-2F were generated with the EDAX Genesis software using a standardless quantification method. The concentration values are not intended as the actual amounts of the elements, they are only used comparatively to show element enrichment across the boundaries. Considering that the line scans are taken in the same region (approximately 2μm apart), and yet only austenite-ferrite interface shows chromium enrichment suggests that it is the preferred site for chromium carbide precipitation in CF8C. These results are significant because dissolution at this boundary in the corrosion test can be interpreted as sensitization.

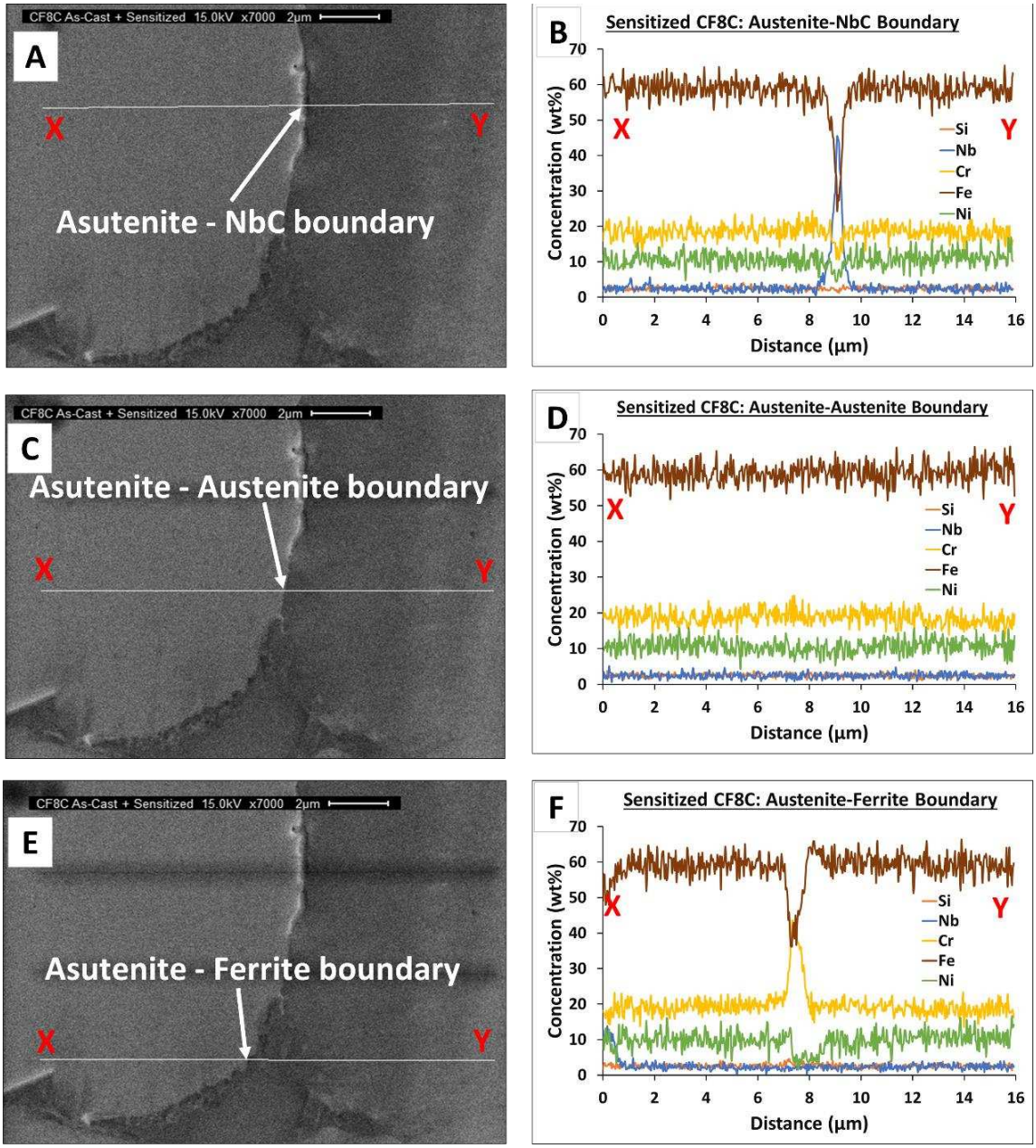

Figure 2- 2: SEM images of various boundaries in CF8C with corresponding EDS line scans across them. (A): Image of austenite-NbC boundary. (B): EDS line scan across austenite-NbC boundary. (C): Image of austenite-austenite boundary. (D): EDS line scan across austenite-austenite boundary. (E): Image of austenite-ferrite boundary. (F): EDS line scan across austenite-ferrite boundary.

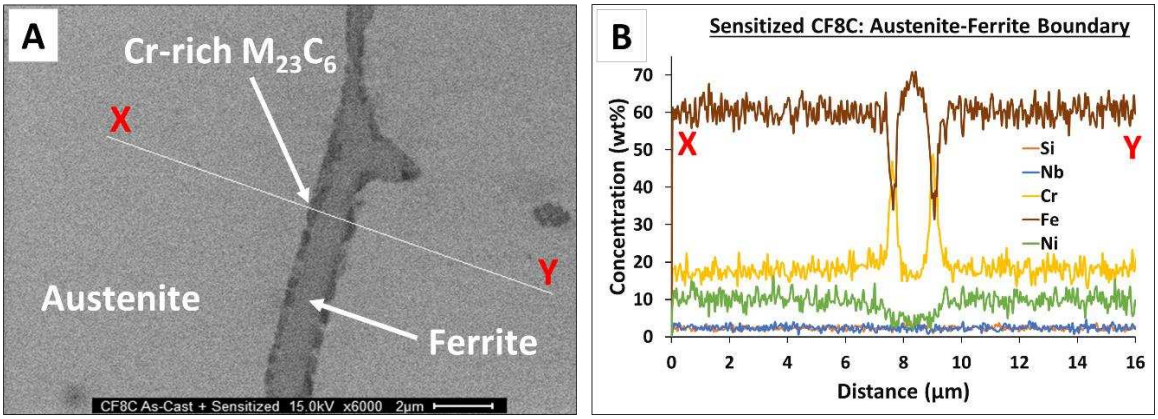

Figure 2- 3: SEM image and EDS line scan across ferrite pool in sensitized CF8C. (A): SEM image of Cr-rich carbides at austenite-ferrite boundary in sensitized CF8C (B): EDS line scan across ferrite pool in sensitized CF8C.

Corrosion Test Results

The DL-EPR test starts at the open circuit potential (OCP) and proceeds with a continuous change in potential up to +200mV (in the passive region), then the potential scan direction is reversed and potential decreased continuously back to the OCP. The peak current during the reverse scan (Ir) is divided by the peak current during the forward scan (Ia) to establish the degree of sensitization (DOS). The forward scan begins in the active region where there is no passive layer, the current measured during this stage comes from uniform corrosion of the entire surface. The reverse scan on the other hand begins in the passive region where the entire sample surface is covered by the protective oxide layer. As the potential scan re-enters the active region, the oxide layer over chromium-depleted areas dissolve preferentially as it is more unstable. Therefore, the anodic current measured during the reverse scan mostly comes from areas of localized corrosive attack. The I_r/I_a ratio thus gives a measure of passive film break down during the test.[23] A sample may reactivate or

not in the DL-EPR scan. An example of a test with no reactivation is shown in Figure 2-4A. In this Figure, the anodic current continuously decreases from the beginning of the reverse scan until it is overtaken by a cathodic current around +30mV, which then persists throughout the rest of the reverse scan. The absence of an anodic current during this stage of the test generally signifies that there was little to no localized corrosion. Reactivation generally depicts sensitization, and the size of the loop indicates the severity of IGA. Figure 2-4B is an example of a test where reactivation was observed. Tests that show no reactivation are the best assurance of the absence of sensitization, although this must be confirmed by post-test SEM examination. Currents measured in the DL-EPR test are net currents at the sample surface.[24] Therefore the cathodic current observed during the reverse scan in Figure 2-4A is actually a net cathodic current. A net cathodic current does not signify the absolute absence of an anodic reaction, it only indicates that the anodic current is very small and surpassed by the cathodic reaction. Following this, an anodic current of 100nA/cm^2 is used to calculate DOS for tests where there is no reactivation. This figure was arbitrarily selected because it is close to the lowest anodic current measured by the potentiostat before the current switches over to a cathodic current. It suggests that the residual anodic reaction rate is around this figure when measurement changes to a net cathodic current. Other researchers assign a DOS of zero for tests where there is no reactivation,[25,26] but this may not be an accurate depiction of the balance of reactions on the sample surface as it implies that there is no corresponding anodic reaction for the cathodic current measured. Current readings in Figures 2-4A and 2-4B span eight orders of magnitude covering different corrosion conditions, and the current drops by three orders of magnitude as the sample transitions from peak active corrosion to passivity. Even in

active corrosion alone, current varies from 1µA to about 40mA. Consequently, if a material is significantly more sensitized than another, it is expected that their DOS values will vary by at least one order of magnitude. Samples with only small variations are considered as similarly sensitized.

The corrosion test is followed by examination in the SEM to confirm intergranular attack. Figure 2-5A is a solution annealed CF3 sample that did not reactivate in the test and shows no dissolution at the ferrite boundary, while Figure 2-5B is a sensitized CF3 sample that reactivated and shows dissolution around the ferrite. The cavities seen in the ferrite phase in both samples likely come from general active dissolution during the forward scan.

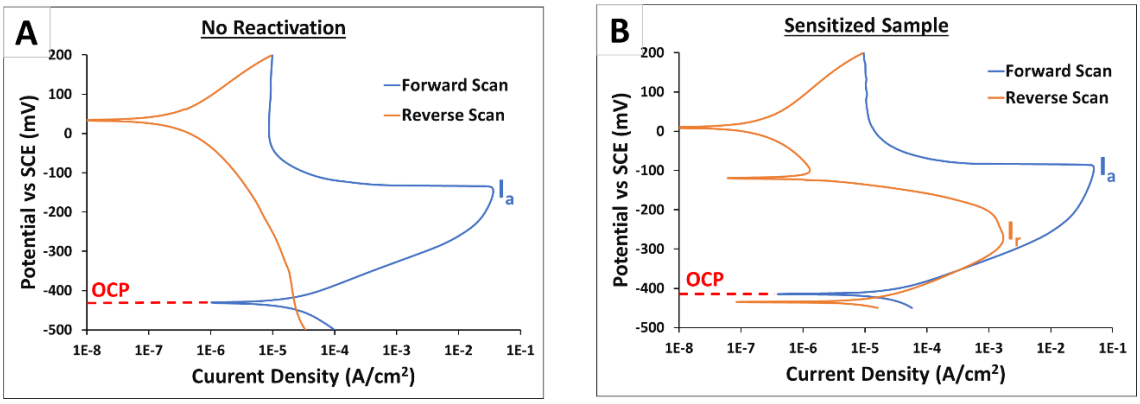

Figure 2- 4: Typical DL-EPR test results plots showing potential vs log of current density. (A): DL-EPR plot showing no reactivation. (B): DL-EPR plot with reactivation.

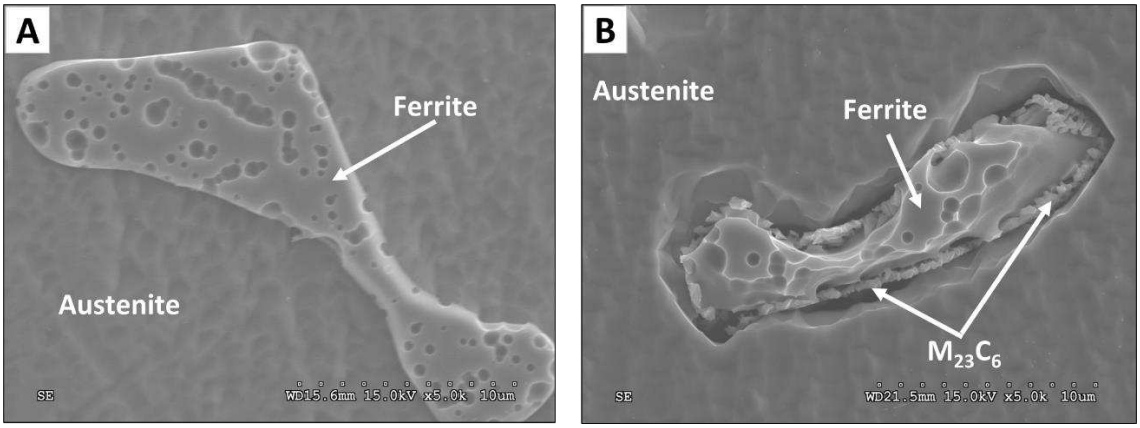

Figure 2- 5: SEM image of CF3 after DL-EPR corrosion test. (A): solution annealed CF3 showing no IGA (B): Sensitized CF3 with dissolution around the ferrite.

CF3 Base Metal and Welds Made with E308L Filler Metal

Figure 2-6 shows the DOS vs heat input plot for CF3/E308L. All base metal samples are shown in blue and weld samples in red. Results from tests conducted on the solution annealed CF3 base metal, which did not reactivate during the test, are shown for comparison. The degree of sensitization generally increases with increasing heat input. Higher heat input processes cool more slowly and allow more time for nucleation and growth of the chromium carbides. There was no reactivation in the solution-annealed and 0.81kJ/mm samples but DOS rises to 2.5×10^{-4} and 1.4×10^{-4} after one thermal cycle at 1.78kJ/mm and 3.75kJ/mm respectively. Figures 2-7A and 2-7B are SEM images of CF3 thermally cycled at 0.81kJ/mm and 3.75kJ/mm respectively, and both samples show attack in and around the ferrite phase. The solution annealed sample showed no boundary attack while the 0.81kJ/mm sample did show attack at the boundary, even though they both did not reactivate. The all-weld metal samples generally exhibited higher DOS values than the base metal samples. The as-deposited weld produced a DOS of 4.9×10^{-4} while the low,

medium, and high heat input all-weld samples had $2.3x10^{-4}$, $2.5x10^{-4}$ and $1.4x10^{-3}$ respectively after one cycle. The higher DOS values suggest that the all-weld metal samples sensitize more readily than the base metal samples. The welds were expected to be more sensitive because fusion zones typically have residual segregation, which will accelerate sensitization. Images of the as-welded and 3.75kJ/mm E308L samples are shown in Figures 2-8A and 2-8B respectively. A different type of local attack is seen in the austenite surrounding the ferrite in Figure 2-8A. In the sensitized base metal, some dissolution can be seen both in austenite and ferrite but in the as-deposited weld, only the austenite appears attacked while the ferrite is preserved. This is clearer when Figure 2-8A is compared with the sample before corrosion test (Figure 2-9). The corrosion pattern in the weld sample thermally cycled at 3.75kJ/mm appears similar to the pattern observed in sensitized base metal where dissolution is present in both the austenite and ferrite phases. From the plot shown in Figure 2-6, all the E308L samples reactivated in the test. Even at low heat input where the base metal DOS was negligible and similar to the solution treated base metal, the weld was attacked. Therefore, there is no heat input level at which the welded assembly can be said to be corrosion-free.

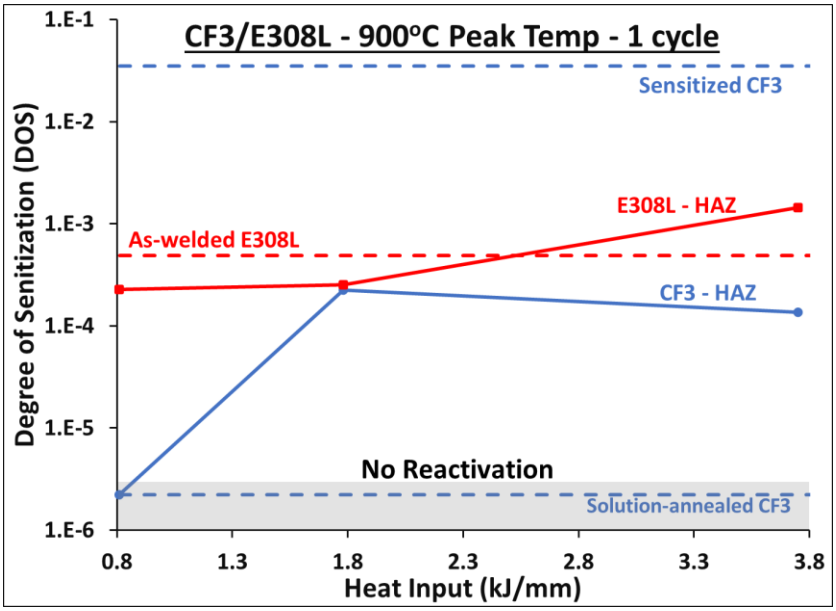

Figure 2- 6: Degree of sensitization vs heat input for CF3 and welds made with E308L filler metal.

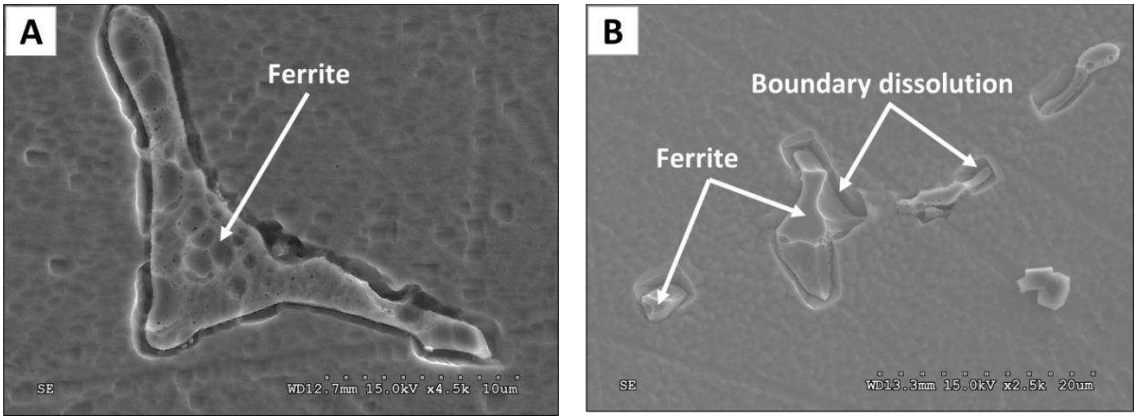

Figure 2- 7: SEM image of CF3 samples after DL-EPR test (A): CF3 thermally cycled at 0.81kJ/mm showing boundary dissolution (B): sample thermally cycled at 3.75kJ/mm showing boundary dissolution.

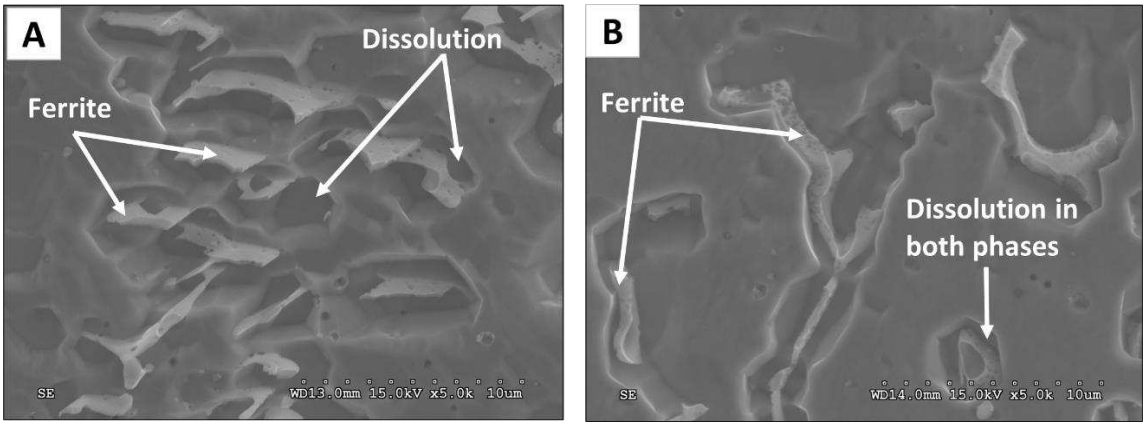

Figure 2- 8: SEM image of E308L samples after DL-EPR test (A): As-welded E308L showing preferential attack in austenite surrounding ferrite (B): E308L thermally cycled at 3.75kJ/mm showing apparent dissolution in both austenite and ferrite.

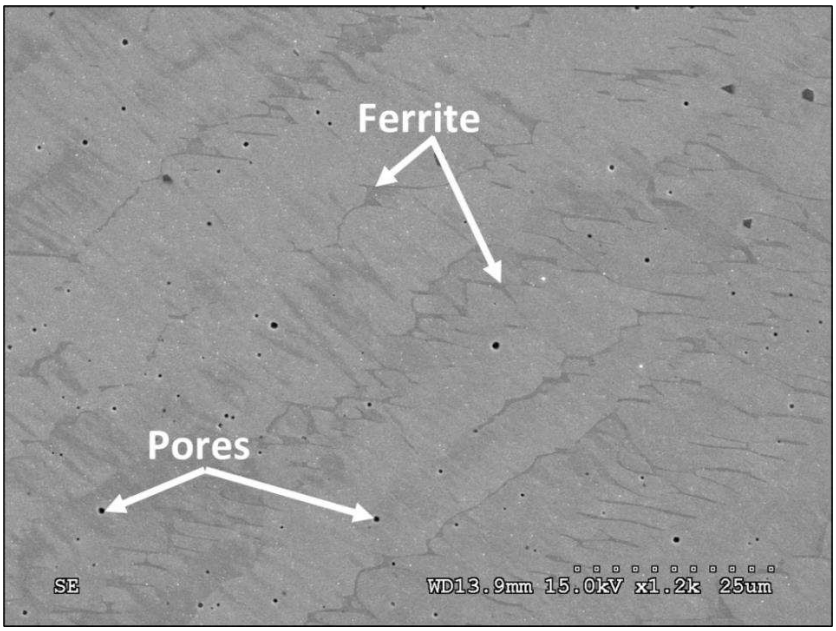

Figure 2- 9: E308L before corrosion test, showing lathy ferrite structure.

CF8 Base Metal and Welds Made with E308L Filler Metal

The corrosion results of CF8 shown in Figure 2-10 depict similar trends as CF3. Susceptibility to sensitization increases with heat input. The DOS values are generally higher than CF3 due to the higher carbon content. This is not surprising as carbon concentration is known to be a major influencer of sensitization kinetics. Unlike the CF3 results shown in Figure 2-6, the weld metal DOS values for CF8 are lower than the base metal, which can be attributed to the lower carbon concentration in the weld metal. Despite the expected sensitive nature of the weld microstructure, the DOS of thermally cycled E308L is still an order of magnitude lower than CF8. Most of the dissolution in CF8 was confined to the austenite-ferrite boundaries as seen in Figure 2-11A but light attack was also observed at some austenite-austenite boundaries (Figure 2-11B), which would have contributed to the higher corrosion currents produced in this alloy.

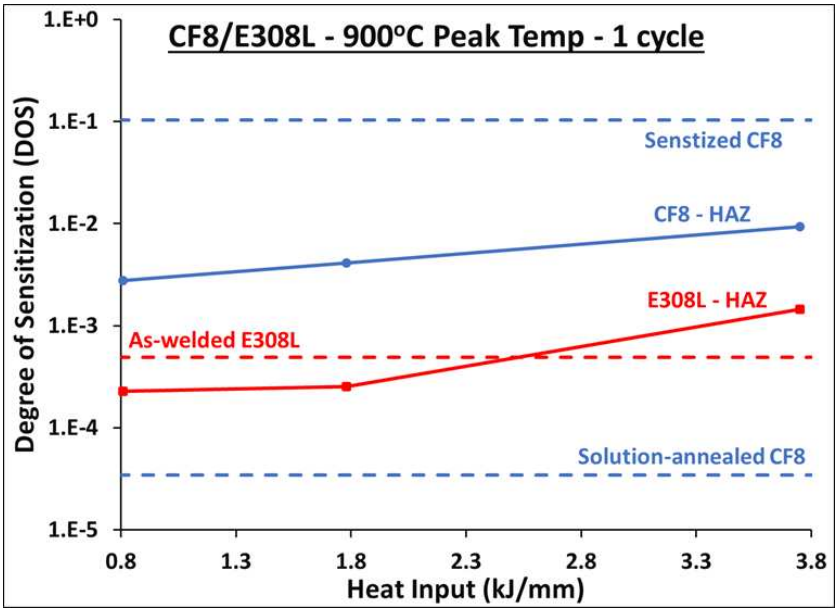

Figure 2- 10: Degree of sensitization vs heat input for CF8 and welds made with E308L filler metal.

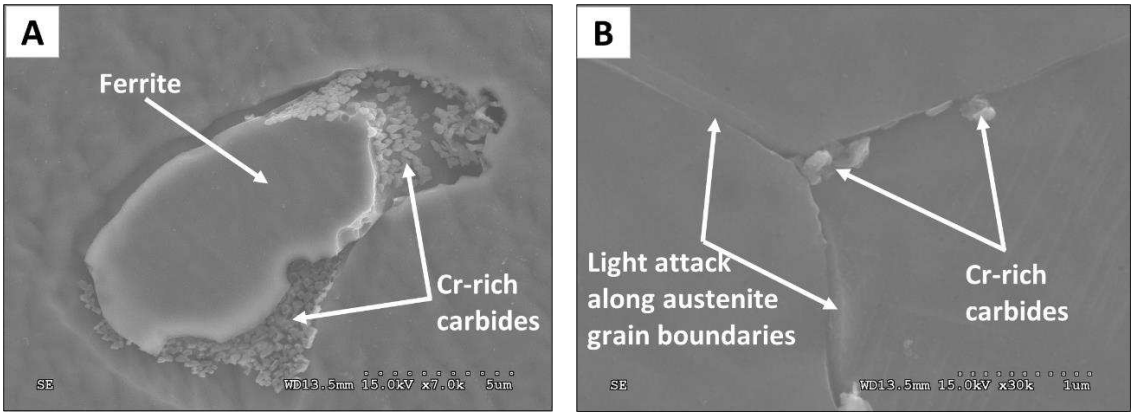

Figure 2- 11: SEM images of CF8 after DL-EPR. (A): CF8 thermally cycled at 1.78kJ/mm showing dissolution at austenite-ferrite boundary. (B): CF8 thermally cycled at 1.78kJ/mm with light attack at austenite-austenite boundary.

CF8C Base Metal and Welds Made with E347 Filler Metal

The corrosion test results of CF8C and E347 are shown in Figure 2-12. The solution annealed sample did not reactivate and showed no boundary attack. The 0.81kJ/mm and 3.75kJ/mm samples also did not reactivate but their microstructure had sparse interphase boundary dissolution as shown in Figure 2-13A for the 3.75kJ/mm sample. The 1.78kJ/mm sample had a DOS of $9.7x10^{-4}$ and showed some boundary attack, although not pervasive as seen in Figure 2-13B. The E347 samples had DOS values very close to the sensitized CF8C sample even in the as-deposited state, again suggesting that the welds were more severely sensitized than the base metal. The SEM images of the all-weld sample shown in low and high magnification in Figures 2-14A and 2-14B respectively, show localized attack in the austenite surrounding the ferrite phase like in the E308L samples. All the E347 samples had a similar corrosion pattern. Here too, the DL-EPR plot shows that the welded assembly cannot be considered as corrosion-free at any heat input value. Higher heat input processes are known to be more sensitizing, but it is interesting that 3.75kJ/mm CF8C sample did not show any reactivation. This "gain" is however nullified by the weld's response at the same heat input. It is not yet understood why only the 1.78kJ/mm sample reacted in the corrosion test when the 3.75kJ/mm thermal cycle is expected to be sensitizing.

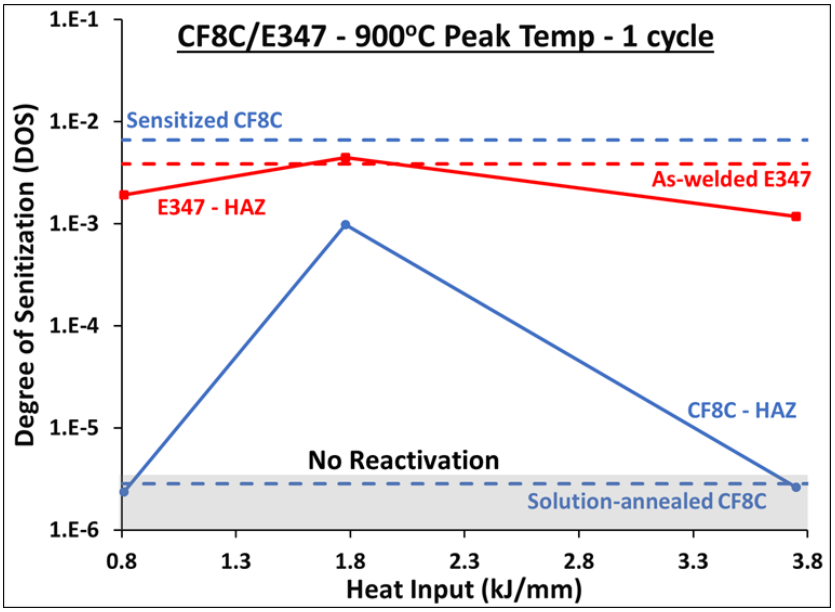

Figure 2- 12: Degree of sensitization vs heat input for CF8C and welds made with E347L filler metal.

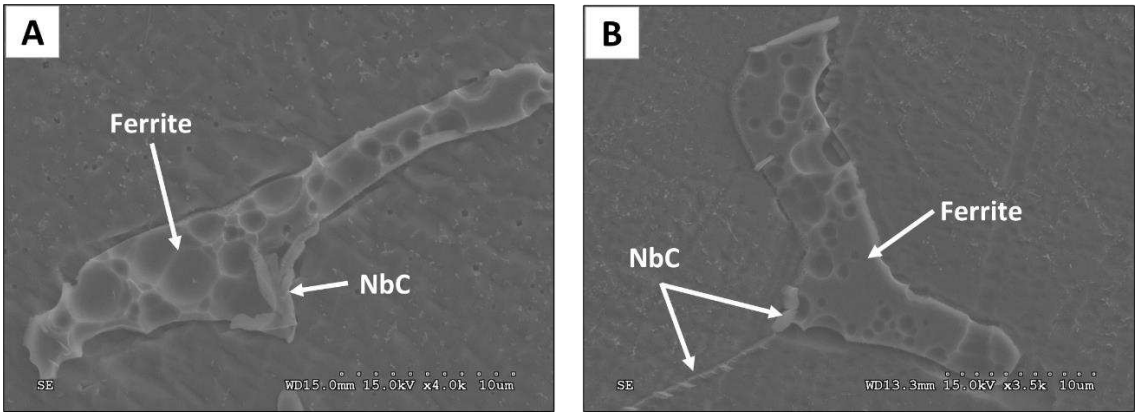

Figure 2- 13: SEM images of CF8C after DL-EPR test. (A): CF8C thermally cycled at 3.75kJ/mm showing very little boundary dissolution (B): CF8C thermally cycled at 1.78kJ/mm showing little boundary dissolution.

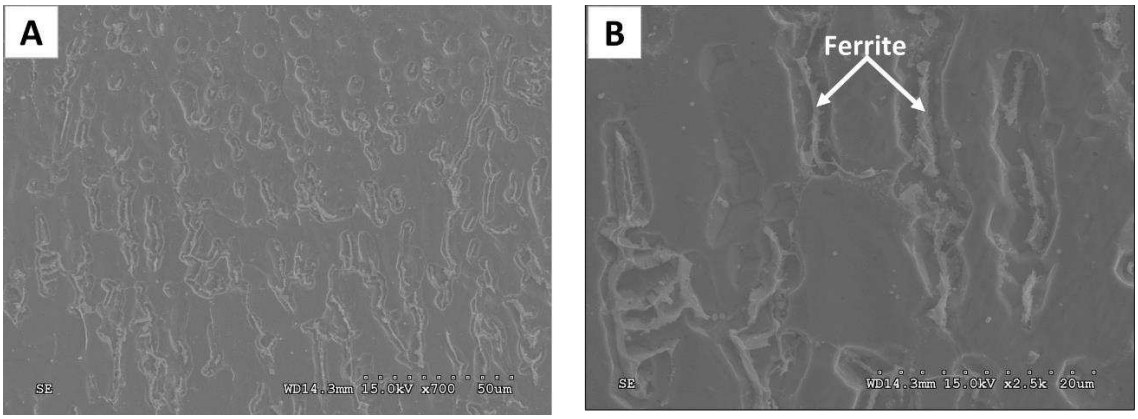

Figure 2- 14: SEM images of E347 after EL-EPR test. (A): low magnification image of E347 thermally cycled at 0.81kJ/mm showing localized corrosion in the austenite around ferrite. (B)high magnification image of E347 thermally cycled at 0.81kJ/mm showing localized corrosion in austenite surrounding ferrite.

CF3MN Base Metal and Welds Made with E316L Filler Metal

The DL-EPR plot for the CF3MN and E316L is shown in Figure 2-15. None of the base metal or weld metal samples reactivated in the corrosion test. The CF3MN samples were thermally cycled to a peak temperature of 800ºC to eliminate any dissolution effects, but they also had the same corrosion results. This was expected as even the sensitized sample did not generate any anodic current during the reverse scan. Multiple thermal cycle tests were deemed unnecessary due to the result from the sensitized sample. The result obtained agrees with the findings of Stansbury et al. that low carbon, high nitrogen CF alloys were difficult to sensitize.[12] Scanning electron micrographs of the sensitized sample are shown in Figures 2-16A and 2-16B at low and high magnification respectively. Unlike the other sensitized CF alloys, there is hardly any attack at the ferrite-austenite boundary, and dissolution appears to be confined to the ferrite as seen in the high magnification image. The scanning electron micrograph in Figure 2-17 shows no dissolution in the CF3MN

sample thermally cycled at 3.75kJ/mm. All the samples subjected to 800°C and 900°C peak temperatures had similar microstructures as that shown in Figure 2-17 after the corrosion test. Low and high magnification images of the as-welded E316L after the corrosion test are shown in Figures 2-18A and 2-18B. General (uniform) corrosion is seen in the austenite while the ferrite appears unattacked. The adverse localized corrosion seen in the E308L and E347 is absent here.

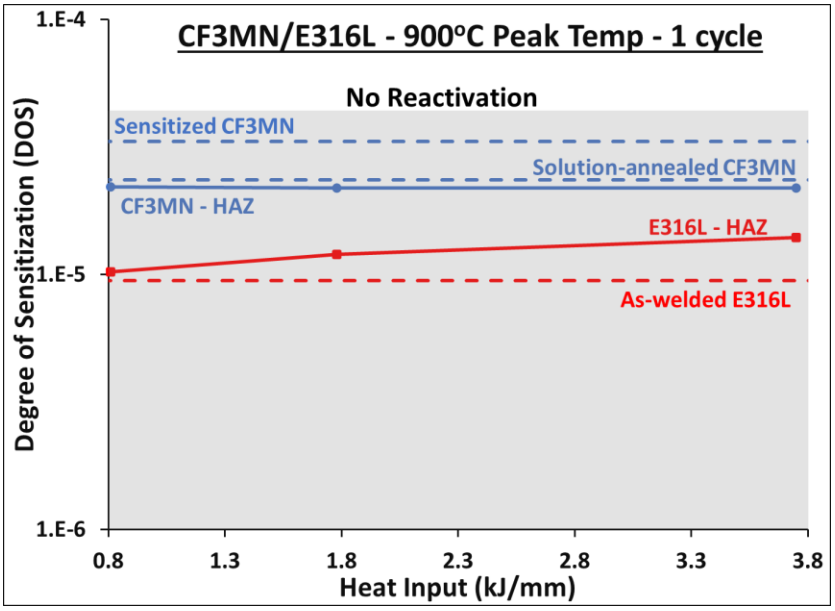

Figure 2- 15: Degree of sensitization vs heat input for CF3MN and welds made with E316L filler metal.

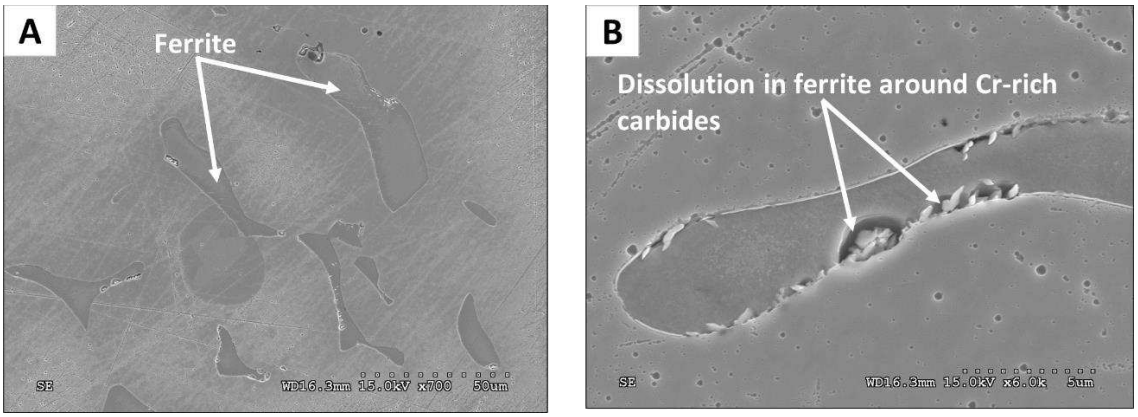

Figure 2- 16: SEM image of sensitized CF3MN after corrosion test. (A): low magnification. (B): high magnification.

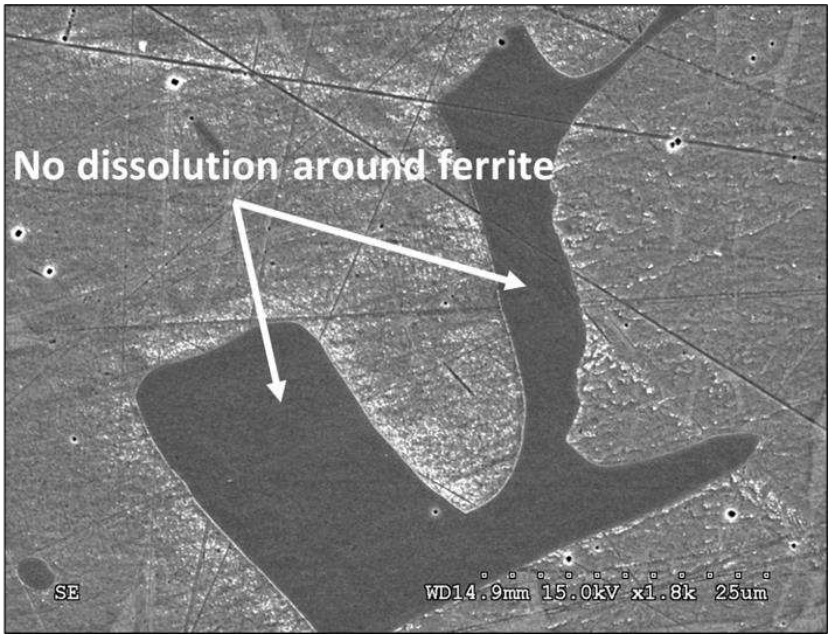

Figure 2- 17: SEM image of CF3MN cycle at 3.75kJ/mm after corrosion test.

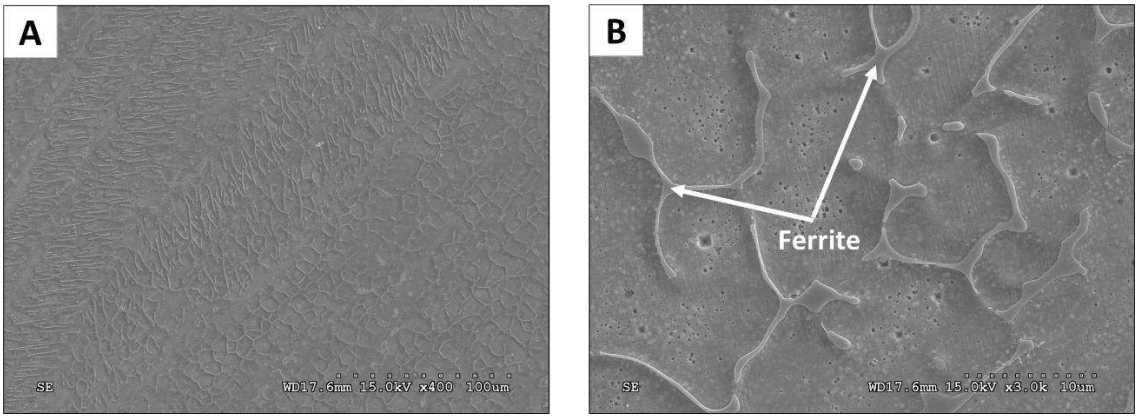

Figure 2- 18: SEM images of as-welded E316L after corrosion test. (A): low magnification image of as-welded E316L (B): high magnification image of as-welded E316L showing uniform corrosion in austenite.

Discussion

Despite being touted as sensitization-resistant, CF3 had some boundary dissolution even at low heat input as seen in Figure 2-7A. That sample, with a DOS of 2.22×10^{-6}, can be classified as sensitized since the chromium-rich carbides are known to precipitate at this interface. Other investigations have categorized such low DOS samples as unsensitized following Majidi and Streicher's[27] suggestion that a DOS of 1×10^{-3} or lower satisfies the criterion of "no discernible sensitization" set by Clarke.[28] Majidi et al.[27] found that such low values corresponded with low corrosion rates in the ferric sulfate-sulfuric acid test. However, the evidence of boundary attack observed in this investigation cannot be overlooked when making general PWHT recommendations.[27] Such low corrosion rates, in practice, may be acceptable for many applications as they may provide long service life spans, but the implications of such seemingly innocuous corrosion rates need to be accounted for in this process of formulating industry requirements. The E308L samples all

showed localized dissolution in the austenite surrounding the ferrite. This appears to be a different form of attack where the ferrite is preserved while the austenite is attacked, unlike in the sensitized CF3 in Figure 2-5B where there is dissolution in both phases, congruent with chromium depletion profiles measured by C.F. Willis[29] in sensitized 308 welds. Willis observed that, although more severe in the austenite, chromium depletion existed on both sides of the austenite-ferrite boundary in sensitized E308 welds. Chromium profile measurements made by other researchers showed no indication of depletion in as-deposited welds.[30–32] Both the skeletal and lathy ferrite were equally attacked despite the known higher crystallographic coherency at lathy ferrite boundaries.[33] This preferential corrosion of austenite in as-deposited welds observed in this and other investigations cannot be attributed to "conventional" sensitization. Energy dispersive spectroscopy (EDS) was used in the TEM to measure the composition across the austenite-ferrite interface in as-deposited and E308L samples. No carbide was detected in the as-deposited weld as can be seen in Figure 2-19A, and the line scan across the interphase boundary in Figure 2-19B also shows no chromium enrichment at the interface. An EDS map of the area, shown in Figure 2-20, and another area in the same sample shown in Figure 2-21, also did not show any chromium carbide formation or chromium depletion in the vicinity of the ferrite, thus further confirming this result. The lack of Cr depletion is consistent with measurements made by other researchers.[30–32] The corrosion in the as-deposited weld could be galvanic attack, and a mix of galvanic attack and sensitization in the thermally cycled ones. Ferrite typically has a higher chromium concentration, which is known to produce a more stable oxide layer, and lower anodic currents in the passive region.[34] Therefore, in the passive region, less dissolution is expected in the ferrite compared to the austenite. This is confirmed by the

"step" structure observed between austenite and ferrite in the solution annealed CF3 sample in Figure 2-5A. When thin strands of austenite are paired with ferrite, as in the lathy ferrite structure, the effect of the higher anodic currents in austenite could be more profound due to the austenite's limited surface area. Notice in Figure 2-8A how the austenite between the ferrite laths have completely dissolved. The as-deposited E308L weld was solution-treated to find out if the PWHT offers any improvement to its IGA resistance since it did not have any chromium carbides. The solution anneal was conducted at 1066°C (1950°F) for one hour, which is the same process used for the CF3 and CF8 plates in the foundry. A ThermoCalc simulated equilibrium phase fraction plot of CF3/E308L, shown in Figure 2-22, confirms the solution anneal temperature lies in the austenite phase field. Since the solution treatment happens in the austenite phase field, more ferrite transforms to austenite during the process and there also appears to be some coalescing and spheroidization of the ferrite, which would serve the purpose of reducing interfacial energy. AghaAli et al. observed similar changes in ferrite volume fraction and shape during multi-pass welding of 316L.[35] The morphological change described above is confirmed in the image of solution annealed E308L weld shown in Figure 2-23. The solution annealed weld was put through the DL-EPR test and it showed no reactivation. Considering that there was no chromium carbide-induced sensitization before the heat treatment, the improvement in corrosion resistance is attributed to the change in ferrite amount and morphology, which eliminates small areas of austenite sandwiched between ferrite. Thus, it appears that the PWHT improves the corrosion resistance of the as-deposited E308L weld by changing its ferrite morphology and amount rather than dissolving carbides.

The CF8C showed good resistance to sensitization. Only the medium heat input sample reactivated with a DOS of $9.7x10^{-4}$, and all the samples showed only sparse boundary dissolution. The DOS of a CF8C sample thermally cycled four times at 3.75kJ/mm increased to $1.51x10^{-3}$, suggesting the alloy becomes susceptible under multi-pass welding conditions. However, the DOS is still low according to Majidi's criterion[27]. The ability to avoid PWHT for a niobium-stabilized stainless steel will not be comprehensive without considering the possibility of knife-line attack (KLA). Since the HAZ experiences peak temperatures from the liquidus to room temperature, there is always a slim band right next to the fusion line where the temperature is high enough to dissolve the niobium carbides and keep niobium in solution due to the rapid cooling conditions.[36,37] The referenced dissolution of NbC in CF8C was simulated with a ThermoCalc equilibrium phase fraction plot, which predicted NbC carbide to dissolve around 1290°C. Li et al. also confirmed NbC dissolution in their investigation of NbC dissolution kinetics in 347 stainless steels.[38] This area now becomes susceptible to IGA if heated to the sensitization temperature range. For this reason, manufacturers of such alloys usually recommend a stabilization treatment after welding to ensure maximum corrosion resistance. This is done by holding the alloy between 900°C and 1000°C for a specified period followed by water quenching.[39–41] Even if CF8C resists sensitization in welding, the post-weld stabilization treatment defeats the aim of "no PWHT". The E347 exhibited a corrosion pattern similar to that observed for E308L. Here too there is localized corrosion in the austenite around the ferrite even in the as-welded condition. The ferrite appears preserved while only the austenite is attacked as would happen in a galvanic couple. Sensitization typically causes chromium depletion in both phases and leads to dissolution in both. Available literature on solidification of E347

suggests that the weld is not sensitized in the as-deposited state.[42,43] The authors believe this to be due to galvanic attack as explained for E308L. An as-welded E347 sample was solution annealed and then inspected in the SEM. The same ferrite morphology change observed in the E308L was seen here too. The skeletal and lathy ferrite structure in the weld changed to isolated and mostly circular islands of ferrite. There was also more proliferate NbC precipitation, suggesting that the "solution treatment" is more a stabilization treatment for the weld. This sample did not reactivate in the DL-EPR test and showed no boundary dissolution. Thus, the PWHT serves as a stabilization treatment for the weld by promoting NbC formation and improving corrosion resistance.

The CF3MN presented the best resistance to sensitization among the alloys tested. None of the samples reactivated, including the one sensitized at 675°C for two and half hours. The CF3MN alloy is essentially CF3 with molybdenum and nitrogen additions, which are proven here to have significant impact on sensitization resistance. Molybdenum is added to stainless steel mainly to improve pitting resistance by stabilizing the protective oxide layer.[44,45] Although not often recognized, Mo also limits anodic dissolution even in the active state.[46,47] Figure 2-24 shows all the DL-EPR curves for the base metals sensitized at 3.75kJ/mm. Notice that the forward scan peak current is around 20mA - 40mA for all the samples except CF3MN, which is one order of magnitude lower. The same trend was observed for the welds, where peak current for E316L was one order of magnitude lower than E308L and E347. Stansbury et al.[46] and Pardo et al.[47] also noticed in their investigations that Mo-containing stainless steels had lower active dissolution currents. In a sensitized material, intergranular attack occurs in the active region by anodic dissolution of the chromium depleted area. Molybdenum thus enhances IGA resistance by limiting the

anodic current from the chromium-starved areas. Nitrogen is added to austenitic stainless steels for pitting corrosion resistance[48,49] and to duplex stainless steels as an austenite stabilizer.[50,51] Nitrogen also improves sensitization resistance by retarding chromium diffusion in austenite.[12] In sensitized nitrogen-bearing dual phase stainless steels, ferrite becomes the sole source of chromium for chromium-rich carbides,[12] and this accounts for the observed dissolution only in the ferrite in the CF3MN sample in Figure 2-16B. Due to the high chromium content in ferrite and chromium's fast diffusion in ferrite, the depletion caused by the carbide is thought to be replenished quicker in ferrite than in the austenite, so that the final chromium profile is not as steep as usually seen in sensitized materials.[12] The E316L samples also did not reactivate in the corrosion test. Examination in the SEM showed general corrosion in the austenite, unlike the localized dissolution noticed in E308L and E347. The Mo in 316L is believed to have inhibited anodic dissolution during the reverse scan. The fact that cathodic current dominated the reverse scan signifies that anodic dissolution was present but insignificant. This contrasts with what happens in E308L and E347 where anodic current exceeds the cathodic component during the reverse scan. The CF3MN/E316L pair possesses the potential to be used in the as-welded state without significant concerns for intergranular corrosion. The authors however recommend testing a multi thermally cycled E316L sample and subjecting the base metal/weld metal pair to other sensitization tests like the weight loss tests in ASTM A262 to corroborate the results obtained here.

A summary of the PWHT recommendations from the discussion so far is presented in Table 2-2.

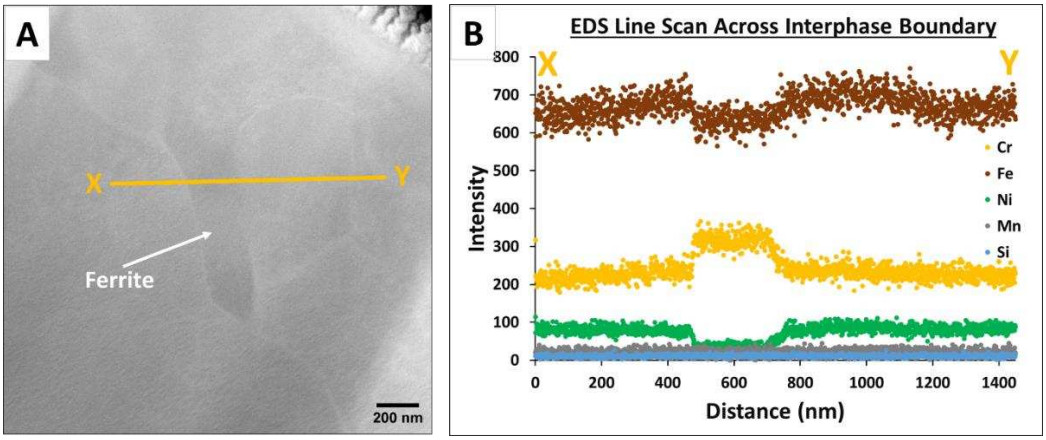

Figure 2- 19: TEM examination of austenite-ferrite boundary in as-deposited E308L weld. (A): HAADF image of ferrite pool in as-deposited E308L (B): EDS line scan across ferrite in 19A.

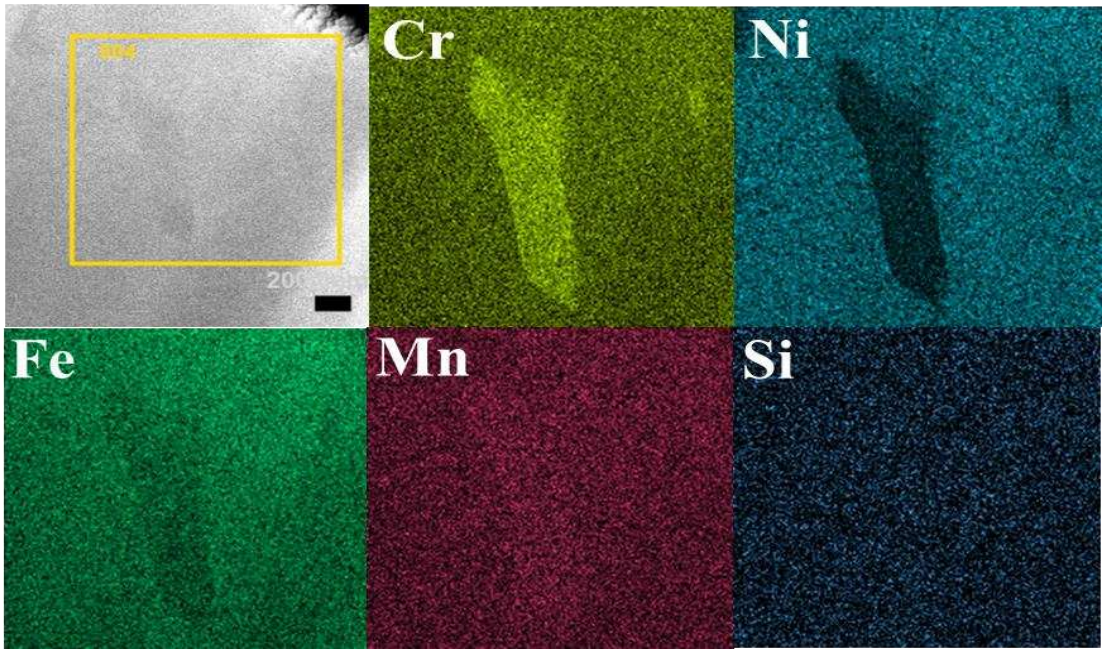

Figure 2- 20: A TEM-EDS map of ferrite pool in as-deposited E308L showing chromium enrichment in the ferrite. No chromium depletion associated with chromium carbide precipitation was detected.

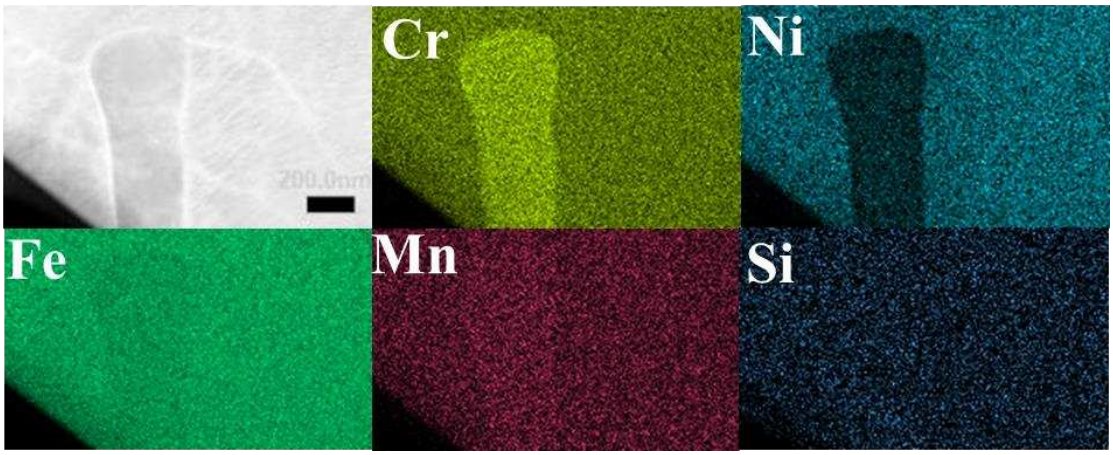

Figure 2- 21: A TEM-EDS map of ferrite pool in as-deposited E308L showing chromium enrichment in the ferrite. No chromium depletion associated with chromium carbide precipitation was detected.

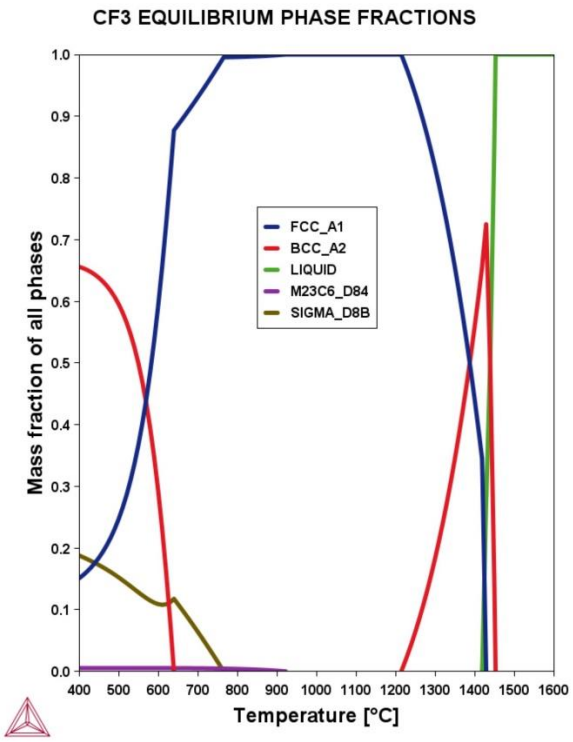

Figure 2- 22: Equilibrium phase fraction plot of CF3/E308L calculated with ThermoCalc 2024a.

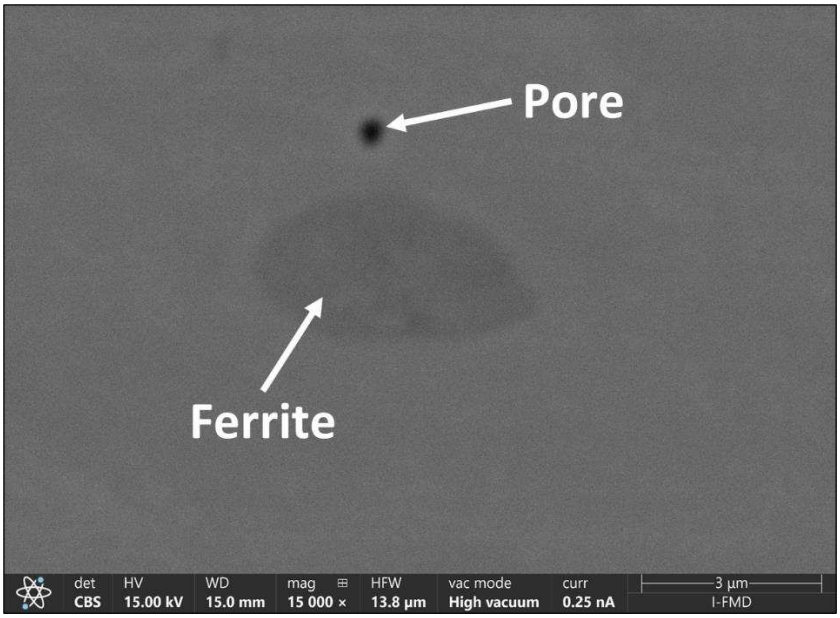

Figure 2- 23: SEM image of "spheroidized" ferrite in solution annealed E308L.

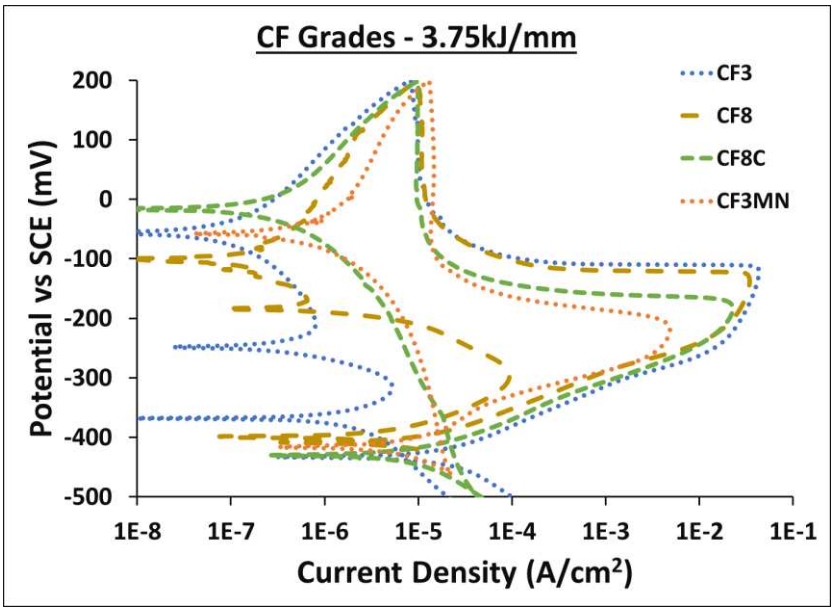

Figure 2- 24: DL-EPR plot of different CF grades thermally cycled with a heat input of 3.75kJ/mm.

Table 2- 2: Summary of PWHT recommendations.

Base metal/Weld metal	Description	PWHT Recommendation	Comments
CF8/E308L	High C	Maintain PWHT requirement	▪ Significant dissolution observed in base metal and weld metal.
CF3/E308L	Low C	Maintain PWHT requirement	▪ Light dissolution observed in base metal. May be used without PWHT in mild environments. ▪ Significant dissolution observed in weld metal.
CF8C/E347	Nb-stabilized	Maintain PWHT requirement	▪ Light dissolution observed in base metal. May be used without PWHT in mild environments. ▪ Significant dissolution observed in weld metal. ▪ PWHT also serves as stabilization treatment for base metal.
CF3MN/E316L	Low C + Mo + N	PWHT can potentially be waived. More extensive testing needed	▪ No interphase boundary dissolution observed in base metal. ▪ Light uniform corrosion observed in austenite phase in weld metal.

Alloying Additions that Promote Sensitization Resistance

Table 2-3 below ranks the alloys tested in increasing order of sensitization resistance from the top of the table to the bottom, based on the DOS values and SEM examination. The CF8 alloy had the least resistance, CF3 and CF8C had good resistance, and the CF3MN alloy had the best resistance to sensitization. The CF3MN alloy's excellent resistance is attributed to its low carbon, and molybdenum and nitrogen additions. The effects of these alloying additions on sensitization factors were investigated with thermodynamic and kinetic modelling.

A well-known effect of increasing carbon concentration is that it accelerates growth of the chromium carbides. Apart of its effect on growth kinetics, carbon concentration could also have thermodynamic effects, which area has not received as much attention in research. The thermodynamic effects of carbon concentration were studied by simulating dissolution temperature and equilibrium volume fraction of $M_{23}C_6$ in a hypothetical CF grade (Fe-19Cr-9Ni) with carbon additions from 0wt% to 0.1wt%. Plots like the one shown in Figure 2-25 were made with ThermoCalc for each composition, from which dissolution temperature and equilibrium volume fraction were obtained as demonstrated in the figure. The data was then plotted against carbon concentration as shown in Figure 2-26. The simulation exercise suggests that $M_{23}C_6$ is more stable at high carbon concentrations and therefore has higher dissolution temperatures and volume fraction. Lowering carbon concentration will thus improve sensitization resistance by, among other things, reducing the dissolution temperature and volume fraction of the $M_{23}C_6$.

It has been suggested in literature, based on the results of corrosion tests, that adding up to 0.2wt% nitrogen to austenitic stainless steels improves sensitization resistance by slowing down chromium diffusion in austenite. To look at the matter more directly, Dictra was used to simulate Cr homogenization in a Fe-19Cr-9Ni-0.03C steel with nitrogen additions from 0wt% to 1wt%. The Cr index of residual segregation was then calculated and graphed against nitrogen concentration. Homogenization heat treatments are performed to rectify the uneven distribution of elements in an alloy after non-equilibrium solidification. Index of residual segregation, δ, is used to check the level of segregation after a period of homogenization. It is calculated with the formula $\frac{C_M - C_m}{C_M^o - C_m^o}$, where $C_M^o \; and \; C_m^o$ are the initial maximum and minimum concentrations respectively, while $C_M \; and \; C_m$ are the

instantaneous maximum and minimum concentrations respectively. Chromium's residual segregation index is used here as a measure of its mobility in the presence of varying nitrogen concentration. A high Cr index of segregation indicates slow Cr diffusion, while a low one represents fast Cr diffusion. The simulation covers Cr homogenization at 1200°C, in the austenite and ferrite phases in a hypothetical 19Cr-9Ni-0.03C-Fe alloy, with initial Cr concentration profile of 14wt% to 24wt%, over a distance of 10μm. Figures 2-27A and 2-27B are the simulated Cr concentration profiles for nitrogen additions of 0.1wt% and 1wt% respectively, after 0, 10, 100, 1000, and 3600 seconds. The 3600s curve is clearly steeper in the 1wt% N alloy, indicating slower chromium diffusion. These plots were repeated for nitrogen concentration from 0wt% to 1wt% in 0.1wt% increments. Index of residual segregation was then calculated and plotted against nitrogen concentration for the austenite and ferrite phases in Figures 2-28A and 2-28B. As seen in the figures, the Cr index of residual segregation generally increases with nitrogen in the austenite phase. In the ferrite, nitrogen is not predicted to make a significant impact as all times beyond ten seconds have a δ of zero. This is likely due to the rapid diffusion of chromium in ferrite. The effect of nitrogen concentration on Ni and Fe diffusion was also checked with the same method to determine if this diffusion-related effect is peculiar to chromium. Figures 2-29A and 2-29B show the influence of nitrogen concentration on nickel index of residual segregation in the austenite and ferrite phase respectively, while Figures 2-30A and 2-30B show the influence of nitrogen concentration on iron index of residual segregation in austenite and ferrite respectively. An initial nickel concentration profile of 4wt% to 14wt% was used for the nickel homogenization simulation, while 67wt%Fe to 77wt%Fe was used for the iron homogenization simulation. Diffusion distance and homogenization

temperature were 10μm and 1200ºC respectively. The plots predict that nickel diffusion in austenite is independent of nitrogen concentration, while iron diffusion increases with nitrogen concentration. The simulations also predict that iron and nickel diffusion in ferrite are not significantly affected nitrogen concentration. In both ferrite plots, the nickel and iron initial concentration profiles are completely homogenized for all times greater than ten seconds. The simulation results suggest that, of the three main elements in a basic CF grade (i.e. Fe, Cr, Ni), nitrogen only impedes chromium mobility. Nitrogen likely achieves this by reacting with chromium to form chromium nitride. Stansbury et al. found CrN in sensitized nitrogen-bearing CF grades, they hypothesized that forming CrN was more beneficial for sensitization resistance than $Cr_{23}C_6$ because the former had a smaller Cr-depletion zone.[46] Thermodynamic simulation also confirms CrN as one of the equilibrium phases in CF3MN.

Molybdenum's effect in limiting active corrosion current has already been discussed in earlier paragraphs. Whiles some researchers suggest this effect could be due to molybdenum impeding chromium diffusion, others also attribute it to a molybdenum oxide layer present in the active region. The same kinetic simulation described in the preceding paragraph was used to investigate the effect of molybdenum concentration on chromium diffusion. The results, shown in Figures 2-31A and 2-31B, predict that molybdenum concentration has no effect on the rate of chromium diffusion in the austenite and ferrite phases in a Fe-19Cr-9Ni-0.03C alloy. From these results, molybdenum's influence in curtailing active corrosion current does not appear to be diffusion-related. It could be due to the molybdenum oxide found by Pardo et al.[47]

Table 2- 3: Ranking of alloys' sensitization resistance. Listed from least resistant at the top of the table to most resistant at the bottom of the table.

Alloy	Description	Phases	Low Heat Input DOS	Intermediate Heat Input DOS	High Heat Input DOS	SEM Examination
CF8	High C	Austenite + Ferrite	2.77×10^{-3}	4.11×10^{-3}	9.37×10^{-3}	Significant interphase boundary dissolution
CF3	Low C	Austenite + Ferrite	No Reactivation	2.25×10^{-4}	1.36×10^{-4}	Light interphase boundary dissolution
CF8C	Nb-stabilized	Austenite + Ferrite	No Reactivation	9.74×10^{-4}	No Reactivation	Light interphase boundary dissolution
CF3MN	Low C Mo N	Austenite + Ferrite	No Reactivation	No Reactivation	No Reactivation	No interphase boundary dissolution

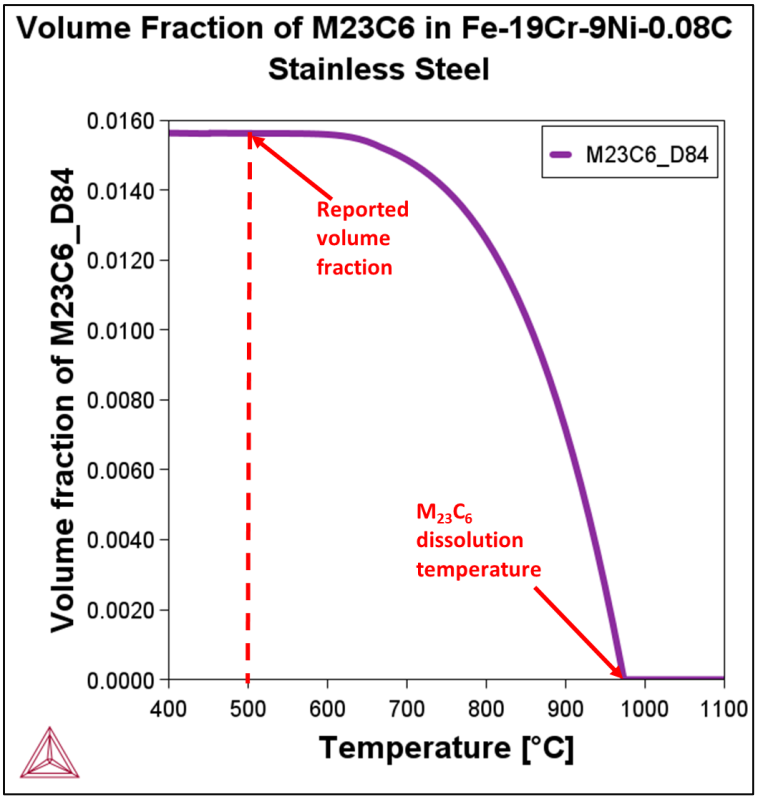

Figure 2- 25: Equilibrium phase fraction plot for M23C6 in Fe-19Cr-9Ni-0.08C Simulated with ThermoCalc 2024A.

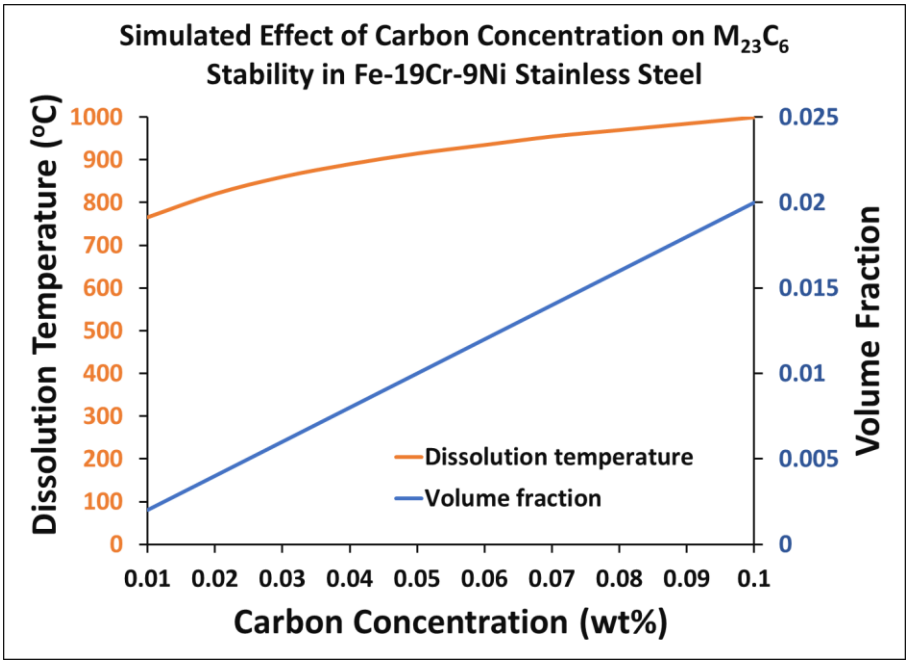

Figure 2- 26: Effect of carbon content on dissolution temperature and volume fraction of M23C6 in a Fe-19Cr-9Ni alloy.

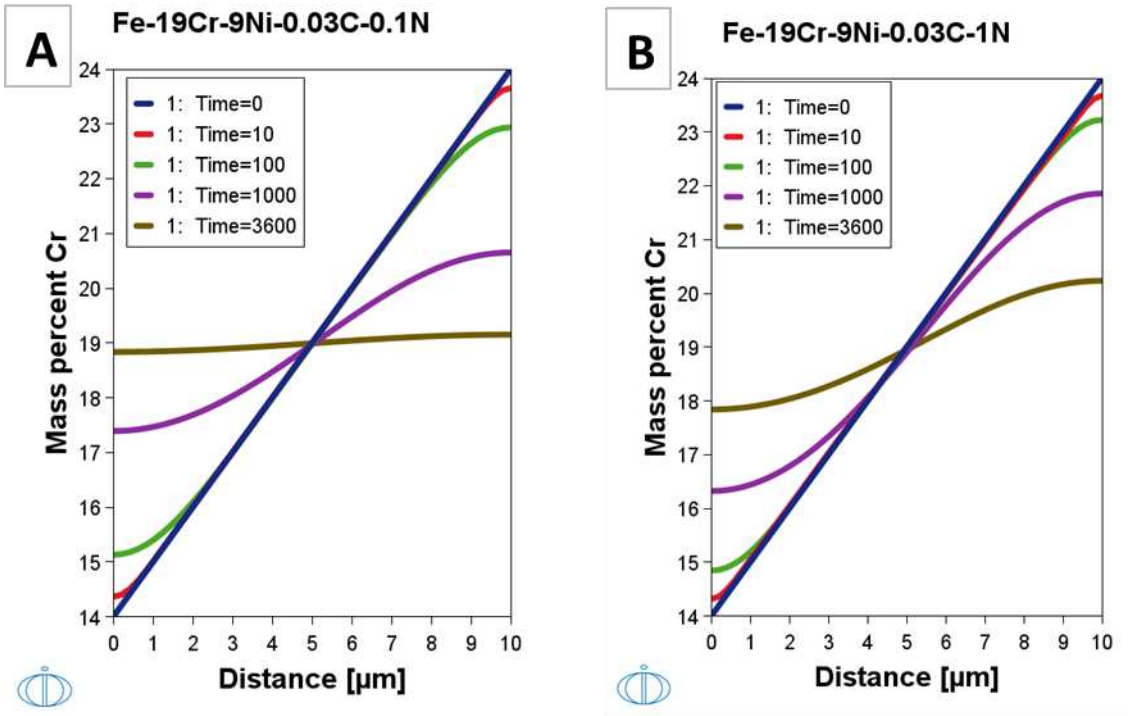

Figure 2- 27: Simulated Cr concentration profiles during homogenization of Fe-19Cr-9Ni-0.03C with different nitrogen additions. (A): 0.1wt% N. (B): 1wt% N.

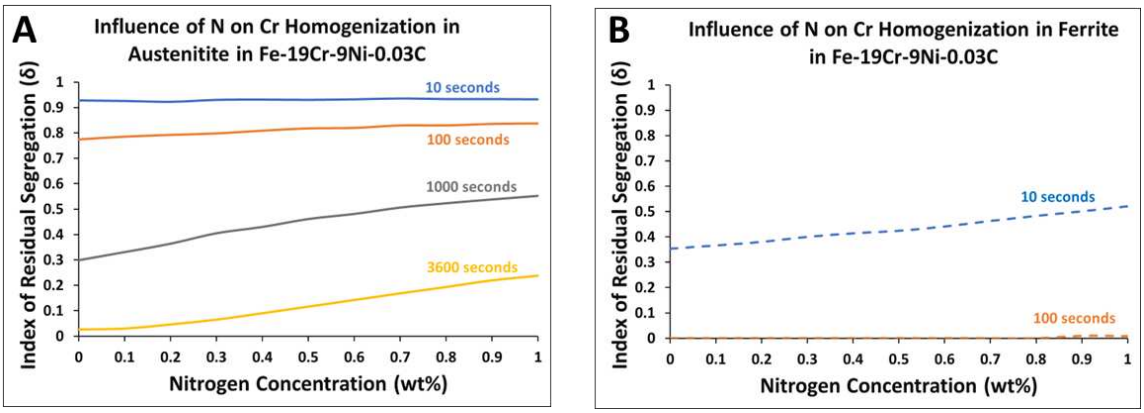

Figure 2- 28: Simulated influence of nitrogen content on Cr homogenization in Fe-19Cr-9Ni-0.03C. (A): Cr homogenization in austenite. (B): Cr homogenization in ferrite.

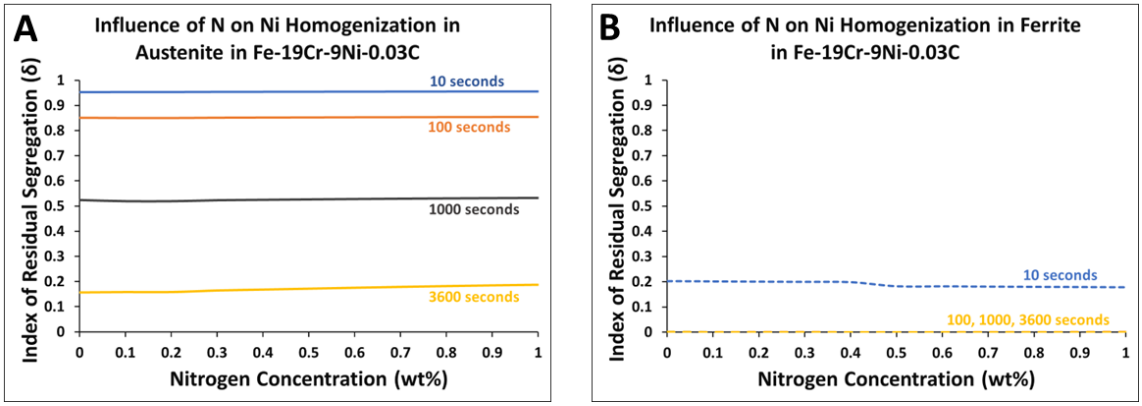

Figure 2- 29: Simulated influence of nitrogen content on Ni homogenization in Fe-19Cr-9Ni-0.03C. (A): Ni homogenization in austenite. (B): Ni homogenization in ferrite.

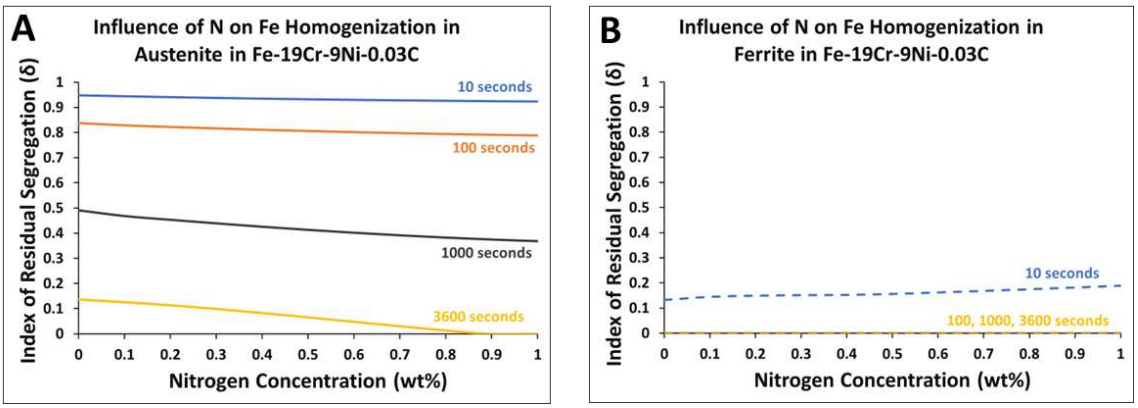

Figure 2- 30: Simulated influence of nitrogen content on Fe homogenization in Fe-19Cr-9Ni-0.03C. (A): Fe homogenization in austenite. (B): Fe homogenization in ferrite.

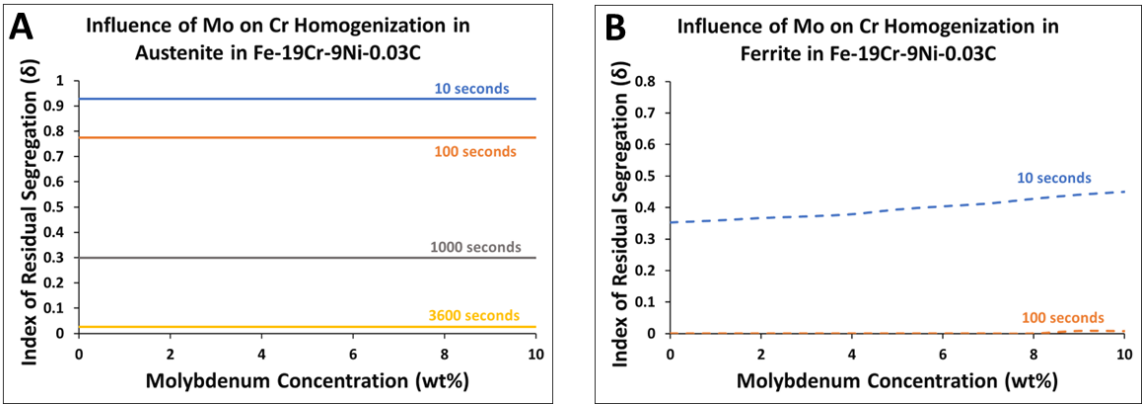

Figure 2- 31: Simulated influence of nitrogen content on Mo homogenization in Fe-19Cr-9Ni-0.03C. (A): Mo homogenization in austenite. (B): Mo homogenization in ferrite.

Conclusion

Different CF stainless steel base metals together with their weld metals were examined under different welding conditions for susceptibility to sensitization. The goal is to determine if any of the base metal/weld metal pairs can be deployed in service without post weld heat treatment. This investigation found that:

1. Though touted as sensitization-resistant, the low carbon grade (CF3) exhibited low DOS values under all heat input conditions and was considered mildly sensitized with evidence of interphase boundary attack. Depending on the service conditions, samples that exhibit such low levels of corrosion may be deployed without PWHT. However, the PWHT requirements in the ASTM standards were recommended to be maintained to ensure maximum corrosion resistance. The welds made with E308L filler metal exhibited higher DOS values due to preferential attack in the austenite. Post weld heat treatment is believed to improve the intergranular corrosion resistance of the E308L weld by changing the ferrite amount and morphology. It was concluded that both the CF3 base metal and E308L weld benefit from the PWHT.

2. The niobium stabilized CF8C grades showed sparse interphase boundary attack under all heat input levels and are considered quite resistant. However, stabilized grades often require a post-weld stabilization heat treatment to prevent knife-line attack, which defeats the goal of avoiding PWHT. The E347 welds exhibited higher DOS values than the CF8C base metal due to localized preferential attack of austenite in the weld. Post weld heat treatment is believed to improve the intergranular corrosion resistance of the E347 weld by changing the ferrite amount and morphology, and serving as a stabilization treatment.

3. The nitrogen-bearing CF3MN base metal and the welds made with E316L filler metal did not reactivate in the corrosion test. They also did not show any interphase

boundary attack after the test. This pair presented the best chance to waive PWHT. More extensive corrosion tests are recommended for this base metal/weld metal pair to generate more comprehensive data on PWHT requirements.

References

1. A.J. Sedriks: Corrosion of Stainless Steels, 2nd edition., John Wiley & Sons Inc, New York, NY, 1996.
2. R.J. Schmitt and C.X. Mullen: in Stainless Steel for Architectural Use, ASTM International100 Barr Harbor Drive, PO Box C700, West Conshohocken, PA 19428-2959, 1969, pp. 124–36.
3. D.A. Jones: Principles and Prevention of Corrosion, 2nd edition., Prentice Hall, Upper Saddle River NJ, 1996.
4. M. Blair: in Properties and Selection: Irons, Steels, and High-Performance Alloys, ASM International, 1990, pp. 908–29.
5. C.P. Dillon: Corrosion Resistance of Stainless Steels, 1st edition., Marcel Dekker Inc, New York, NY, 1995.
6. J. Lippold and D. Kotecki: Welding Metallurgy and Weldability of Stainless Steels, 1st edition., John Wiley & Sons, Inc, Hoboken, New Jersey, 2005.
7. T.M. Devine: Corros Sci, 1990, vol. 30, pp. 135–51.
8. E.A. Trillo and L.E. Murr: Acta Materalia, 1998, vol. 47, pp. 235–45.
9. R.M. Davison, T. DeBold, and M.J. Johnson: in ASM Handbook, Volume 13A Corrosion: Fundamentals, Testing, and Protection, vol. 13A, ASM International, Materials Park OH, 1987.

10. R. Ayer, C.F. Klein, and C.N. Marzinsky: Metallurgical Transactions A, 1992, vol. 23, pp. 2455–67.
11. P. Aneesh Kumar, S.P. Kumaresh Babu, and B. Thirumaran: J Test Eval, 2019, vol. 47, pp. 3690–704.
12. Steel Founders Society of America: The Role of Nitrogen in the Corrosion Behavior of Cast Austenitic and Duplex Stainless Steels, Des Plaines IL, 1988.
13. A. Poonguzhali, M.G. Pujar, and U. Kamachi Mudali: J Mater Eng Perform, 2013, vol. 22, pp. 1170–8.
14. N. Parvathavarthini and R.K. Dayal: Journal of Nuclear Materials, 2010, vol. 399, pp. 62–7.
15. M.A. Streicher: Corrosion, 1958, vol. 14, pp. 19–30.
16. Steel Founders Society of America: Sensitization Behavior of Cast Stainless Steels Subject to Weld Repair, Des Plaines IL, 1984.
17. Lawrence Livermore National Laboratory: An Overview of Low Temperature Sensitization, Livermore CA, 1983.
18. M.J. Povich: Corrosion, 1978, vol. 34, pp. 60–5.
19. J.L. Mitchiner, S.D. Kleban, B. V Hess, K.W. Mahin, and D. Messink: Proceedings of the AI and Manufacturing Research Planning Workshop, 1996, pp. 129–35.
20. C.F. Willis, R. Gronsky, and T.M. Devine: Metallurgical Transactions A, 1991, vol. 22A, pp. 2889–902.
21. H. Kokawa, M. Shimada, and Y.S. Sato: JOM, 2000, vol. 52, pp. 34–7.
22. Y. Zhou, K.T. Aust, U. Erb, and G. Palumbo: Scr Mater, 2001, vol. 45, pp. 49–54.

23. M.A. Streicher: in Intergranular Corrosion of Stainless Steels, ASTM STP 656, R.F. Steigerwald, ed., ASTM International, 1978, pp. 3–84.
24. S. Fajardo and G.S. Frankel: Electrochem commun, 2017, vol. 84, pp. 36–9.
25. S.S.M. Tavares, M.T.G. de Sampaio, G. Perez, B.B. de Almeida, and E.A. Ponzio: Materials and Corrosion, 2022, vol. 73, pp. 866–75.
26. L. Sun, Y. Sun, C. Lv, Y. Liu, N. Dai, Y. Jiang, J. Li, and D.D. Macdonald: Corros Sci, 2021, vol. 185, p. 109432.
27. A.P. Majidi and M.A. Streicher: Corrosion, 1984, vol. 40, pp. 584–93.
28. W.L. Clarke and R.L. Cowan: The EPR Method for the Detection of Sensitization in Stainless Steels, Palo Alto, 1980.
29. C.F. Willis: A Study of Chromium Carbide Precipitation at Interphase Boundaries in Stainless Steel Welds, Berkeley CA, 1990.
30. C.L. Leone and H.W. Kerr: Weld J, 1982, vol. 61, pp. 13s–21s.
31. T. Takalo, N. Suutala, and T. Moisio: Metallurgical transactions A, 1979, vol. 10A, pp. 1173–81.
32. S.A. David: 62nd AWS Annual Meeting in Cleveland OH April 1981, 1981, pp. 61s–71s.
33. C.F. Willis, R. Gronsky, and T.M. Devine: Metallurgical Transactions A, 1991, vol. 22A, pp. 2889–902.
34. J.R. Myers, F.H. Beck, and M.G. Fontana: Corrosion, 1965, vol. 21, pp. 277–87.
35. A. AghaAli, M. Farzam, M.A. Golozar, and I. Danaee: Materials & Design , 2014, vol. 54, pp. 331–41.
36. M.L. Holzworth, F.H. Beck, and M.G. Fontana: Corrosion, 1951, vol. 7, pp. 441–9.

37. M.G. Fontana: Ind Eng Chem, 1952, vol. 44, pp. 87A-90A.
38. L. Li and R.W. Messler: Metallurgical and Materials Transactions A, 2002, vol. 33A, pp. 2031–42.
39. V. Moura, A.Y. Kina, S.S.M. Tavares, L.D. Lima, and F.B. Mainier: J Mater Sci, 2008, vol. 43, pp. 536–40.
40. A.Y. Kina, V.M. Souza, S.S.M. Tavares, J.A. Souza, and H.F.G. de Abreu: J Mater Process Technol, 2008, vol. 199, pp. 391–5.
41. R. Barbosa Gonçalves, P. Henrique Dias de Araújo, F. José Villela Braga, L. Augusto Hernandez Terrones, and R. Pinheiro da Rocha Paranhos: Welding International, 2017, vol. 31, pp. 196–205.
42. B.A. Senior: Materials Science and Engineering, 1988, vol. 100, pp. 219–27.
43. C.D. Lundin, C.H. Lee, R. Menon, and V. Osorio: AWS 66th Annual Meeting, Las Vegas, NV, 1985, pp. 35s–46s.
44. H.Y. Ha, T.H. Lee, J.H. Bae, and D.W. Chun: Metals (Basel), 2018, vol. 8, p. 653.
45. Y.-T. Sun, X. Tan, L.-L. Lei, J. Li, and Y.-M. Jiang: Tungsten, 2021, vol. 3, pp. 329–37.
46. Steel Founders' Society of America: Sensitization Behavior of Cast Stainless Steels Subject to Weld Repair, Des Plaines IL, 1984.
47. A. Pardo, M.C. Merino, A.E. Coy, F. Viejo, R. Arrabal, and E. Matykina: Corros Sci, 2008, vol. 50, pp. 780–94.
48. U.K. Mudali, R.K. Dayal, J.B. Gnanamoorthy, and P. Rodriguez: Materials Transactions, JIM, 1996, vol. 37, pp. 1568–73.

49. R.F.A. Jargelius-Pettersson: Corros Sci, 1999, vol. 41, pp. 1639–64.

50. Z. Zhang, H. Jing, L. Xu, Y. Han, L. Zhao, and C. Zhou: Appl Surf Sci, 2017, vol. 404, pp. 110–28.

51. N. Sridhar and J. Kolts: Corrosion, 1987, vol. 43, pp. 646–51.

Chapter 3: PWHT-Free Cast CN Stainless Steel Grades

Abstract

Molybdenum-bearing nickel-rich stainless steels are popular in the chemical processing industry for their excellent resistance to pitting and chloride-induced stress corrosion cracking. The CN7M alloy and its low carbon version CN3MCu fall in this group, and additionally have great resistance to hot dilute sulfuric. This makes them popular for making components like pump and valve bodies used in harsh environments. Industry standards that regulate the production of these alloys require post weld heat treatment to restore corrosion resistance. Manufacturing processes for these castings will benefit from avoiding the post weld heat treatment (PWHT) since it can distort large machined castings, leading to high scrap rates and operational costs. This research used a combination of heat affected zone (HAZ) simulation, electrochemical corrosion tests, thermodynamic simulation, and energy dispersive spectroscopy (EDS) to comprehensively investigate sensitization resistance of the selected stainless steel grades in their base metal, heat affected zone, and weld fusion zone, under different welding conditions. Evidence of sensitization was found in the CN7M heat affected zone, and in the fusion zone of welds made with E320 filler metal even at low heat input levels. The CN3MCu/E320LR base metal/weld metal pair had no sensitization in the fusion zone and very little sensitization in the base metal heat affected zone. Results from thermodynamic and kinetic modelling suggest that adding nitrogen to CN3MCu could potentially improve its resistance to intergranular corrosion, and possibly permit the CN3MCu/E320LR base metal/ weld metal pair to be used without PWHT.

Introduction

The CN7M alloy was first developed by M.G. Fontana in 1935 to be used in applications that require sulfuric acid resistance.[1] It is part of a group of Ni-rich Cr-Mo-Cu fully austenitic stainless steels known for their excellent resistance to pitting corrosion and stress corrosion cracking.[2–4] It is often made into pump and valve bodies to be used in the chemical processing industry.[5] Despite these excellent properties, it was found susceptible to sensitization when exposed to the chromium carbide precipitate temperature range (500ºC – 900ºC) for sufficient periods.[6] Sensitization is the condition where chromium-rich carbides precipitate at grain boundaries in austenitic stainless steels, leading to a depletion of chromium in the area adjacent to the boundary.[7] The stability of the protective layer in stainless steels depends on chromium concentration, [8,9] therefore a reduction in chromium makes the oxide layer unstable and renders the area susceptible to corrosive attack. A low carbon version (CN3MCu) and a niobium-stabilized version (Alloy 20-Cb3) have since been developed to mitigate the alloy's susceptibility to sensitization, and there is evidence available in literature that point to the success of these alloys.[4,6] McCaul investigated a CN7MS alloy with a 0.02wt% carbon concentration and reported that it could be used in the as-welded state without any significant concern for intergranular attack (IGA).[6] He found that all the base and weld metal samples tested met the 1.22mm/year corrosion rate threshold set by Brown[10] as an indication of the absence of sensitization. Other researchers have also reported a corrosion rate of 0.10mm/year for Alloy 20-Cb3 in sulfuric acid concentrations up to 90% at different temperatures all below 100ºC.[11] Despite the successes of these alloys, the ASTM standards A743, 744, and A351, which regulate the production of these alloys, require post weld solution anneal for all stainless

steel grades it covers.[12–14] This requirement has been considered by some as redundant for certain grades considering their improved compositions and modern casting processes cable of producing steels with extremely low contaminant levels. Furthermore, heat treating large austenitic castings can dimensionally distort them because of the high thermal expansion of these alloys, leading to high scrap rates. In light of this, it has become necessary to consider modifying the PWHT requirements to reflect the current state of alloy performance. To accomplish this, a thorough investigation of the sensitization resistance of CN3MCu and CN7M is required. There is the need to establish the effect of different welding conditions in each region of a welded assembly. A review of available literature shows that previous sensitization studies are usually limited to the base metal or the heat affected zone (HAZ) or fusion zone.[15,16] Since the welded structure is deployed as a unit, it is necessary to establish the sensitization behavior of all weld regions, that includes the base metal, base metal heat affected zone (BM-HAZ), weld metal and weld metal heat affected zone (WM-HAZ). The fusion zone typically has residual element segregation not found in a solution annealed parent metal,[17,18] which is expected to significantly influence its sensitization kinetics. In that sense, the HAZ in the fusion zone (i.e., the re-heated weld metal) will behave differently from the HAZ in the base metal. Complete knowledge of the alloy's sensitization resistance is necessary to make generic PWHT recommendations. In addition, much work done so far in this area usually concludes that the improved compositions are unsensitized because they show low corrosion rates in weight loss tests.[6,19,20] While low corrosion rates are acceptable in most applications, they cannot be interpreted as the absence of sensitization. Boiling acid tests/weight loss tests measure intergranular attack through grain dropping, which happens when the entire circumference

of a grain dissolves. There must be enough attack to dislodge the grain before significant weight loss can be detected. Materials with large grains (like castings), that are not fully surrounded by the depletion layer may be erroneously judged as unsensitized since they will not drop many grains. A similar phenomenon applies to slightly sensitized samples where the depletion zone around the grain may not be wide enough to cause grain dropping. This consideration makes the weight loss method relatively insensitive to low levels of sensitization.[21,22] To modify PWHT requirements in the applicable standards, it is important that even mild levels of sensitization are detected. The type of corrosion associated with sensitization is termed intergranular corrosion (IGC), and occurs when sensitized material is exposed to a corrosive medium. The severity of the attack will depend on many factors including the extent of chromium depletion and the medium's corrosiveness.[23] Care must be taken in generalizing an alloy's corrosion resistance based on results obtained with a one medium under a specific set of conditions. Low corrosion rates in a medium does not guarantee that the alloy is only slightly sensitized, and even if it is, it can be still be attacked more aggressively in another medium. Thus, when establishing general PWHT needs, the focus must be to detect any occurrence of IGA associated with chromium carbide precipitation. The determination of a threshold corrosion rate that qualifies a material to be put in service without PWHT must be done by owners and suppliers based on the specific application. In this investigation, the double loop electrochemical potentiokinetic reactivation (DL-EPR) test was used as the corrosion testing method to indirectly detect chromium depletion since this test is known to be very sensitive to low levels of sensitization.[24–26] The DL-EPR test measures corrosion current emanating from areas of passive film breakdown during intergranular attack, and modern

electronics make it possible to measure current down to the nanoampere range, making it suitable for this investigation. This research aims to comprehensively examine all areas of the weld in alloys CN7M and CN3MCu with a sensitive corrosion test and microstructural examination to determine if the PWHT requirement can be waived under some conditions.

Experimental Procedure

Welding procedure specifications (WPS) designed for the alloys under investigation and other austenitic stainless steels were sourced from foundries around the USA to help tailor the weld simulations to industry practices. The CN7M base metal was paired with E320 weld metal, while CN3MCu base metal was paired with E320LR weld metal. The cast plates were received in the solution annealed condition. The solution treatment was done at 1177ºC (2150ºF) for two hours followed by water quenching. All-weld metal samples were made with the filler metals by overlaying weld beads on a 304L plate to a thickness of 32mm, Gleeble samples were then extracted from the top 16mm to avoid dilution from the 304L plate. The E320LR weld metal samples were made with gas metal arc welding (GMAW) using 100% Ar gas, 1.0kJ/mm heat input and 350ºF maximum interpass temperature. The E320 all-weld metal samples were made with submerge arc welding (SAW) using a Lincoln Electric P200 subarc flux, 1.0kJ/mm heat input and 350ºF maximum interpass temperature. The SAW process was used to avoid porosity that occurred when attempts were made to use the GMAW process. The E320 filler wire was custom-made for this project as it is hardly available commercially now. The lack of a standard manufacturing procedure may have led to the weld defects. The material

certificate provided by the electrode manufacturer indicated a silicon concentration of 0.27wt% in the E320 filler metal, which was suspected to be insufficient to fully deoxidize the weld. The flux was therefore chosen to further deoxidize the weld. The welds were made with a Miller Jetline automated welder.

Table I shows the chemical composition of the cast plates and deposited weld beads as determined with optical emission spectroscopy (OES). Nitrogen content was determined by inert gas infusion-thermal conductivity method.

Ten WPS's were received, all specifying different heat input ranges. For each WPS, the parameters that produced the highest heat input were used to generate heat affected zone thermal (HAZ) cycles in the SmartWeld program[27] with peak temperatures between 500°C and 900°C. The maximum interpass temperature specified in the WPS (350°F) was selected as the base metal's starting temperature. The total time spent in the sensitization range was calculated and plotted against peak temperature for each WPS as shown in Figure 3-1. For each WPS, thermal cycles that reached a peak temperature of 900°C were determined to be the most deleterious, i.e. the points in the HAZ that experienced these thermal cycles stayed the longest in the sensitization temperature range (500°C – 900°C). These harmful thermal cycles were selected for the heat input levels, 0.81kJ/mm, 1.78kJ/mm and 3.75kJ/mm, to be applied to base metal and weld metal samples in the Gleeble 3500 thermomechanical simulator. The Gleeble samples were φ12mm x 110mm long with threaded ends. All the Gleeble work was done under zero force conditions to avoid plastic deformation. After the thermal cycling, samples were cut at the point of thermocouple attachments, mounted and metallographically prepared.

Corrosion testing was accomplished with the Double Loop Electrochemical Potentiokinetic Reactivation (DL-EPR) test. Samples from the Gleeble were cut, mounted in conductive Bakelite powder and metallographically prepared with silicon carbide paper, diamond polishing compound and 0.05 micron colloidal silica. They were then thoroughly rinsed with ASTM type I deionized water to remove any contaminants. The corrosion tests were done with a Gamry 1010E potentiostat and Gamry ParaCell kit for flat specimens. Sample masks were used to isolate 1cm^2 of the sample surface for testing. They were then set up in the corrosion cell and allowed to stabilize for thirty minutes before testing. The potential scan was done at 1.67mV/s from the open circuit potential (OCP) to 200mV and back in a 2M H_2SO_4 + 0.5KCl solution at ambient temperature (approximately 24^{o}C). The OCP was usually between -300mV and -400mV, the auxiliary electrode used was saturated calomel electrode (SCE). Plots of potential vs current were made for each test. Peak current during the reverse scan, I_r was divided by the peak current during the forward scan I_a to establish a degree of sensitization (DOS).[28–30] The DOS is a measure of passive film break down during the reverse scan. The electrolyte was prepared with ASTM type I deionized water. After the corrosion test, the samples were lightly rinsed with deionized water and ethanol, dried and examined in the SEM.

Imaging was done in a Hitachi 4300 SEM with the backscattered electron detector and Everhart Thornley secondary electron detector. All EDS line scans and maps were taken with the EDS detector in the same equipment using 15kV accelerating voltage and 7.68μs process time

Electron Probe Microanalysis (EPMA) was used to measure concentrations of alloying elements across dendrites in the fusion zone using a JEOL JXA-8900. Fusion zone samples

were mounted in conductive Bakelite and metallographically prepared to a final finish with 50nm colloidal silica but were not etched. Measurements were made with a working distance of 11mm, accelerating voltage of 20kV and a beam current of 30nA. Monte Carlo simulations performed with WinXRay version 1.4.2.1 predicted an interaction volume of 2µm in the alloys under investigation.[31] An accelerating voltage higher than 20kV will generate an interaction volume upwards of 2µm, which will not exclusively sample some of the regions of interest. Quantification was done with the Xtreme Edition EPMA software v. 12.8.1 using the Armstrong/Love-Scott matrix correction procedure and ISO-9001 and 17025 certified metal standards.[32,33]

Table 3- 1: Chemical composition of base metals and deposited welds. All compositions in weight percent.

CHEMICAL COMPOSITION OF BASE METALS. All compositions in weight percent.												
	C	**Mn**	**P**	**S**	**Si**	**Cr**	**Ni**	**Mo**	**Nb**	**Cu**	**N**	**Fe**
CN3MCu	0.03	1.14	0.024	0.002	0.54	19.63	30.45	2.45	0.04	3.41	0.08	Bal
CN7M	0.09	0.96	0.023	0.031	0.63	20.07	29.01	2.25	0.03	3.86	0.08	Bal
CHEMICAL COMPOSITION OF DEPOSITED WELDS. All compositions in weight percent.												
E320LR	0.01	1.95	0.012	0.007	0.1	19.74	32.92	2.38	0.31	3.27	0.03	Bal
E320	0.04	0.66	0.023	0.008	0.42	16.78	36.02	2.17	0.69	4.22	0.03	Bal

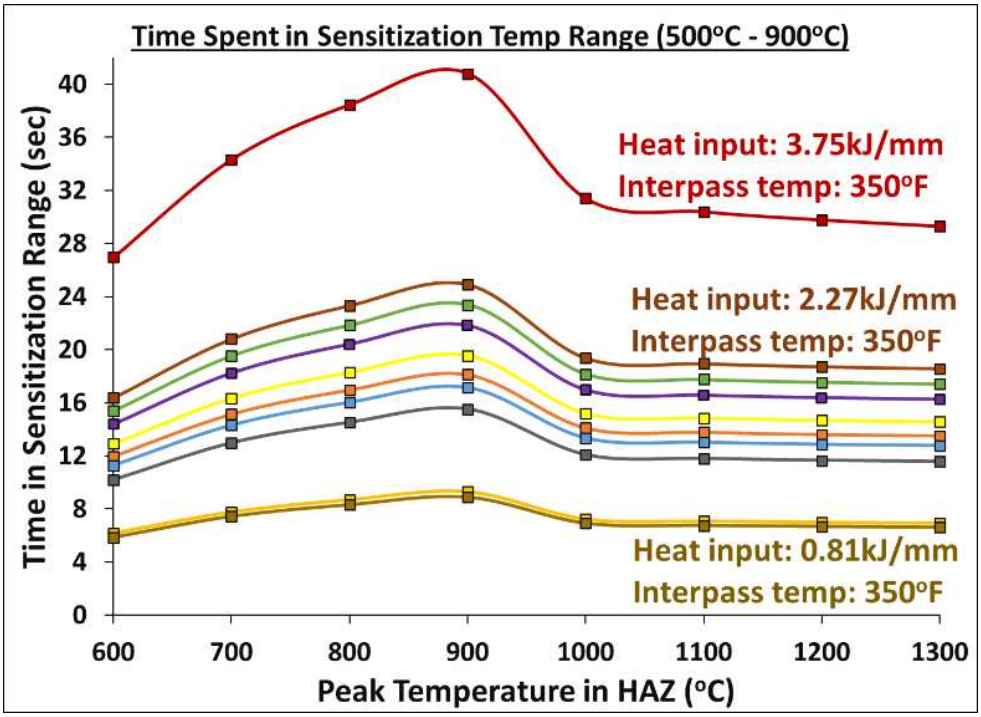

Figure 3- 1: Plot showing time spent in the sensitization temperature range for each peak temperature in the HAZ. Times were calculated from thermal cycles simulated with SmartWeld.

Results and Discussion

Corrosion Test Results

The DL-EPR test was done with 2M H2SO4 + 0.5M KCl because the alloys were found to be passive in the commonly used 0.5M + 0.01M KSCN solution. Replacing the potassium thiocyanate with potassium chloride lowered the open circuit potential into the active region to allow for the polarization test. Figures 3-2A and 2B show example plots for two types of results that can be obtained from the DL-EPR test. Figure 3-2A is the plot for CN3MCu thermally cycled at with a heat input of 1.78kJ/mm, where the sample produced a reactivation current I_r, while Figure 3-2B shows results for solution annealed CN3MCu

where there was no reactivation current. The absence of a reactivation current in the DL-EPR test is the best assurance of the absence of sensitization. As seen in both plots, the corrosion current varies by large factors depending on the applied potential. In the active region alone, the measured current spans the interval from 100nA to 1μA as seen in Figure 3-2A. Corrosion current density can vary dramatically depending on the specific redox reactions and the reaction conditions. For example, the exchange current density for H^+ reduction to H_2 is nine orders of magnitude higher on a platinum electrode than a mercury electrode.[1,34] The same reaction on a Hg electrode in a 5N HCl solution has an exchange current density one order of magnitude higher than in a 1N HCl solution.[1,34] Severely sensitized materials are therefore expected to produce current densities significantly higher than mildly sensitized or unsensitized materials. In this research, samples with DOS values of the same order of magnitude are considered similarly sensitized. Where there was no reactivation current, an anodic current of 100nA was assumed to calculate DOS. The corrosion current measured in the test is actually a net current.[35,36] In Figure 3-2B where there is no reactivation, the anodic current continuously decreases from the start of the reverse scan until it is overtaken by the cathodic current around -10mV, which then persists throughout the remainder of the test. The net cathodic current does not represent the absolute elimination of anodic reactions on the sample surface. Rather, it signifies that the anodic current is very small and has been overtaken by the cathodic component, which is nicely illustrated by the diminishing anodic current and eventual switch to cathodic current. The 100nA reactivation current used to calculate a DOS for such tests was selected to represent the rate of the residual anodic reaction during the period when the potentiostat measures a net cathodic current. The 100nA figure was selected because it is close to the

lowest anodic current measured (in this research) before the change over to a net cathodic current, suggesting that the residual anodic current is in the nanoampere range. This approach of accounting for a residual anodic current in "no reactivation tests" is consistent with the balance of reactions on the surface of the test sample. Other researchers assign a DOS of zero for "no reactivation" tests, which implies the complete absence of an anodic reaction during the period when the potentiostat measures a cathodic current.[37,38]

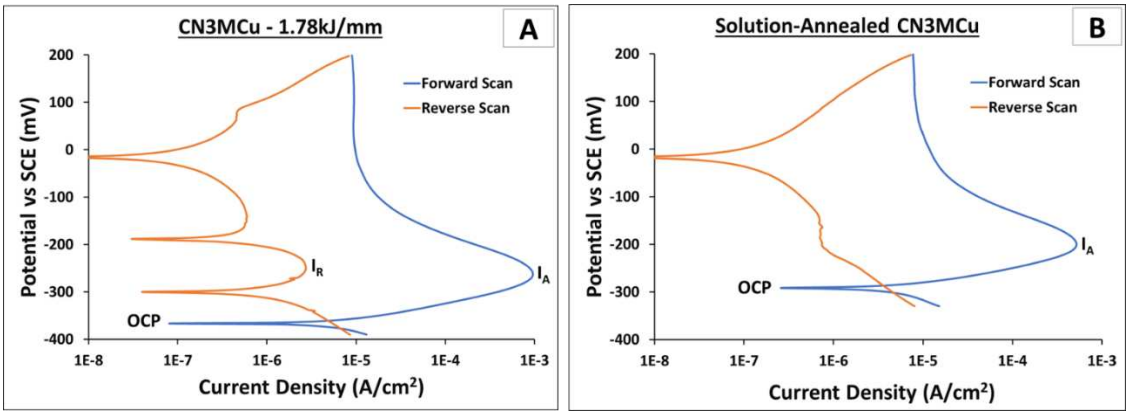

Figure 3- 2: Typical DL-EPR test plots showing potential vs log of current density (A): DL-EPR plot of CN3MCu sample thermally cycled with a heat input of 1.78kJ/mm showing reactivation during the reverse scan. (B): DL-EPR plot of solution annealed CN3MCu base metal showing no reactivation during reverse scan.

CN7M Base Metal and Welds Made with E320 Filler Metal

Figure 3-3 shows the DOS vs heat input plot for CN7M base metal (in blue) and weld metal made with E320 filler metal (in red). The DOS values are provided for as deposited weld metal along with thermally cycled base metal and weld metal, solution annealed base metal and sensitized base metal. The solution annealed and sensitized samples were included as controls to define the upper and lower bounds for sensitization of the material.

Sensitization treatments in this research were done at 675ºC for 2.5 hours, which is known to rapidly sensitize austenitic stainless steels.[39] As expected, the CN7M sensitizes easily because of its high carbon concentration. Even the solution-annealed samples exhibited some level of sensitization, suggesting that the solution treatment may not have been adequate. All the CN7M samples reactivated and generally had higher DOS values than the low carbon CN3MCu base metal. The risk of grain dropping is generally high in fully austenitic grades like these because at the chromium-rich carbides mostly precipitate at the austenite-austenite grain boundaries, unlike in dual-phase stainless steels where the austenite-ferrite interphase attracts most of the chromium carbides, leaving the austenite grain boundaries free of attack. No grain dropping was observed in the corrosion test samples, likely because the test only lasts about 15 minutes, which is not long enough to dislodge approximately 100μm-wide grains. In the weight loss tests where grain dropping is often observed, the samples are held at the acid's boiling temperature for periods ranging from 24 hours to 120 hours.[39] Figure 3-4 is a scanning electron microscope (SEM) image of CN7M sample thermally cycled with a heat input of 1.78kJ/mm. Figure 3-4A shows an austenite grain at low magnification, fully surrounded by dissolution, while Figure 3-4B shows the same phenomenon at a triple point at higher magnification. The particles at the grain boundary in Figure 3-4B are too small to be characterized in the SEM but they are suspected to be chromium carbides because an EDS map of similar grain boundary dissolution, shown in Figure 3-5, showed chromium and carbon enrichment at the boundary. All the welds made from E320 filler metal also reactivated, but with lower DOS values. This is likely due to the lower carbon concentration in the E320 deposited weld, which is only 0.04wt% C compared to 0.09wt% C in the CN7M base metal. The as-welded

E320 sample had the lowest DOS among the CN7M/E320 base metal/weld metal samples. Figures 3-6A and 3-6B are SEM images of the as-deposited E320 sample after the corrosion test. No chromium carbides were observed in the E320 weld, but it had a Mo and Nb rich secondary phase at grain boundaries around which scant and random dissolution occurred. No other grain boundary dissolution was observed in the E320 weld metal. The EDS map shown in Figure 3-7 confirms the Nb and Mo enrichment in the secondary phase. The low DOS of this sample is believed to come from the sparse dissolution associated with the secondary phase. The secondary phase is suspected to be laves based on simulation done with ThermoCalc and evidence found in literature.[40] The Scheil solidification simulation of welds made with E320LR and E320 filler metals are shown in Figures 3-8A and 3-8B respectively. Figure 3-8B, which is the plot for E320, predicts the formation of laves phase at the end of solidification. Niobium and molybdenum are both known to segregate to the liquid during solidification in super austenitic stainless steels,[41] so a Mo-Nb rich secondary phase forming at the end of solidification in a weld made with E320 agrees with the studied segregation behavior of this class of alloys. The thermally cycled E320 samples had higher DOS values than the as-welded E320 samples, and more grain boundary dissolution believed to be caused by the secondary phase and chromium carbides. Examples of the grain boundary attack observed in the E320 weld thermally cycled with a heat input of 1.78kJ/mm are shown in Figure 3-9A and 3-9B. The boundary attack is more severe than the sparse dissolution present in the as-welded E320. Overall, the CN7M/E320 pair will benefit from the post-weld heat treatment as the process will dissolve both the secondary phase and any chromium carbides present.

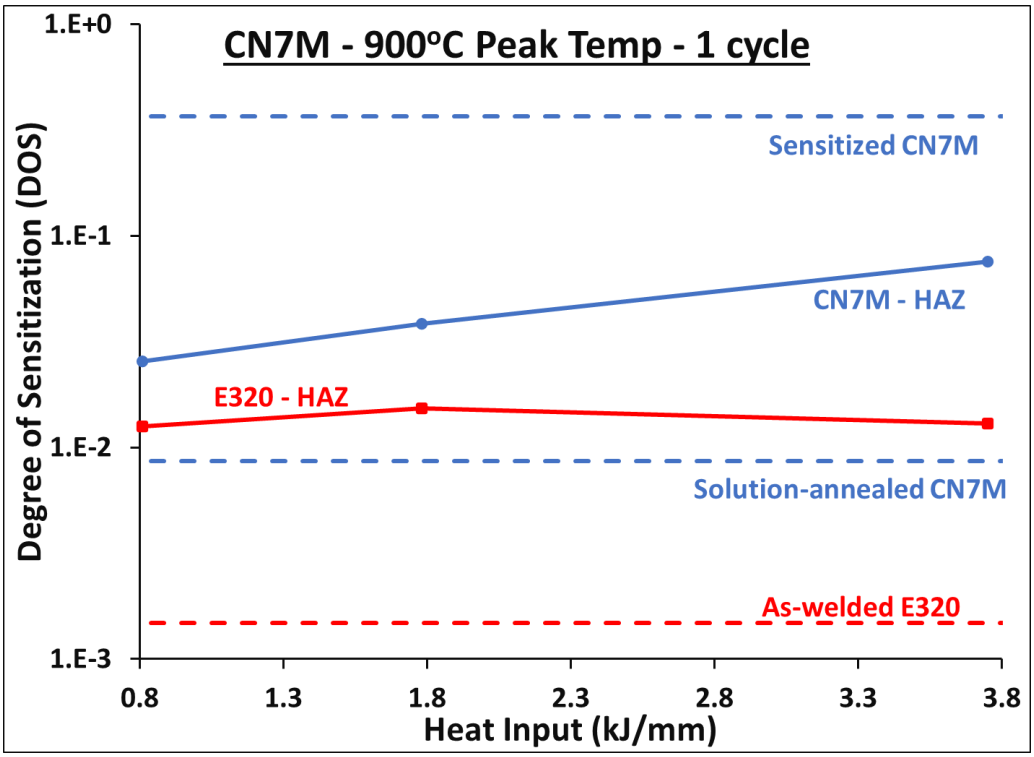

Figure 3- 3: Degree of sensitization (DOS) vs heat input plot for CN7M base metal and welds made with E320 filler metal.

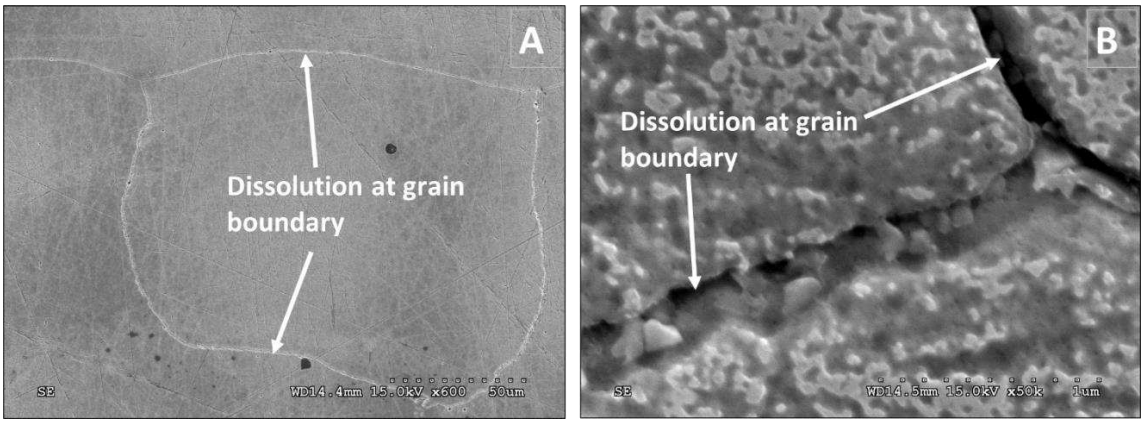

Figure 3- 4: Post-corrosion test SEM micrograph of CN7M base metal thermally cycled with a heat input of 1.78kJ/mm. (A): low magnification image of grain boundary dissolution. (B): high magnification image showing grain boundary dissolution at a triple point.

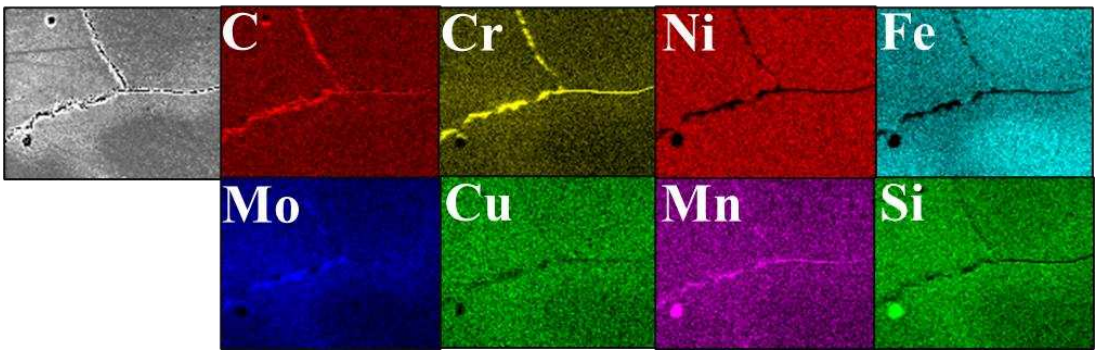

Figure 3- 5: An SEM-EDS map of a grain boundary triple point in sensitized CN7M base metal showing chromium and carbon enrichment at the grain boundary.

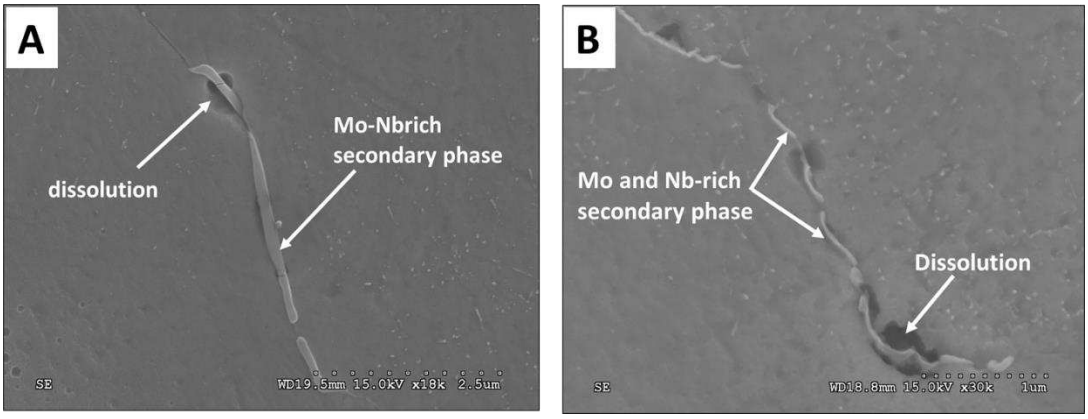

Figure 3- 6: SEM image of as-deposited welds made with E320 filler metal after corrosion testing. (A): Image of as-deposited weld showing sparse dissolution around secondary phase on a grain boundary. (B): Image of as-deposited weld showing sparse dissolution around secondary phase on grain boundary.

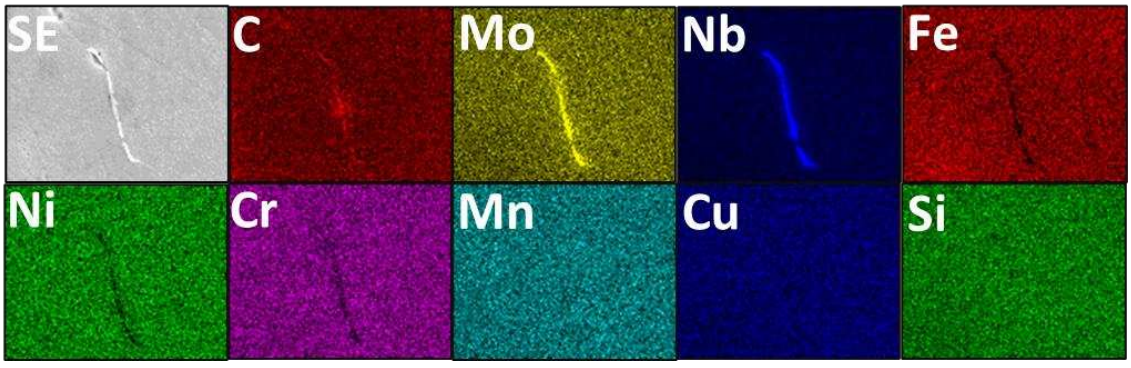

Figure 3- 7: SEM-EDS map of Nb-Mo rich secondary phase in as-deposited weld made with E320 filler metal.

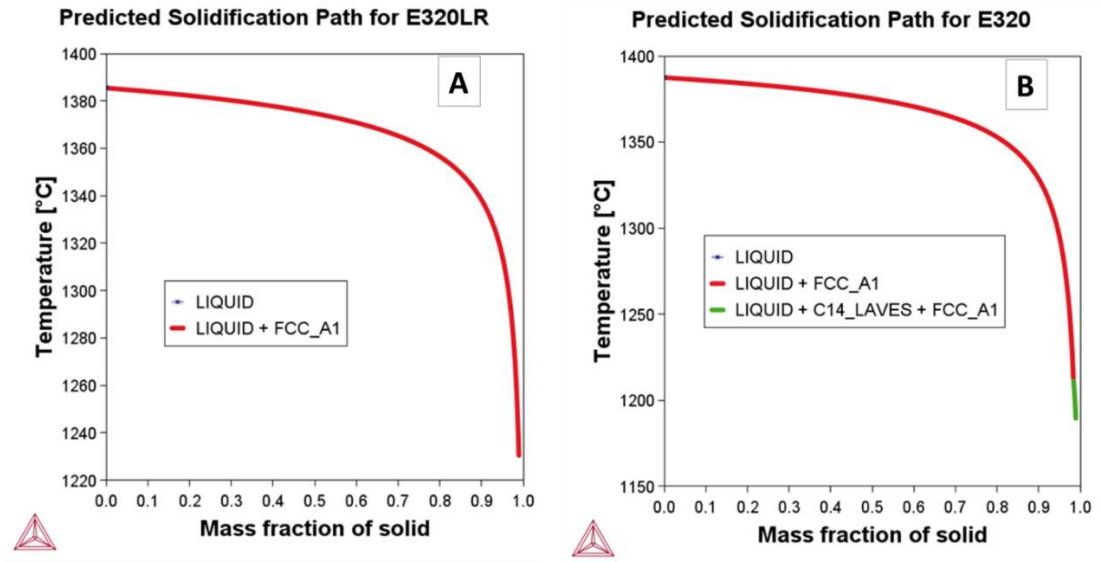

Figure 3- 8: Scheil solidification path simulated with ThermoCalc 2024a. (A): solidification path for welds made with E320LR filler metal. (B): solidification path for welds made with E320 filler metal.

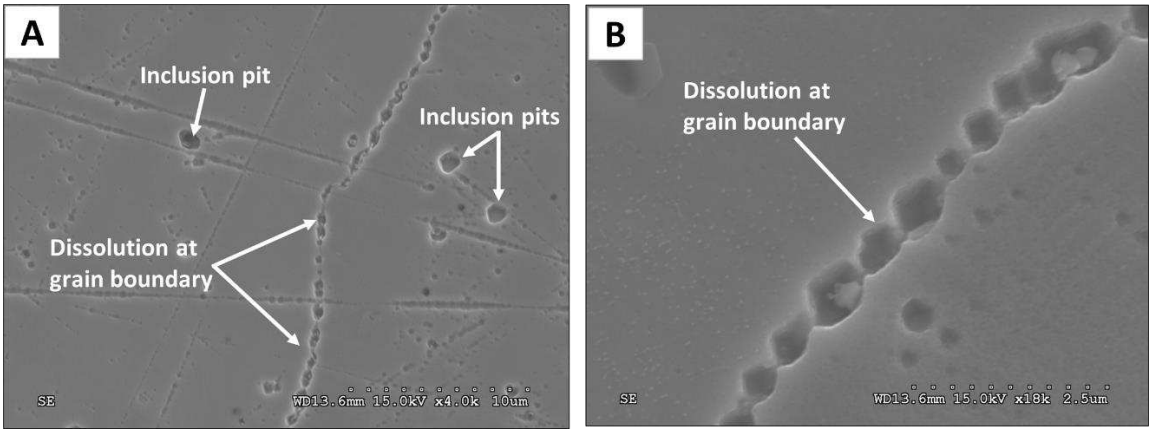

Figure 3- 9: Post-corrosion test SEM image of weld made with E320 filler metal thermally cycled with a heat input of 1.78kJ/mm. (A) Low magnification image showing grain boundary dissolution. (B). High magnification image showing grain boundary dissolution.

CN3MCu Base Metal and Welds Made with E320LR Filler Metal

The corrosion test results for the CN3MCu base metal and welds made with the E320LR filler metal are shown in Figure 3-10. The welds made with E320LR filler metal outperformed the CN3MCu base metal as none of the weld metal samples reactivated in the corrosion tests. In fact, subsequent DL-EPR tests showed that the welds made with E320LR still did not reactivate after it was sensitized at 675^{o}C for 2.5 hours. The DL-EPR test scans for the E320LR weld samples that demonstrate their "no reactivation" results are shown in Figure 3-11. This result made it unnecessary to test for multiple thermal cycles. Examination in the SEM after corrosion testing also did not show any dissolution at grain boundaries either. This is demonstrated in Figures 3-12A and 3-12B, which are SEM images of welds made with E320LR in the as-welded condition and thermally cycled with a heat input of 3.75kJ/mm. As shown in Table 1, the deposited E320LR weld had 0.01wt% carbon compared to 0.03wt% in the CN3MCu base metal. The superior resistance to sensitization is attributed to the extra low carbon concentration. This result suggests that an extra low carbon E320LR fusion zone will not sensitize. Unlike E320, no Mo-Nb-rich secondary phase was observed in the weld made with E320LR filler metal and therefore no dissolution associated with secondary phases was seen. The E320LR filler metal was first developed by Brown et al. to improve upon the solidification cracking susceptibility of E320 welds.[42] They limited carbon to 0.025wt%, and lowered Si, Nb and P concentrations.[42] The elimination of the secondary phase is attributed to this improved composition, especially the lower niobium levels. Line scans taken with EPMA across dendrites in both welds showed that while other elements had similar segregation profiles,

niobium varied from 0.21wt% to 0.84wt% in welds made with E320LR, and from 0.27wt% to 1.74wt% in welds made with E320. The milder niobium segregation in E320LR likely prevented the secondary phase from forming. The secondary phase was typically too small to be measured with EPMA, but is believed to be laves phase based on evidence in literature an ThermoCalc simulations, as earlier mentioned.[40] ThermoCalc 2024A predicts austenite and laves to form in E320 welds, and only austenite to form in E320LR welds during non-equilibrium solidification as shown in Figures 3-8A and 3-8B. The simulation was done with concentration values of Mn, Si, Ni, Cr, Mo, C and Fe found in Table I.

All three thermally cycled CN3MCu base metal samples had DOS values between $1x10^{-3}$ and $4x10^{-3}$. Despite the low DOS values, examination of the CN3MCu base metal samples in the SEM after the corrosion test showed grain boundary attack, and EDS maps of the same samples depicted chromium and carbon enrichment at the grain boundaries. The SEM images that confirm grain boundary corrosion in the CN3MCu base metal thermally cycled with heat input levels of 0.81kJ/mm and 3.75kJ/mm are shown in Figures 3-13A and 3-13B respectively. The EDS map of the 3.75kJ/mm CN3MCu base metal sample, which depicts chromium and carbon enrichment at the attacked grain boundary is shown in Figure 3-14. The low carbon CN3MCu base metal was sensitized, with DOS values between $1.6x10^{-3}$ and $3.1x10^{-3}$, even when processed with low heat input. In the work done by Majidi and Streicher, DOS values around $1x10^{-3}$ translated to approximate corrosion rates of 10-20mils/year in the ferric sulfate-sulfuric acid test for 304L.[24] Other researchers have adopted this DOS value as the upper limit for unsensitized samples. While such low corrosion rates may support the ability to avoid PWHT in certain applications,[10,43] aggressive attack may occur in certain other media or further sensitization may occur at

low service temperatures.[44,45] Sensitization has been found to be possible below the classic carbide precipitation range in a phenomenon is known as low temperature sensitization (LTS).[45,46] Schmidt et al. found that chromium carbides that were present in the as-welded condition grew during isothermal holds at 360ºC for 72 and 2592 hours.[47] Girija et al. also observed that DOS values increased in pre-sensitized 304L samples during LTS holds at 500ºC for one and eleven days. They found that 0.02wt%C 304L was more resistant to LTS than 0.03wt% 304L.[48] It is insightful that stainless steels with such low carbon concentrations were still susceptible to this phenomenon. Once an alloy starts corroding in an aqueous environment, the electrolyte gradually gets enriched in metal cations. These cations, acting as oxidizers, raise the corrosion potential and corrosion current.[49,50] They can possibly raise the potential into the passive region, but this is not guaranteed in most applications since their release into the electrolyte is not controlled.[51] Therefore, the low corrosion rates of mildly sensitized materials are not guaranteed to stay the same as cations build up in the service fluid. In addition, the low corrosion rates observed in pristine laboratory electrolytes cannot be guaranteed in the field if the component is exposed to a spent service fluid already loaded with these cations. The carbides themselves can also be attacked in certain environments. Stansbury et al. conducted different corrosion tests on similarly processed CF8 and CF8M, and observed that while CF8M performed better in the DL-EPR test, both alloys were about equally attacked in the oxalic acid test. They concluded that since the oxalic acid test attacked the chromium carbides directly, the benefit of the molybdenum in enhancing corrosion resistance was not realized in oxalic acid test.[52] Thus, based on these considerations, the PWHT required in ASTM A744 for CN3MCu appears warranted. Since the welds made with the E320LR filler metal did not

sensitize in this research, more extensive testing is recommended to generate comprehensive data on its PWHT needs. The DOS values obtained for the CN3MCu base metal are low enough that marginal improvements to its intergranular corrosion resistance might permit both the base metal and E320LR weld metal to be used without PWHT.

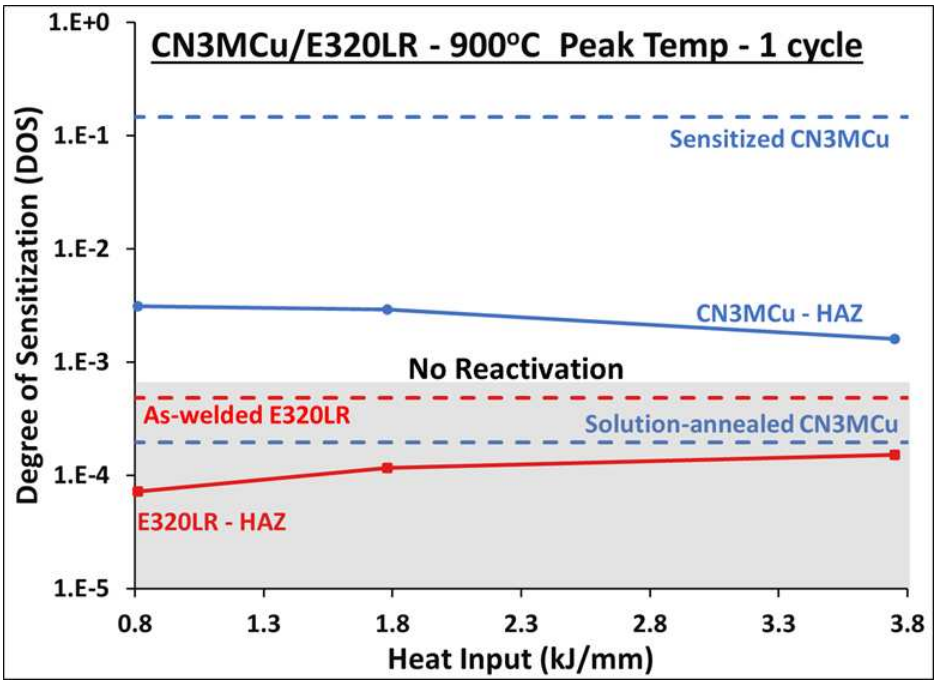

Figure 3- 10: Degree of sensitization (DOS) vs heat input plot for CN3MCu base metal and welds made with E320LR filler metal.

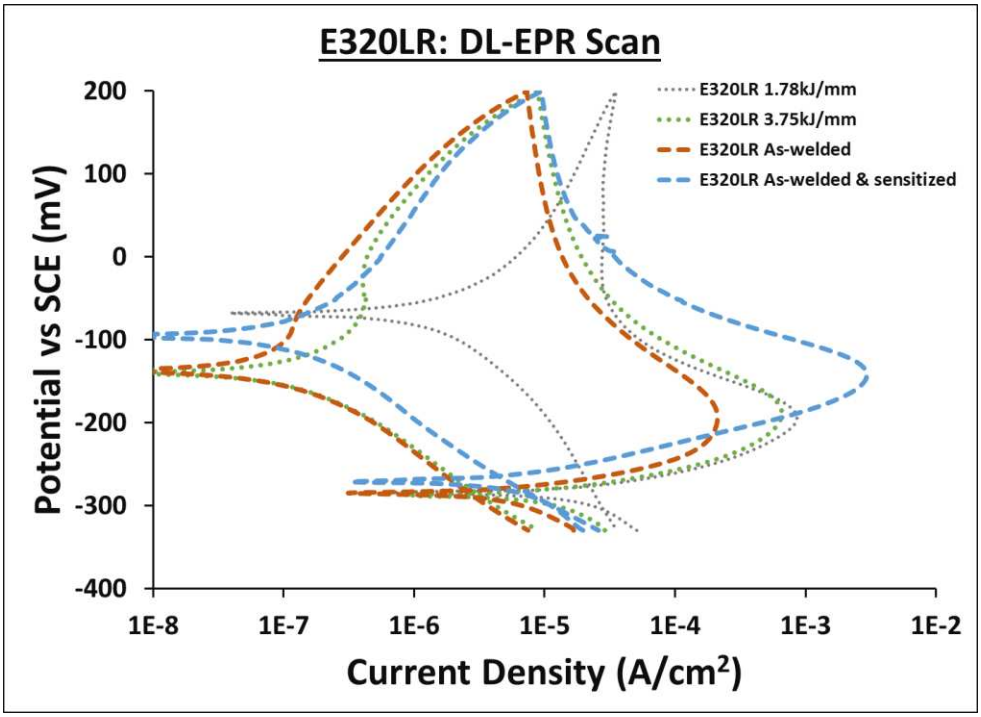

Figure 3- 11: DL-EPR scans for weld metal samples with different thermal histories, all showing no reactivation in the corrosion test. All the welds were made with E320LR filler metal.

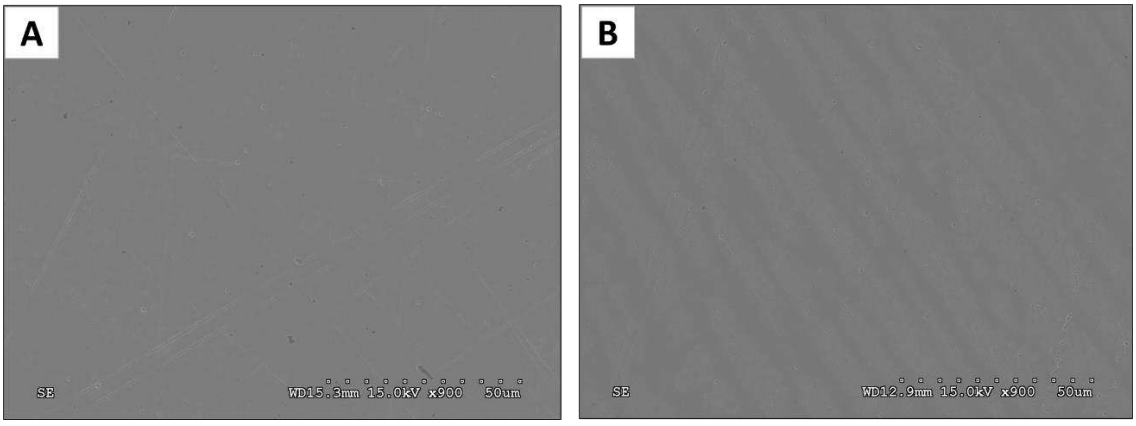

Figure 3- 12: SEM images of E320LR weld samples after the DL-EPR corrosion test, both showing no evidence of intergranular attack. (A): As-welded E320LR. (B) E320LR weld sample thermally cycled with a heat input of 3.75kJ/mm.

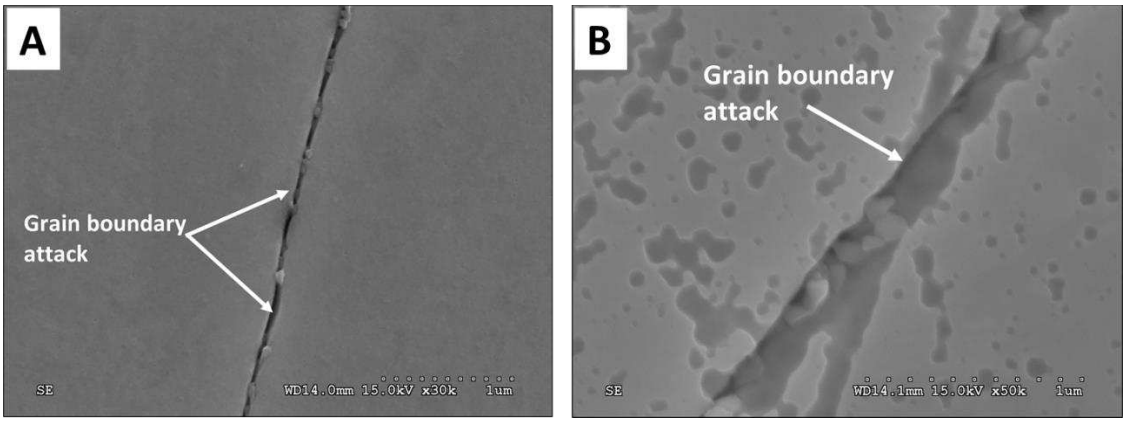

Figure 3- 13: SEM images of CN3MCu base metal samples after corrosion testing. (A): CN3MCu base metal sample thermally cycled with a heat input of 0.81kJ/mm showing grain boundary corrosion. (B) CN3MCu base metal sample thermally cycled at 3.75kJ/mm also showing grain boundary corrosion.

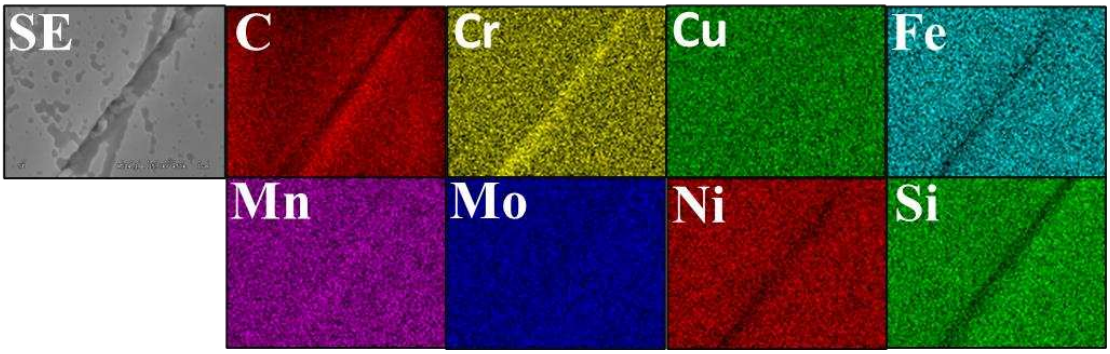

Figure 3- 14: EDS map of CN3MCu base metal sample thermally cycled at 3.75kJ/mm showing Cr and C enrichment at a grain boundary that was attacked in the corrosion test.

Proposed Improvement to CN3MCu Base Metal

Influence of Nitrogen Content on Cr Diffusion in CN3MCu

The CN3MCu comes close to avoiding sensitization as evidenced by the low DOS values, but it must still be improved upon before PWHT can be completed waived. Carpenter Technologies developed Alloy 20-Cb3 (UNS N08020) in the mid 1900's as an

improvement of CN7M and CN3MCu (UNS N08007). The nickel content was increased from 27-30wt% to 32-35wt% for better chloride stress corrosion cracking resistance and niobium was added for sensitization resistance. Alloy 20Cb-3 has enjoyed considerable success in the chemical processing industry, but like all stabilized grades, a post-weld stabilization heat treatment is recommended by the manufacturer to maximize corrosion resistance and prevent knife-line attack (KLA).[3,23,53] Knife-line attack is a well-studied corrosion phenomenon that happens in stabilized stainless steels. During welding, there is small area in the HAZ, usually right next to the fusion line, where peak temperature is high enough to dissolve the niobium or titanium carbides and keep them in solution due to rapid cooling.[54,55] This area becomes susceptible to sensitization if later heated in the chromium carbide precipitation temperature range. Manufacturers usually recommend holding these alloys between 900°C and 1000°C to precipitate the niobium/titanium carbides.[53,56,57] A post weld stabilization treatment defeats the aim of avoiding PWHT.

A promising solution lies in incorporating nitrogen in CN3MCu. Nitrogen addition up to about 0.2wt% to austenitic stainless steels has been shown to improve resistance to pitting corrosion and sensitization.[58] Stansbury et al. investigated the role of nitrogen on corrosion resistance in austenitic stainless steels and concluded that low carbon, nitrogen bearing CF grades were very difficult to sensitize.[58] They noticed that in sensitized nitrogen-bearing CF grades, the chromium-depleted layer shifted from the austenite side of the interphase boundary into the ferrite as nitrogen content increased. Ferrite became the main source of the chromium in the chromium-rich carbides as nitrogen impeded the mobility of Cr in austenite. That chromium still diffused from ferrite to form the carbide somewhat diminished the effect of nitrogen in dual phase stainless steels. However,

chromium depletion was not severe because of its high concentration in ferrite. The nitrogen advantage is expected to be more prominent in fully austenitic stainless steels as chromium mobility will be uniformly hampered throughout the microstructure. Another way they found nitrogen improved sensitization resistance is that it precipitated chromium nitride whose depletion zone is relatively smaller. To investigate nitrogen's potential effect on chromium diffusion in CN3MCu, ThermoCalc was used to simulate Cr homogenization in CN3MCu with varying nitrogen content. The simulations were done at 1200°C, over a distance of 10μm, and for 0.1wt% nitrogen increments from 0wt% to 0.6wt%. Figures 3-15A and 3-15B are examples of simulated Cr profiles in homogenized CN3MCu and CN3MCu with 0.5wt% N respectively. The 1000-second and 3600-second curves are clearly steeper in the nitrogen-containing composition, indicating slower Cr diffusion. Similar plots were made for CN3MCu with nitrogen additions from 0wt% to 0.6wt%. The CN3MCu composition used was Fe-22Cr-30.5Ni-3Mo-3.5Cu-0.03C, picked from the recommended concentrations in Table 2 of ASTM A744. An initial Cr profile of 17wt% to 27wt% was used. From the simulated homogenization profiles, Cr index of residual segregation was calculated for each composition and time, and plotted against nitrogen concentration. Index of residual segregation, δ, is a measure of relative elemental segregation over a distance (usually from the dendrite core to the interdendritic region) after a period of homogenization. It is calculated with the formula $\frac{C_M - C_m}{C_M^o - C_m^o}$, where $C_M^o \; and \; C_m^o$ are the initial maximum and minimum concentrations respectively, and $C_M \; and \; C_m$ are the instantaneous maximum and minimum concentrations respectively. Chromium index of residual segregation is used here as a measure of chromium mobility in each alloy. A high δ means slow chromium diffusion, while a low δ represents rapid

chromium diffusion. Figure 3-16 is a plot of Cr residual segregation index in austenite versus nitrogen concentration. The simulation predicts that chromium diffusion slows down as nitrogen concentration increases. The potentially beneficial addition of nitrogen to CN3MCu to improve corrosion resistance and avoid PWHT thus warrants further investigation.

The Benefit of Lower Mo Content in CN3MCu

The CN3MN alloy is the only nitrogen-bearing CN grade in ASTM A743 and A744. Other similar alloys in the standards are CK35MN and CK3MCuN. The CN and CK grades have somewhat similar Ni/Cr ratios, and all the three alloys mentioned above have 6-7wt% Mo. Such high Mo concentrations impart excellent pitting resistance but also make the alloy vulnerable to sigma phase precipitation. DuPont et al. found that molybdenum segregation in as-cast and as-welded CN3MN and CK3MCuN led to sigma phase formation and reduced corrosion resistance.[41] It is possible that the corrosion improvement benefits of nitrogen were masked by molybdenum's aggressive partitioning. No sigma phase was seen in the as-cast CN3MCu studied in this research. The CN3MCu composition potentially curtails sigma formation by increasing Ni to 27.5-30.5wt%, limiting Mo to 2-3wt% and introducing 3-3.5wt% Cu. A similar compositional design is seen in other Ni-rich alloys like Alloy 825. The copper and molybdenum combination imparts about the same level of resistance to chloride-induced attack as the high Mo concentration.[3] ThermoCalc 2024A was used to predict sigma phase stability under equilibrium conditions in CK3MCuN (20.5wt% Cr, 19.5wt% Ni, 7wt% Mo, 0.24wt% N) and CN3MCu with nitrogen (22wt% Cr, 30.5wt% Ni, 3wt% Mo, 3.5wt% Cu, and 0.24wt% N). The results shown in Figures 3-

17A and 3-17B predict that sigma will be stable in CK3MCuN from 440ºC - 1215ºC, and in "CN3MCuN" from 550ºC to 910ºC. Further simulation with the same program predicted a sigma phase volume fraction of 0.03 and 0.007 in CK3MCuN and "CN3MCuN" respectively, under non-equilibrium cooling conditions. This suggests that sigma formation may be limited in a "CN3MCuN" composition during non-equilibrium solidification.

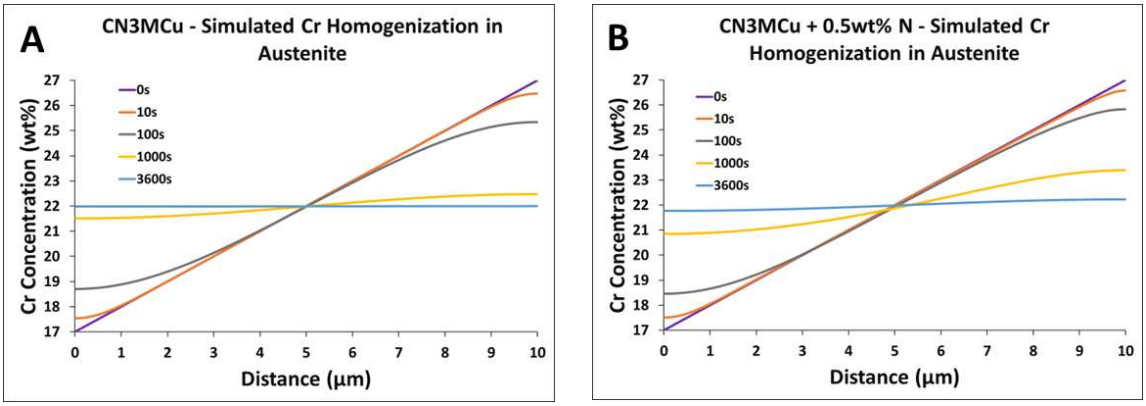

Figure 3- 15: Thermo-Calc-simulated homogenization of Cr profile in (A): CN3MCu and (B): CN3MCu with 0.5wt% N.

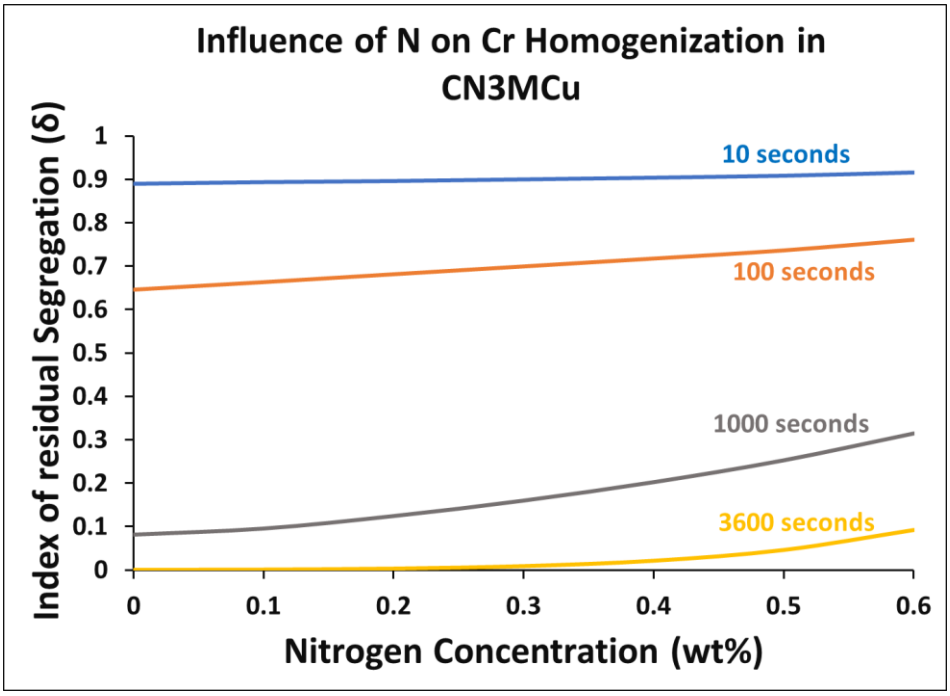

Figure 3- 16: Simulated influence of nitrogen on chromium homogenization in CN3MCu

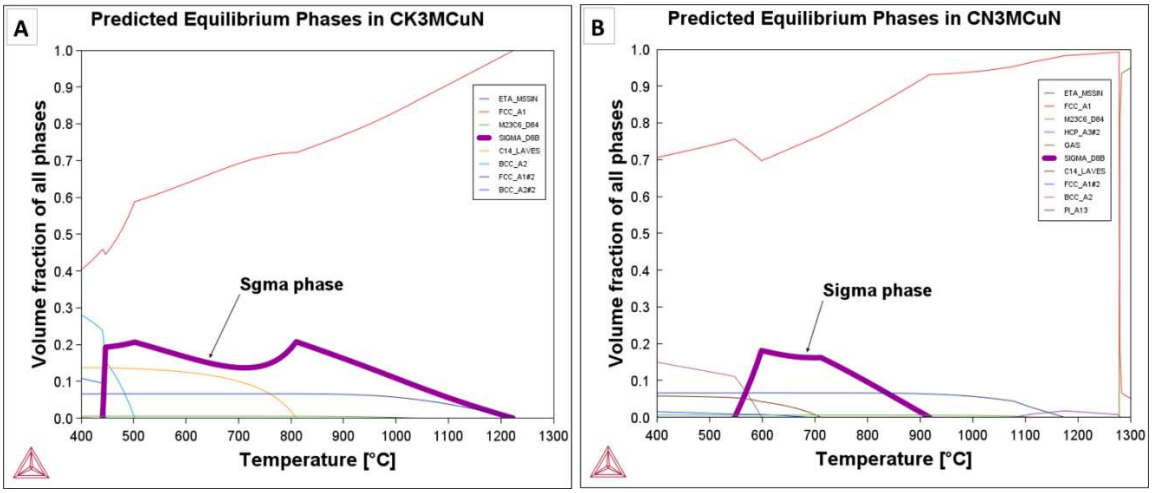

Figure 3- 17: Equilibrium phase fractions predicted with Thermo-Calc in (A): CK3MCuN (7wt% Mo, 0.24wt% N). (B): CN3MCu with nitrogen (3wt% Mo, 0.24wt% N).

Conclusion

Two base metal/weld metal pairs, CN3MCu/E320LR and CN7M/E320 were evaluated for the possibility of waiving the PWHT requirement in ASTM A743 and A744. The research produced the following findings:

1. Austenite boundary dissolution was seen in both CN7M base metal and welds made with E320 after the corrosion test. It was determined that a solution anneal will be beneficial for this pair to dissolve the chromium carbides in the base metal and weld metal, and secondary phases in the weld metal.
2. The CN3MCu/E320LR base metal/weld metal pair generally had lower DOS values. None of the weld metal samples made with E320LR reactivated in the corrosion test, including the isothermally sensitized one, indicating excellent resistance to intergranular corrosion. This was attributed to the extra low carbon concentration (0.01wt%) in the deposited weld. Its base metal, CN3MCu, exhibited very low DOS values, with IGA confirmed by the presence of boundary dissolution. Although such low DOS values may permit use in mild environments, it is recommended that the PWHT requirement be maintained since such materials could still be attacked in other certain environments.
3. Results from thermodynamic and kinetic modelling suggest that adding nitrogen to CN3MCu could potentially improve its resistance to intergranular corrosion, and possibly permit the CN3MCu/E320LR base metal/ weld metal pair to be used without PWHT.

References

1. M.G. Fontana: Corrosion Engineering, 3rd edition., McGraw-Hill, New York, 1986.
2. A.J. Sedriks: International Metals Reviews, 1982, vol. 27, pp. 321–53.
3. C.P. Dillon: Corrosion Resistance of Stainless Steels, 1st edn., Marcel Dekker, Inc., New York, 1995.
4. M. Blair, T.L. Stevens, and B. Linskey: Steel Castings Handbook - Chapter 20, 6th Edition., ASM International, Materials Park, Ohio.
5. J. Van der Geer, J.A.J. Hanraads, and R.A. Lupton: Nickel Development Institute Publication, 2000, vol. 266, pp. 1–52.
6. C. McCaul: British Corrosion Journal, 1991, vol. 26, pp. 239–43.
7. D.A. Jones: Principles and Prevention of Corrosion, 2nd edition., Prentice-Hall Inc., Upper Saddle River, NJ, 1996.
8. F.H. Stott and F.I. Wei: Materials Science and Technology, 1989, vol. 5, pp. 1140–7.
9. T. Ohmi, Y. Nakagawa, M. Nakamura, A. Ohki, and T. Koyama: Journal of Vacuum Science & Technology A: Vacuum, Surfaces, and Films, 1996, vol. 14, pp. 2505–10.
10. M.H. Brown: Corrosion, 1974, vol. 30, pp. 1–12.
11. I.-S. Forest: The International Nickel Company, 1983, vol. 1, pp. 51–82.
12. ASTM International: ASTM A743-21, 2021, pp. 1–8.
13. ASTM International: ASTM A744-21a, 2021, pp. 1–6.
14. ASTM International: ASTM A351-18, 2018, pp. 1–7.

15. S. Zhang, Z. Jiang, H. Li, H. Feng, and B. Zhang: J Alloys Compd, 2017, vol. 695, pp. 3083–93.
16. J.M. Aquino, C.A. Della Rovere, and S.E. Kuri: Corros Sci, 2009, vol. 51, pp. 2316–23.
17. J.C. Lippold: Welding Metallurgy and Weldability, 1st edition., John Wiley & Sons Inc, Hoboken, NJ, 2015.
18. S. Kou: Welding Metallurgy, 3rd edition., Wiley, Hoboken, NJ, 2020.
19. L.R. Scharfstein and G.N. Maniar: British Corrosion Journal, 1965, vol. 1, pp. 36–41.
20. J.F. Grubb: NACE Corrosion Conference and Expo 2011, 2011, pp. 4753–9.
21. K. Vivekanand, R.C. Prasad, and P.K. De: High Temperature Materials and Processes, 1997, vol. 16, pp. 183–200.
22. M.F. Maday, A. Mignone, and M. Vittori: Corros Sci, 1988, vol. 28, pp. 887–900.
23. A.J. Sedriks: Corrosion of Stainless Steels, 2nd edition., John Wiley & Sons Inc, New York, NY, 1996.
24. A.P. Majidi and M.A. Streicher: Corrosion, 1984, vol. 40, pp. 584–93.
25. L. Sun, Y. Sun, C. Lv, Y. Liu, N. Dai, Y. Jiang, J. Li, and D.D. Macdonald: Corros Sci, 2021, vol. 185, p. 109432.
26. J. Hong, D. Han, H. Tan, J. Li, and Y. Jiang: Corros Sci, 2013, vol. 68, pp. 249–55.
27. J.L. Mitchiner, S.D. Kleban, B. V Hess, K.W. Mahin, and D. Messink: Proceedings of the AI and Manufacturing Research Planning Workshop, 1996, pp. 129–35.

28. M.A. Streicher: in Intergranular Corrosion of Stainless Steels, ASTM STP 656, R.F. Steigerwald, ed., ASTM International, 1978, pp. 3–84.
29. D.L. Reichert and G.E. Stoner: J Electrochem Soc, 1990, vol. 137, pp. 411–3.
30. T. Amadou, C. Braham, and H. Sidhom: Metallurgical and Materials Transactions A, 2004, vol. 35A, pp. 3499–513.
31. H. Demers, P. Horny, R. Gauvin, and E. Lifshin: Microscopy and Microanalysis, 2002, vol. 8, pp. 1498–9.
32. J.J. Donovan, J.W. Singer, and J.T. Armstrong: American Mineralogist, 2016, vol. 101, pp. 1839–53.
33. S.M. Seddio and J.J. Donovan: Microscopy and Microanalysis, 2016, vol. 22, pp. 444–5.
34. D.A. Jones: Principles and Prevention of Corrosion, 2nd edition., Prentice Hall, Upper Saddle River NJ, 1996.
35. S. Fajardo and G.S. Frankel: Electrochem commun, 2017, vol. 84, pp. 36–9.
36. A.D. Gabbardo and G.S. Frankel: J Electrochem Soc, 2019, vol. 166, pp. C3254–65.
37. R.L. Holtz, P.S. Pao, R.A. Bayles, T.M. Longazel, and R. Goswami: DoD Corrosion 2011, pp. 1–12.
38. L. Sun, Y. Sun, C. Lv, Y. Liu, N. Dai, Y. Jiang, J. Li, and D.D. Macdonald: Corros Sci, 2021, vol. 185, pp. 1–12.
39. ASTM International: ASTM A262-15, 2021, pp. 1–20.
40. J.N. DuPont: Weld J, 1999, vol. 78, pp. 253s–63s.
41. J.N. DuPont and J.D. Farren: Corrosion, 2011, vol. 67, pp. 055002/1-055002/11.

42. R.S. Brown and J.B. Koch: Weld J, 1978, vol. 57, pp. 38s–42.
43. C. McCaul: NACE Corrosion Conference and Expo 1992, 1992, pp. 297/1-297/11.
44. Steel Founders' Society of America: Sensitization Behavior of Cast Stainless Steels Subject to Weld Repair, Des Plaines IL, 1984.
45. Lawrence Livermore National Laboratory: Overview of Low Temperature Sensitization, Livermore, CA (United States), 1983.
46. M.J. Povich: Corrosion, 1978, vol. 34, pp. 60–5.
47. C.G. Schmidt, R.D. Caligiuri, L.E. Eiselstein, S.S. Wing, and D. Cubicciotti: Metallurgical and Materials Transactions A, 1987, vol. 18A, pp. 1483–93.
48. G. Suresh, P.K. Parida, S. Bandi, and S. Ningshen: Mater Chem Phys, 2019, vol. 226, pp. 184–94.
49. Z. Liu, L.M. Zhang, W.Q. Chen, A.L. Ma, Y. Zheng, W. Yan, Y.F. Li, E.F. Daniel, Y.Y. Shan, and Y.G. Zheng: Electrochim Acta, 2023, vol. 442, pp. 141917/1-141917/15.
50. M.A. Streicher: J Electrochem Soc, 1959, vol. 106, p. 161.
51. M.A. Streicher: Corrosion, 1958, vol. 14, pp. 19–30.
52. Steel Founders Society of America: Sensitization Behavior of Cast Stainless Steels Subject to Weld Repair, Des Plaines IL, 1984.
53. Carpenter Technology: CarTech 20Cb-3 Stainless - Technical Data Sheet, 2002.
54. M.G. Fontana: Corrosion, 1952, vol. 44, pp. 87A-90A.
55. M.L. Holzworth, F.H. Beck, and M.G. Fontana: CORROSION, 1951, vol. 7, pp. 441–9.

56. L. Shoemaker and J. Crum: NACE Corrosion Conference and Expo 2011, 2011, pp. 4924–36.

57. M. Henthorne and T.A. DeBold: Corrosion, 1971, vol. 27, pp. 255–64.

58. Steel Founders Society of America: The Role of Nitrogen in the Corrosion Behavior of Cast Austenitic and Duplex Stainless Steels, Des Plaines IL, 1988.

Conclusions

This project investigated the possibility of waiving PWHT among CF and CN grades of cast stainless steels. Four CF alloys and two CN alloys were selected to include low carbon compositions, niobium-stabilized compositions, and nitrogen-containing compositions, which are popular alloy designs for mitigating sensitization. All these base metals were paired with welds made with their corresponding filler metals. The double loop electrochemical potentiokinetic reactivation (DL-EPR) test was used as the preferred corrosion test for its ability to detect even mild levels of sensitization. The research conclusions are as follows:

1. Though touted as sensitization-resistant, the low carbon grade (CF3) exhibited low DOS values under all heat input conditions and was considered mildly sensitized with evidence of interphase boundary attack. Depending on the service conditions, samples that exhibit such low levels of corrosion may be deployed without PWHT. However, the PWHT requirements in the ASTM standards were recommended to be maintained to ensure maximum corrosion resistance. The weld metal made with E308L filler metal exhibited higher DOS values due to preferential attack in the austenite. Post weld heat treatment is believed to improve the intergranular corrosion resistance of the E308L weld by changing its ferrite amount and morphology. It was concluded that both the CF3 base metal and E308L weld benefit from the PWHT.
2. The niobium stabilized CF8C base metal showed sparse interphase boundary attack under all heat input levels tested, and are considered quite resistant to intergranular corrosion. However, stabilized grades often require a post-weld stabilization heat

treatment to prevent knife-line attack, which defeats the goal of avoiding PWHT. The E347 welds exhibited higher DOS values than the CF8C base metal due to localized preferential attack of austenite in the weld. Post weld heat treatment is believed to improve the intergranular corrosion resistance of the E347 weld by changing its ferrite amount and morphology. The PWHT also acts as a stabilization treatment for both the base metal and weld metal.

3. The nitrogen-bearing CF3MN and welds made with the E316L filler metal did not reactivate in the corrosion test. They also did not show any interphase boundary attack after the test. This pair presented the best chance to waive PWHT. More extensive corrosion tests are recommended for this pair to generate comprehensive data on its PWHT needs.
4. The CN3MCu base metal exhibited mild levels of sensitization evidenced by low DOS values. Intergranular attack was observed in this alloy through SEM examination. The welds made with E320LR, on the other hand, exhibited excellent resistance to intergranular corrosion, no grain boundary attack was observed in the weld samples after the corrosion test. Results from thermodynamic and kinetic modelling suggest that nitrogen additions to CN3MCu could potentially improve its resistance to intergranular corrosion, and permit the CN3MCu/E320LR base metal/weld metal pair to be used without PWHT.

Vita

Michael Annor was born and raised in Accra, Ghana. He attended Mfantsipim High School in Cape Coast, Ghana and graduated in 2006. From 2007 to 2011, he was enrolled at the Kwame Nkrumah University of Science and Technology in Kumasi, Ghana and graduated with a Bachelor of Science in Materials Engineering. After his undergraduate studies, he worked in welding inspection roles in the gold mining and oil and gas industries in Ghana. In Fall of 2020, he was got admitted into Lehigh University for his graduate studies under Professor John DuPont in the Engineering Metallurgy Group. He graduated with a Master of Science in Materials Science and Engineering in Spring of 2022 and continued with his PhD studies under Professor John DuPont. He graduated with his PhD in Spring of 2024 and accepted a role as an Advanced Research and Development at Honeywell UOP in Chicago, USA.